

DESIGN OF AN OXYGEN FLOW METER
FOR HOSPITAL APPLICATION

Thesis by

James R. Barnes

In Partial Fulfillment of the Requirements
For the Degree of
Mechanical Engineer

California Institute of Technology
Pasadena, California

1966

(Submitted September 8, 1965)

ACKNOWLEDGMENTS

The author wishes to thank Professor D. A. Morelli for suggesting the research subject, and for his advice and constructive criticism during the instrument design.

Thanks are due also to Dr. Boris Auksmann for his advice on tooling, and to Mr. James McCloud for his assistance during the design of the flow meter totalizer section. Mr. Donald W. Laird and his personnel in the Mechanical Engineering shop did a creditable job in producing the prototype.

The author further wishes to express his gratitude to many persons for their help in the preparation of the manuscript.

The author is indebted to the California Institute of Technology for financing this project. During the investigation, the author received financial assistance from General Electric Foundation Fellowships for which he wishes to express his appreciation.

ABSTRACT

A general description of the need for hospital flow meters is given along with an analysis of some common flow measurement methods.

The design criteria, establishment of the basic configuration of the instrument, and the evolution of the final design are presented in detail. The ability of the magnetic crossover mechanism to extract the square root of an input is explained, and design curves are presented. The action of the flow totalizer is described in relation to the rest of the instrument. A complete set of manufacturing drawings for the instrument and its tooling is included in the thesis.

In conclusion, an evaluation of the completed instrument is made, and improvements and modifications are indicated. Mention is made of the adaptability of the magnetic crossover mechanism to other instrumentation.

TABLE OF CONTENTS

Acknowledgments	ii
Abstract	iii
List of Figures	vi
I. Introduction	1
Accepted Flow Measurement Techniques	2
II. General Description of the Device	6
III. The Capsule Section	10
The Orifice Design	10
The Diaphragm Capsule Design	14
The Throttling Valve Design	17
The Diaphragm Capsule Chamber Casing and Anvil Casing Design	18
IV. The Magnetic Crossover Assembly Section	20
Theoretical Considerations	20
1. Determination of the Flux Path	20
2. Tilted Ring Calculations	24
Design of the Magnetic Crossover Assembly	30
V. The Flow Totalizer Assembly Section	37
Operation of the Totalizer	37
VI. Instrument Evaluation	42
Test of the Magnetic Crossover Assembly	42
Overall Test of the Instrument	45
Conclusions	45

TABLE OF CONTENTS (continued)

Appendixes

I.	Isentropic Gas Laws for Orifice Flow	48
II.	Calculations for Curves of Magnet Excursion Angle, α - β , versus Tilted Ring Rotation Angle, γ , for Various Fixed Angles of Tilt, σ .	52
III.	References	61
IV.	Manufacturing Drawings	63

LIST OF FIGURES

<u>Figure</u>		<u>Page</u>
1	Schematic Diagram of the Instrument	7
2	Photograph of the Completed Instrument	9
3	Torque Analysis of the Tilted Ring	22
4	Torque Analysis of the Tilted Ring	23
5	Torque Analysis of the Tilted Ring	23
6	Torque Analysis of the Tilted Ring	23
7	Geometrical Configuration of the Tilted Ring within the Sphere	26
8	Orthogonal Projection of the Spherical Triangle ABC	26
9	Plot of Magnet Excursion versus Tilted Ring Rotation Angle	27
10	Expanded View of Fig. 9 for Magnet Excursion Angles from One to Ten Degrees	28
11	The Magnetic Crossover Assembly	31
12	Comparison of the Configurational Aspects of the Tilted Ring to the Magnet for Circular and Square Cross Sections	31
13	Photograph of the Swiss Die Set Used to Fabricate the Tilted Ring	34
14	Photograph of the Stretch-Former Die Used to Fabricate the Tilted Ring Support Frame	34
15	Plot of Magnet Excursion versus Tilted Ring Rotation for $\sigma = 30^\circ$ Showing Comparison of Errors at Different Flow Rates Due to Error in Zero Setting of Instrument	36

LIST OF FIGURES (continued)

<u>Figure</u>		<u>Page</u>
16	The Flow Totalizer Assembly	38
17	Diagram of the Quick-Return Mechanism	39
18	Comparison of Theoretical and Experimental Results for Tilted Ring Rotation as a Function of Magnet Excursion	43
19	Schematic Diagram of Flow Meter Calibration Equipment	46

Chapter I

INTRODUCTION

There is a need in industry for a reliable and accurate gas flow meter which can measure small flow rates, and also totalize the amount of flow through the instrument. This need is evident in present day hospital applications, where oxygen is no longer administered to the patient from a bedside cylinder, but is delivered from a central, high-pressure source through a system of supply lines maintained at 50 psi. Flow rate must be set remotely, i. e., at the surgery room, the recovery room, or the ward, depending on the usage, such as for masks, tents, catheters, cannulas, or incubators. Breathing flow rates vary from 5 liters per minute for children to 10 liters per minute for adults. The totalized amount of flow is necessary so that the cost of oxygen used can be allocated to each patient.

Determination of the rate of oxygen delivery may be quite critical, such as when oxygen is being supplied through a nebulizer to atomize liquids for inhalation. Therefore, the flow meter must indicate the rate of flow accurately and totalize the amount of flow while located in a position remote from the main line regulator. A throttling device must be located downstream of the calibrated measuring device in order to vary the flow rate. Furthermore, the instrument requires protection against fluctuations in back pressure on the measuring device that may cause variations in a predetermined

flow rate. Such fluctuations may be encountered, for example, when a nebulizer is inserted in a line downstream of an orifice. Finally, the very nature of the application dictates that the flow meter be compact, portable, and accurate with a minimum of maintenance.

Accepted Flow Measurement Techniques

All presently available hospital flow meters suffer from a lack of accuracy. In order to develop a more accurate instrument, it is helpful to examine some existing methods of monitoring low flow rates. The advantages or disadvantages of each to the design of an instrument for hospital application can then be noted along with the requirement for inexpensive production and profitable marketing.

A generally accepted flow meter design uses the moment-of-momentum principle, where the torque on an impeller in the line of flow is measured and related to the mass flow rate, or to the volumetric flow rate for fluids of constant density. The impeller has many blades, each radial at its exit section, so that the applied torque, T , is determined by

$$T = \dot{m} \omega r^2 ,$$

where \dot{m} is the discharge mass rate, ω is the speed of rotation, and r is the impeller outer radius. By holding the speed fixed by adjusting the torque applied, the mass rate can be computed as a function of the measured torque and its correction for losses in the bearings and for disk friction.

To totalize the flow, however, a hydrodynamically balanced,

low-mass, paddle-bladed rotor, requiring no thrust bearing, is used in the line of flow. In operation, a magnetic pick-off coil, located externally to the duct, but adjacent to the rotor, has generated within it an electric current whose frequency is directly proportional to the rotation of the rotor, which, in turn, is proportional to the fluid flow. These generated pulses are fed directly into any of many recording, indicating, or control devices commercially available. The cost of these devices eliminates this method from further consideration for hospital application.

If instead, a mechanical counter is driven by the rotating rotor at a constant torque output, the rotor speed would indicate the through flow. This principle is presently used by some hospital flow meters, but the low power available at small flow rates (0 - 15 lpm) limits accuracy to $\pm 15\%$ of total flow.

Other accepted flow meter types show similar disadvantages, namely low accuracy for small flow rates, or high cost. For example, the electromagnetic type flow meter, used to measure flows of molten corrosive metals, sets up a magnetic field across a non-conducting tube through which flows a conductive fluid, producing an induced voltage across the flow which may be measured if electrodes are embedded in the tube walls. The voltage is a linear function of the volume rate passing through the tube. A disadvantage of the method is the small signal received and the large amount of amplification needed, which is costly.

The bellows-type orifice meter, prominent in the natural gas industry, measures the differential pressure across a restriction placed in the flow line. A modern bellows-type orifice meter is composed of a center plate connecting two bellows, the interiors of which are completely filled with a liquid which can pass through an orifice in the center plate. This system constitutes a sort of frictionless piston, free to move from one side to the other as pressure is applied to the outside of the bellows. Pressure applied to the exterior of the bellows causes its volume to decrease; liquid is moved through the orifice to the opposite bellows, which increases in volume, resulting in linear movement along the axis of the bellows. This motion, proportional to differential pressure applied, is picked up by a drive arm and transmitted to a square root device, and then to a pointer, pen arm, or other indicator or recorder. In order to obtain popular differential ranges used in flow measurement, additional spring loading of the bellows unit is necessary, which can cause nonlinearities of output if the instrument is not calibrated or maintained properly. Of course, this meter merely indicates flow rate and makes no attempt to totalize the flow.

This brief look at several flow measurement techniques has pointed out weaknesses in their adaptation to low flow rate flow meters. Further study leads to the following design guides. First, for overall accuracy an orifice must be employed and designed not only to deliver specified flow, but constructed in such a way that gaseous expansion on the downstream side will not affect the measurement. Secondly, the bellows, or diaphragm capsule, provides a very adequate

way of transferring pressure changes into linear motion if the inherent nonlinearities can be controlled. And last, the magnetic crossover is an excellent method of transmitting information from a hermetically sealed chamber to the outside of that chamber, if some amplification of the information can be obtained in order to power a counting device, or to provide an indicating level against which an externally powered counting device can compare. It is deemed necessary to keep the counter mechanism exterior to the hermetically sealed oxygen container because of its need for periodic lubrication, which would not only contaminate the oxygen but could produce a combustible mixture.

Chapter II

GENERAL DESCRIPTION OF THE DEVICE

The resulting design will now be described generally, with detailed descriptions being presented in the following chapters and appendices. Referring to Figure 1, flow enters the instrument from the wall at the inlet port (1) and passes into the diaphragm capsule chamber (2) and then through the orifice at (3) into the diaphragm capsule (4) and out through the throttling valve (5) to the oxygen user. Magnet chamber (6) is also maintained at line pressure, and supports a permanent magnet (7) which is free to rotate about a horizontal axis, being controlled by a linkage (8) from the diaphragm capsule below it. Mounted exterior to the hermetically sealed chamber is the crossover ring assembly (9), which rotates about a vertical axis with amplification very nearly proportional to the square root of the excursion of the permanent magnet within the chamber. Attached to this assembly is a pointer (10) which may be held against a calibrated anvil, integral to casing (11), by clamp (12) which is actuated for a period of each cycle of ball cam (13), driven by gear motor (14). The mechanical counter housing (15) and counter drive wheel (16) are also driven by the gear motor through the ball cam by a slot arrangement in the counter housing base. However, as the counter drive strikes the crossover assembly pointer, an overrunning slip clutch (17) engages the lower counter disk while the counter housing and other

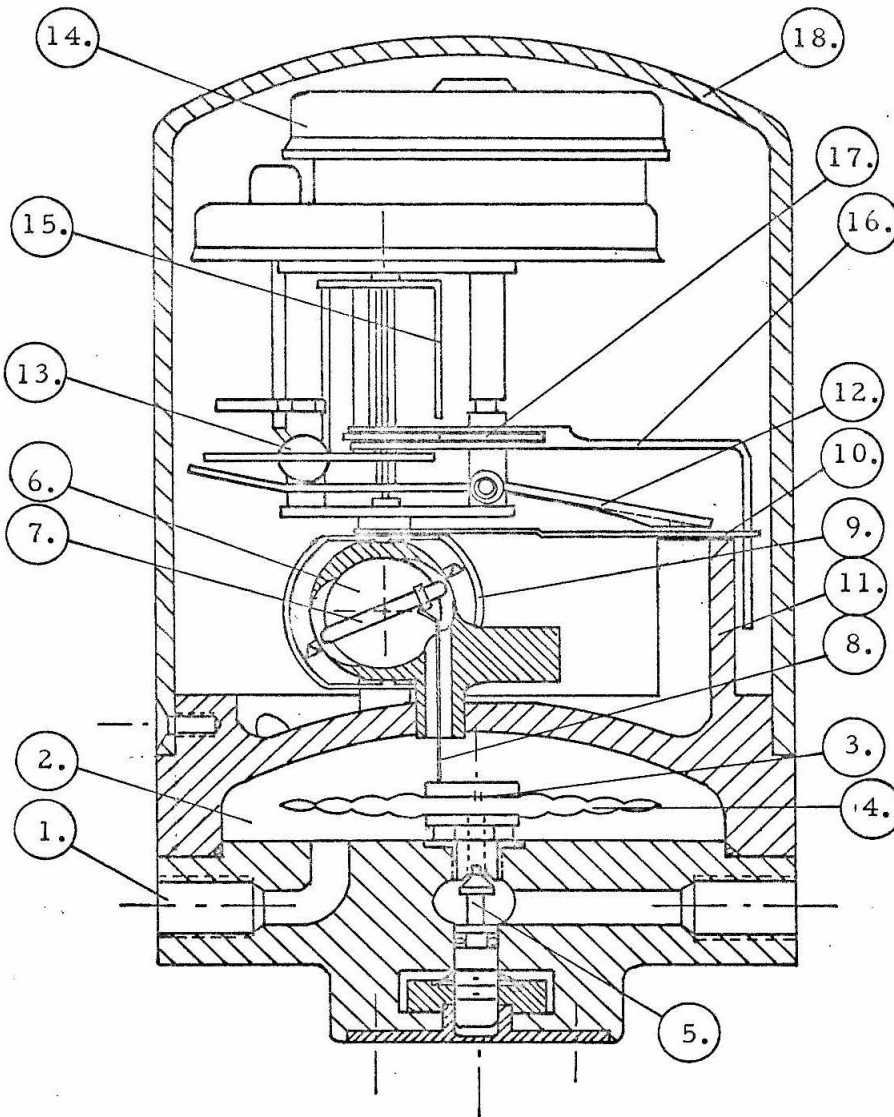


Fig. 1. Schematic Diagram of the Instrument.

- | | |
|------------------------------|---------------------|
| 1. inlet port | 10. pointer |
| 2. diaphragm capsule chamber | 11. anvil casing |
| 3. orifice | 12. clamp |
| 4. diaphragm capsule | 13. ball cam |
| 5. throttling valve | 14. gear motor |
| 6. magnet chamber | 15. counter housing |
| 7. permanent magnet | 16. counter drive |
| 8. linkage | 17. slip clutch |
| 9. crossover ring assembly | 18. enclosure |

counter disks continue rotating, putting a count into the meter. After the lower counter disk has turned through a full revolution, a pawl is engaged which actuates the upper disks to keep count, in typical odometer action. Both the anvil scale and meter counter can be read through the transparent enclosure (18).

Therefore, this instrument employs orifice metering through a diaphragm capsule linked to a magnetic crossover mechanism, allowing indication of both fluid flow rate and totalization of flow. The accuracy of the instrument suffers only from friction in the bearings of the crossover ring suspension and nonlinearities in the diaphragm capsule and linkage arrangement, which are designed to be minimal. Resolution is dependent upon the construction of the magnet and magnetic crossover assembly, and on the angle of tilt of the tilted ring, which determines the angular scan of the pointer on the anvil. Commercial manufacture is possible as shown by the manufacturing drawings of all components, Appendix IV, and the photograph of the working model, Figure 2. The exact shapes, dimensions, and materials of each component were determined on the basis of design calculations for strength and rigidity where applicable, with due consideration to the machining operations necessary for construction, the availability of materials, and overall instrument cost.



Fig. 2. Photograph of the Completed Instrument. (The closure plate to the magnet chamber has been removed.)

Chapter III

THE CAPSULE SECTION

The purpose of the capsule section of the instrument, which includes the diaphragm capsule, the valve casing, and the anvil casing, is to provide a means for transforming a pressure drop through an orifice to lineal motion. To do this, a sharp-edged orifice plate is used as the center pad of the upper diaphragm of a diaphragm capsule mounted within a chamber maintained at line pressure, 50 psig. In accordance with equation 21 of Appendix I, a pressure differential occurs across the orifice plate as a function of the orifice diameter, the flow rate, and the properties of the gas. Since a diaphragm is a pressure-responsive element which is movable in a direction substantially perpendicular to its flexible surface, motion parallel to the cylindrical axis of the diaphragm capsule results. This motion may be made a linear function of the applied force by proper design of each of the diaphragm's corrugations and is transmitted by means of a linkage to a pivoted permanent magnet within its support chamber, located above the diaphragm capsule within the instrument.

The Orifice Design

The design of the orifice meets three specifications:

1. The pressure differential across the orifice must not collapse the diaphragm capsule.

2. The diameter ratio, $\beta = \frac{d_{\text{orifice}}}{d_{\text{reservoir}}}$, must be chosen such that the contraction coefficient, C, and the expansion factor, Y, of equation 20, Appendix I, $Q = CA_o Y \sqrt{\frac{2\Delta P}{\rho_1}}$, remain reasonably constant for the Reynolds numbers in the operating range.
3. The orifice plate must be designed to allow a connection with the linkage which will not disturb the flow on the upstream side of the orifice and will permit joining in a manner not susceptible to fatigue failure.

The following values for oxygen will be used in the subsequent analysis:

Reservoir pressure, $p_1 = 50 \text{ psig} = 64.7 \text{ psia}$

Absolute viscosity, $\mu = 4 \times 10^{-7} \text{ lb. sec/ft}^2$

Kinematic viscosity, $\nu = 1.7 \times 10^{-4} \text{ ft}^2/\text{sec}$ at S. T. P.

Specific heat ratio, $k = 1.40$

Density, $\rho = \frac{\mu}{\nu} = 7.56 \times 10^{-2} \text{ lb/ft}^3$ at S. T. P.

Specific weight at reservoir,

$$\rho_1 = \frac{\rho_{\text{S. T. P.}}}{g} \left(\frac{p_1}{p_{\text{S. T. P.}}} \right)^{1/k} = 6.78 \times 10^{-3} \text{ lb. sec}^2/\text{ft}^4$$

Upstream Reynolds numbers,

$$R = \frac{4}{\pi} \frac{Q}{D_1} \frac{\rho_1}{\mu} = \begin{cases} 2.03 \times 10^3 & \text{for } Q = 5 \text{ lpm} \\ 6.08 \times 10^3 & \text{for } Q = 15 \text{ lpm} \end{cases}$$

where $D_1 = .375''$

To satisfy specifications 1 and 2, the orifice type must be selected before any stipulation is made as to the diameter ratio, β . Then the orifice area will be chosen to provide a small pressure differential over the diaphragm capsule, leaving a larger Δp over the throttling valve. It has been shown experimentally (reference 13) that for large Reynolds numbers, laminar flow influences are small contrasted to inertial influences, and the exact geometry of the orifice opening is not important as long as the upstream edge is sharp and the throat thickness small enough, so that the jet remains free of the influence of the orifice throat boundary. However, for low Reynolds numbers, such as those of concern in this design, the combined discharge coefficient, $K = CY$, is a function of the flow pattern through the orifice, which is described by the exact geometry of the boundary, particularly the boundary in the vicinity of the orifice opening. Velocity gradients with corresponding shear stresses will vary between orifices with thick throat sections and thin throat sections. The angle of the beveled downstream edge also produces discernible differences for small variations. The choice of orifice plate type must present stable, nearly constant values for K for a specified geometric configuration and the range of Reynolds number through the orifice.

It is helpful to look at completed experimental work to eliminate some design choices. Grace and Lapple (reference 11) have made extensive calibrations to determine the discharge coefficients of small diameter orifices, i. e., orifices with $d \leq .750$ ". Their results, conducted on sharp edged orifices with 45° bevels on the downstream

faces, show that thick throated orifices, throat lengths $\geq .032''$, do not give reproducible results at low Reynolds numbers, even with calibration. Spreads of as much as 30% in discharge coefficient were obtained for a given Reynolds number. However, they were able to determine discharge coefficients for thin-throated, sharp-edged orifices within $\pm 0.5\%$, as a function of the Reynolds number, when the precision of fabrication and measurement of the actual orifice diameter was held at ± 0.002 mm. For $d_o = .093''$, throat length $\leq .001''$, $\beta = .05$, gives $K = 0.635$ to 0.615 for Reynolds numbers 2.03×10^3 to 6.08×10^3 , respectively. For comparison, a VDI orifice (as given by reference 18), with $d_o = .084''$, throat length $\leq .007''$, $\beta = .05$, gives $K = 0.618$ to 0.605 for the same Reynolds number range. The VDI orifice specifies a 30° bevel for the downstream face.

It is evident, then, that the orifice could be designed with an approximate diameter of $5/64''$, throat length $.005''$, and downstream bevel taking the angle of the deburring tool, giving discharge coefficients that are constant within $\pm 1\%$ for the desired Reynolds number range. Careful calibration of the orifice, mounted within the instrument, would then be necessary to design the calibrated scale mounted on the anvil casing. The plenum chamber upstream of the orifice will generally cause smaller coefficients than those calculated. It is noted that Δp across the orifice, as calculated by equation 21, Appendix I, is only 3.35 psi, well within the pressure-deflection characteristics of many commercially available diaphragm capsules. This satisfies specification 1.

Specification 3 calls for the attachment of the linkage to the orifice plate in such a way as not to disturb the upstream flow and not to be subject to fatigue failure. These conditions require, first, that the linkage not be located on the centerline of the orifice, and second, that the linkage not be anchored by a soldered butt joint which might experience fatigue failure. The use of solder in making the joint is also questionable because the orifice plate may become unsoldered to the upper diaphragm in the joining process. Fabrication of the linkage to the orifice plate before joining the latter to the diaphragm capsule is thought to be unwise as orientation problems might arise when assembling the capsule to the instrument casing. Therefore, a mechanical joint, tacked with an epoxy resin, is indicated. A .020" stainless steel wire, chosen for its stiffness and nonmagnetic properties, is formed to spring fit into a cylindrical internal groove on the periphery of the orifice plate. The other end of the wire fits into a bracket which slides on the magnet to allow adjustment of the zero point and/or the leverage ratio. The bracket is then glued to the magnet, leaving that end of the linkage to pivot about a fixed point. Elastic preload of the wire takes out any backlash existing between the magnet and its pivot.

The Diaphragm Capsule Design

The design of the diaphragm capsule, the center pad of which is the orifice plate, is quite complicated. Its design is somewhat like that of a mechanical spring, only with a great many more variables

to affect the performance. There are five principal characteristics which have importance, and any changes affecting one often affect others:

1. The pressure constant
2. The safe pressure or deflection
3. The linearity of the pressure deflection curve
4. The energy available
5. The temperature effects.

Some general comments can be made concerning diaphragm materials, diaphragm configurations, and the assembly of diaphragm capsules. The modulus of elasticity of a material has a direct effect on the stiffness of the diaphragm and, therefore, on the pressure and force constants. The hardness of a material affects manufacture and performance. If the material is too hard, it cannot be formed without fracturing; if it is too soft, it will form easily, but the resulting diaphragm will have high hysteresis and drift. Figure 40 of reference 1 determines the pressure and deflection for various percentages of hysteresis for several materials. From this curve the available energy per square inch of effective diaphragm area can be derived, showing beryllium copper, for example, to have 80 times more available energy than stainless steel. The thickness of material affects the pressure and force constants, the linearity of deflection, hysteresis, and available energy.

Diaphragm configurations are quite varied, but, generally, the effective area determines the pressure constant. The pad

diameter and gap width, between the pad and the periphery, affect the pressure and force constants, the effective area, linearity, and available energy. Large pad diameters usually produce nonlinearity with large deflections. The gap width is corrugated to reduce or eliminate nonlinearities in a given deflection range. Usually these corrugations are in the form of single arcs of a circle, with the high pressure applied to the concave side. The number of corrugations and their depth can be traded off to produce the desired linearity.

Diaphragm capsule assembly involves connection of the peripheries of the diaphragms by any of several methods. Joints may be telescoped, flanged, nested, or grooved. The type of solder used and the technique of application greatly affect hysteresis and drift because of the stiffening contribution to the outer edge. Pulsation and baking can be used along with natural aging to reduce hysteresis and drift after assembly.

Most of the useful equations for diaphragm design are empirical, and assembly and testing of capsules require specialized equipment and technology. Since capsules are produced commercially, for such instruments as altimeters and barometers, it was decided to purchase one for this flow meter design which would meet the following specifications:

1. Maximum differential pressure = 5 psi
2. Approximate 2" diameter
3. ± 0.10 " linear deflection (to allow for sufficient rotation of magnet)

4. Suitable mounting fitting in lower diaphragm
5. Approximately 1/2" center pad diameter (to allow for the orifice).

The Throttling Valve Design

The design of the throttling valve meets two requirements:

1. Location must be downstream of the orifice plate so that the orifice plate always sees constant upstream pressure.
2. The throttling valve must provide back pressure protection for the instrument; that is, it must protect the calibration against fluctuations of downstream pressure.

Condition (1) is easily met by designing the throttling valve into the diaphragm chamber casing downstream of the orifice, as shown in the instrument schematic, Figure 1. Condition (2) is satisfied by making use of the fact that the discharge of a gas from an orifice will increase as the downstream pressure decreases, reaching a maximum when the velocity at the throat equals sonic velocity. Any further reduction in downstream pressure will not increase the flow rate, nor will any downstream pressure fluctuation be seen upstream of the orifice because of the shock wave formed. Equation 13 of Appendix I states that sonic flow occurs when $\frac{P}{P_1} \leq 0.528$. Therefore, designing the valve to provide sonic velocity at the maximum

instrument flow rate of 15 lpm protects the diaphragm capsule against downstream back pressures up to 34.1 psia. The valve diameter is chosen so that the pressure drop over the valve is 27.25 psi, allowing the desired 3.35 psi drop over the diaphragm capsule. The diameter must also be large enough to allow calibration of the orifice plate after assembly to the casing by passing a reamer through the valve seat. This requires the valve to be designed with a constant area plug fitting inside the valve seat.

Diaphragm Capsule Chamber Casing and Anvil Casing Design

The diaphragm capsule casing is designed to contain the diaphragm capsule and the throttling valve, and to hold a seal with the anvil casing. Since the flow into the orifice must be axi-symmetrical for proper instrument calibration, this casing is also designed to eliminate swirl of the inlet flow by inserting it into the chamber where the diaphragm capsule itself acts as a baffle. Both casings are designed with an eye towards easy assembly and adjustment of adjacent parts.

Some mention should be made of the sealing of the diaphragm capsule chamber to the anvil casing. Any relative motion between the two brass die castings would appear to the magnet as direct diaphragm movement because of the nearly-straight linkage between them. Therefore, care was taken in the design of the sealing arrangement so that no possible relative movement could exist. A first attempt was made to latch down the transparent top cap by means of the same sealing clamp. This idea was later discarded because the top cap might be

removed after calibration of the instrument to adjust the pointer or counter, releasing the seal of the capsule chamber, which could necessitate recalibration. In the present design, the top cap is screwed to the anvil casing, while six other machine screws hold the chamber seal.

CHAPTER IV

MAGNETIC CROSSOVER ASSEMBLY SECTION

The purpose of this section of the instrument is to take lineal motion from the diaphragm capsule, to transmit it through the hermetically sealed magnet support chamber wall, and to produce a rotation proportional to the flow rate. These ends are achieved by the use of a tilted iron ring mounted to rotate freely about an axis orthogonal to the axis of rotation of the permanent magnet which is linked within the chamber to the diaphragm capsule. The angular displacement of the tilted ring will be shown to be proportional to the square root of the arc of magnet excursion, which, in turn, is proportional to the deflection of the diaphragm capsule, resulting from the pressure differential across it.

Theoretical Considerations

1. Determination of the Flux Path

For a singly excited magnetic system it is well known that forces, due to magnetic flux, are established which tend to move mechanical parts towards the configuration of minimum energy stored in the field, or the position of minimum reluctance.

Since reluctance is determined by

$$R = \frac{l}{\mu A} \quad , \quad \text{ampere-turns/weber,}$$

and the resulting force is determined by

$$F = -\frac{1}{2} \varphi^2 \frac{dR}{d\ell}$$

where ℓ = length of the flux path
 μ = magnetic permeability
 A = cross sectional area of the flux path
 φ = magnetic flux in the air gap,

the length of the flux path will be minimized for any particular mechanical configuration, and this minimization will certainly occur in the air gap if the adjacent mechanical configuration is rigid. By designing a magnetic circuit where the air gap is variable, the developed torque will drive a properly mounted tilted ring to seek a position of minimum air gap.

Now consider this torque acting upon the ring of Figure 3, tilted at an angle, σ , to the horizontal equatorial plane of diameter d and pinned at points E and G , where $F = \frac{T}{d}$. If the magnetic force is applied perpendicularly to the tilted ring at point A , components will exist in both the x - and y -directions, and the subsequent torque about the z -axis will rotate the ring an angular amount to conform to the position of minimum reluctance of the ring with respect to the permanent magnet within the chamber. If, however, the magnetic force acts at point B , the position of maximum tilt from the horizontal equatorial plane, no resultant torque about the z -axis will exist because there is no force in the x -direction, as shown in Figures 4 and 5. At position B ,

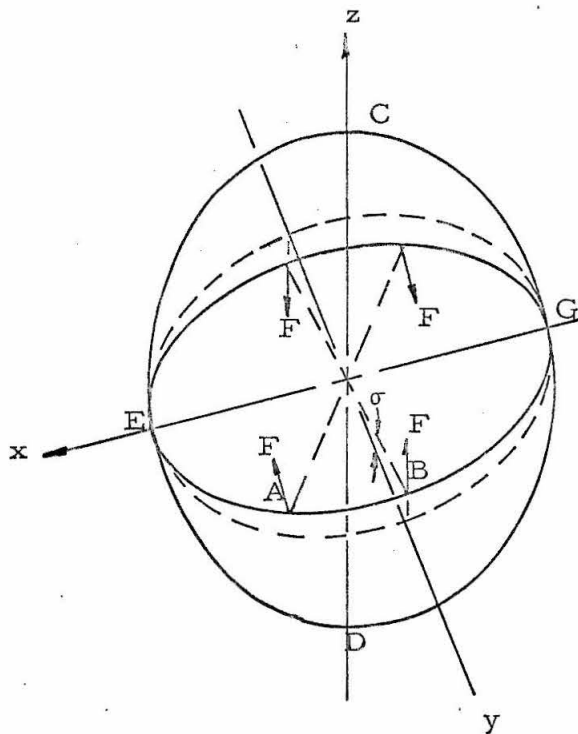


Fig. 3. Torque Analysis of the Tilted Ring.
(The horizontal equatorial plane is shown dotted.)

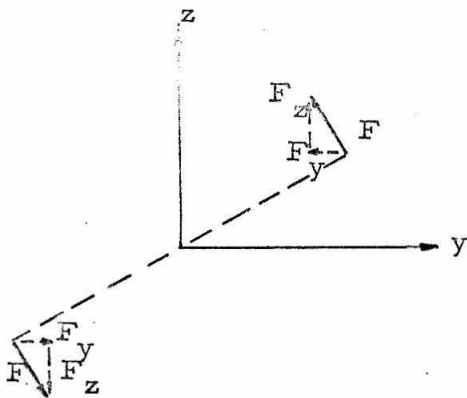


Fig. 4. Torque Analysis of the Tilted Ring. Forces acting on the ring at point A cause rotation about z axis. (F_x is developed perpendicular to the page.)

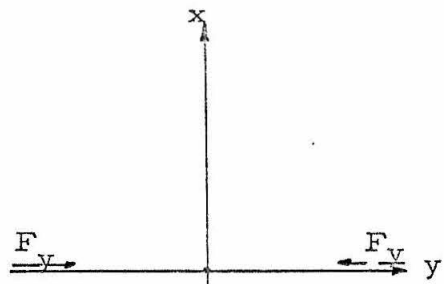


Fig. 5. Torque Analysis of the Tilted Ring. Forces acting on the ring at point B cause no resultant torque about z axis.

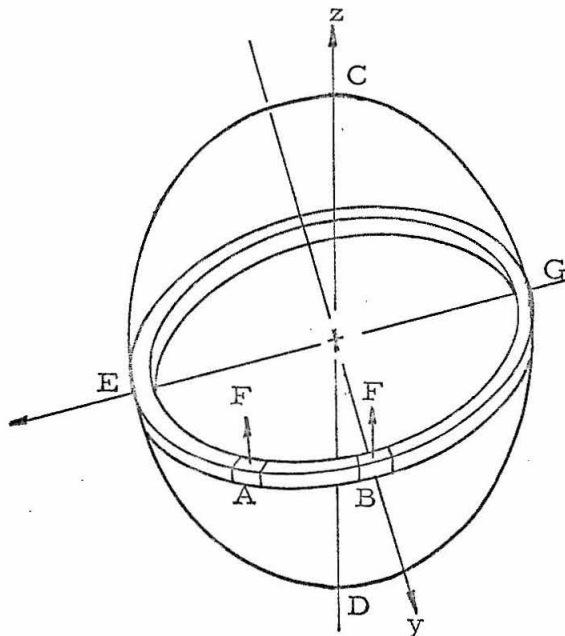


Fig. 6. Torque Analysis of the Tilted Ring.

incremental angular motion could occur clockwise or counterclockwise unpredictably. This fact must be borne in mind when designing the tilted ring and support frame so as to avoid this location within the angular limits of their rotation.

Another way of considering this phenomenon is to look at the degree of tilt from the vertical, or z-axis, of an incremental segment of the ring. As shown in Figure 6, any force perpendicular to the ring at point A must give rise to a component acting in such a direction as to rotate the ring. However, at position B, the incremental segment of the ring is virtually horizontal, and a force perpendicular to it at that point can give no rotation about the z-axis, but only a torque about the x-axis, which must be absorbed by the bearings of the support frame at C and D.

2. Tilted Ring Calculations

It is obvious that some tilt must be given to the ring so that a variable air gap can be developed. The next question to be answered is how much tilt should be provided so that sufficient angular output is realized for the limits of angular excursion of the permanent magnet. It would also be helpful if the angular rotation of the ring versus the indicated flow rate were linear so as to aid in the calibration of the instrument scale. This property is mandatory if a stepwise integration of flow is to be made by referring to the angular location of the pointer from a known zero position.

The configuration of the tilted ring is again presented in Figure 7 with arcs a and b of two vertical equatorial planes inter-

secting the tilted ring perpendicularly at point A and obliquely at point B, forming a right-spherical triangle, ABC, with respective included angles α , β , γ . An orthogonal view of this triangle is presented for clarity in Figure 8.

By Napier's rules for right spherical triangles,

$$\cos \gamma = \cot a \tan b$$

where the angle of ring tilt $\sigma = 90^\circ - b$, or

$$\cos \gamma = \cot a \cot \sigma .$$

Therefore, the angle of rotation of the tilted ring and its support frame is directly proportional to the angle of tilt and the arc length, in an equatorial plane, from the spherical apex to successive positions of minimum air gap between the ring and the magnet within the chamber. By holding fixed various angles of tilt, σ , and varying the arc length, a , the resulting angular displacement, γ , can be calculated. Since the magnet rotates through an arc length $a-b$, which is directly proportional to the pressure differential, Δp , over the diaphragm capsule, it is handier to plot the results for γ versus that parameter on a logarithmic scale as shown in Figure 9. Figure 10 shows an expanded scale for magnet excursion angles of $1-10^\circ$. (The calculations for these curves are presented in Appendix III.) Table I, developed from Figures 9 and 10, shows an interesting result, namely, that the tilted ring rotation angle, γ , is proportional to the square root of the magnet excursion angle, $a-b$, for angles of tilt between 15° and 45° for a large range of γ . Since flow rate is proportional to the square root of the pressure differential

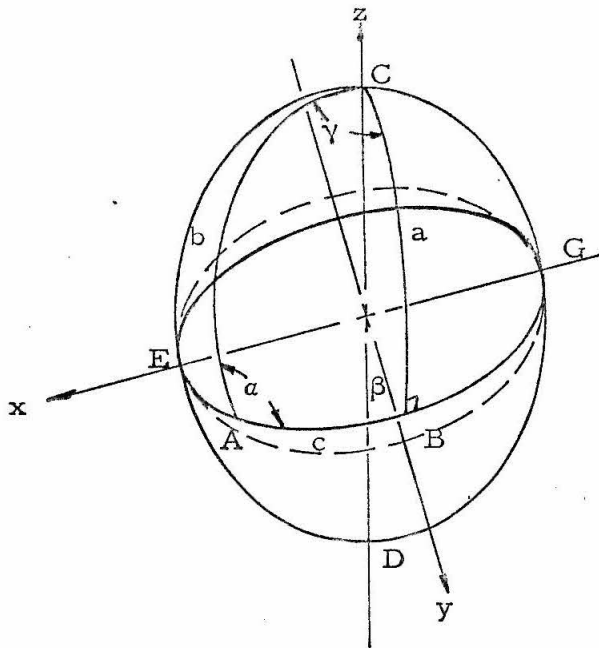


Fig. 7. Geometrical Configuration of the Tilted Ring within the Sphere. (The horizontal equatorial plane is shown dotted.)

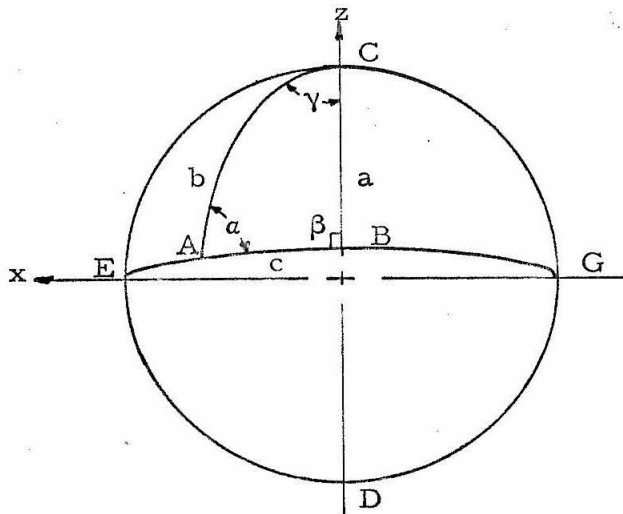


Fig. 8. Orthogonal Projection of the Spherical Triangle ABC .

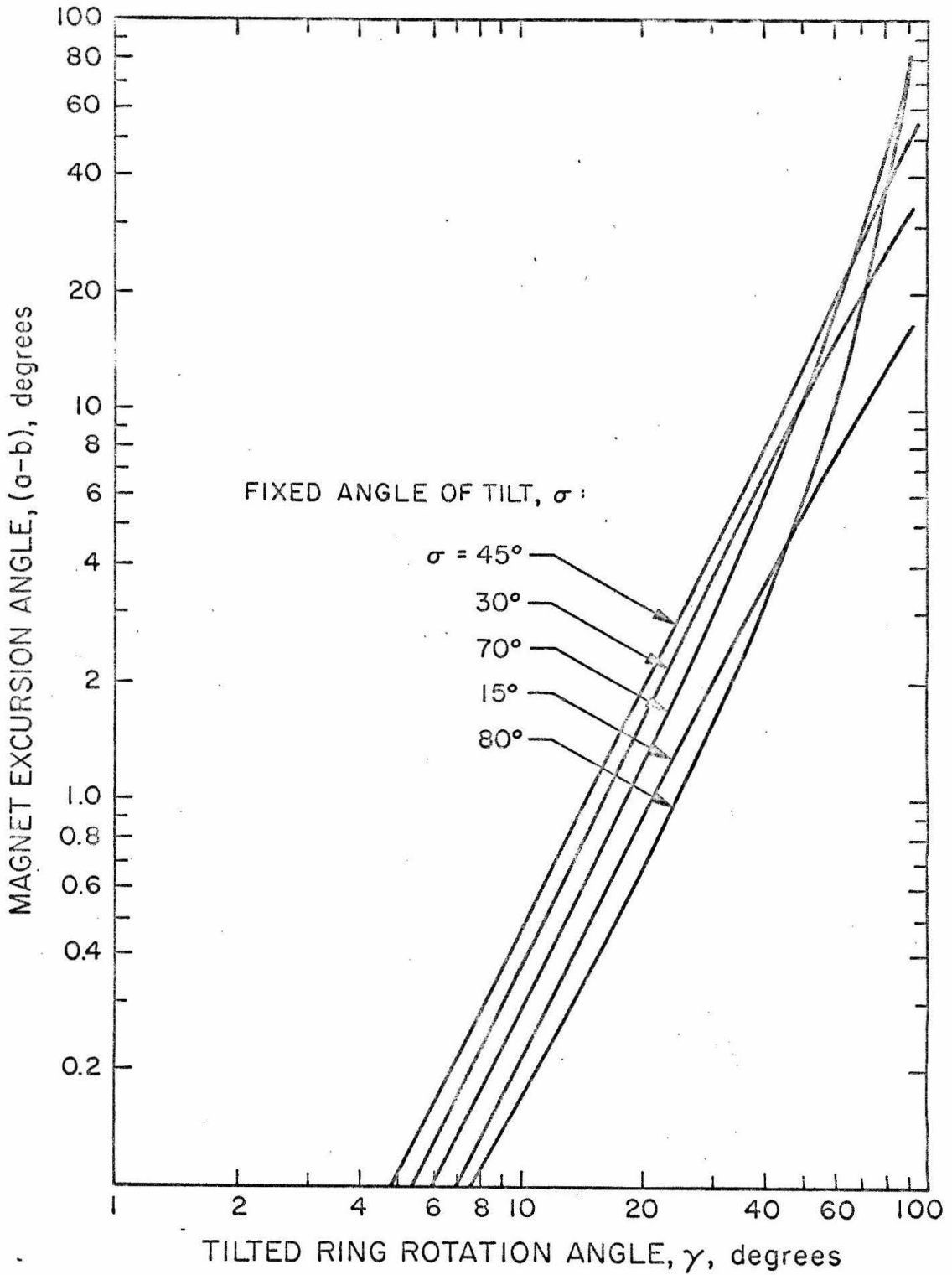


Fig. 9. Plot of Magnet Excursion versus Tilted Ring Rotation.

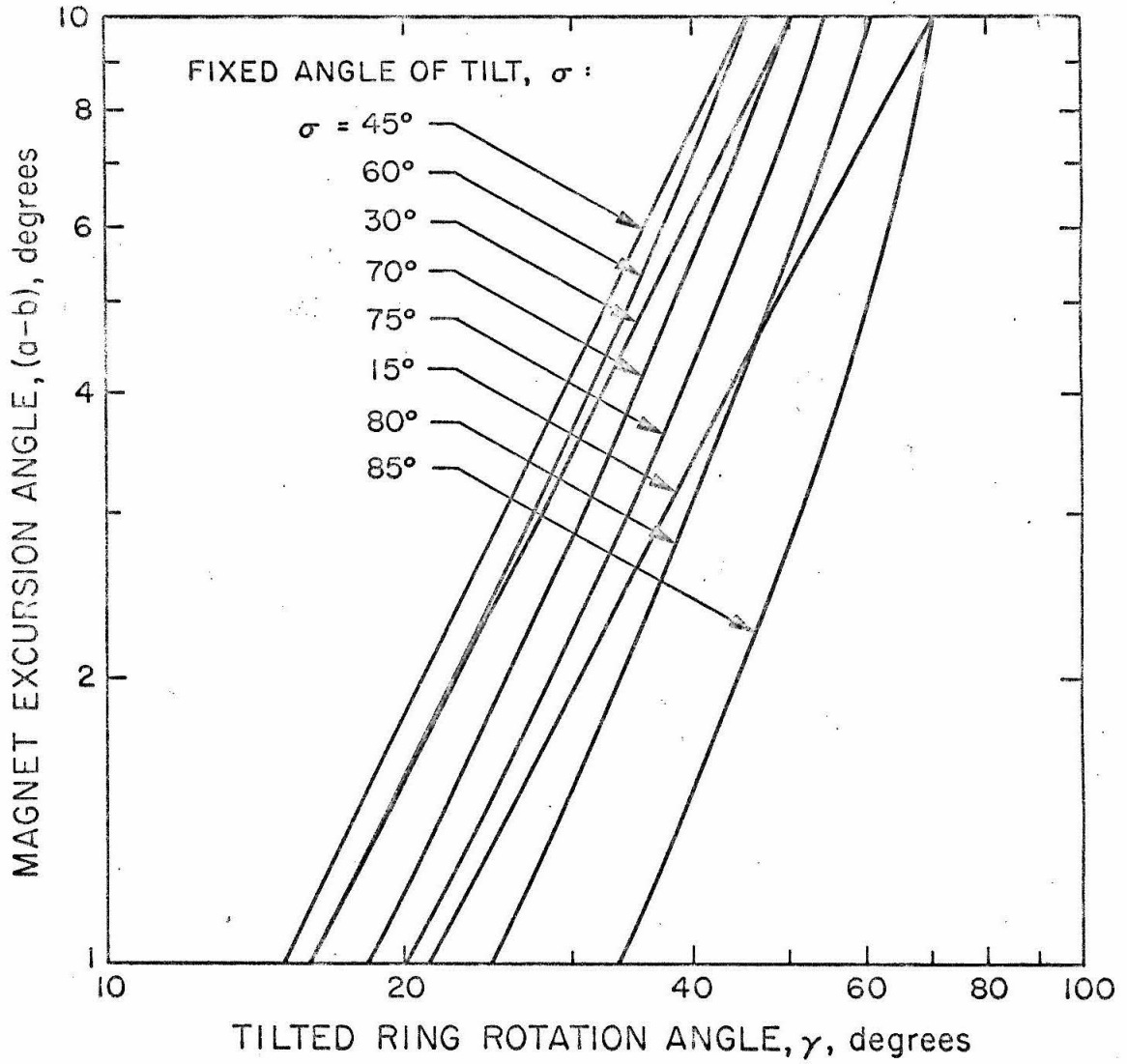


Fig. 10. Expanded View of Fig. 9 for Magnet Excursions between One and Ten Degrees.

across an orifice, by equation 20 of Appendix I, it is also proportional to γ .

Table I

ring tilt, σ	linear range of ring rotation angle, γ	slope, $\frac{\Delta(a-b)}{\Delta \gamma}$
15	7-49°	1.9797
30	5-50°	2.0594
45	4-55°	2.0145
60	5-28°	2.0778
70	6-30°	2.1543
75	6-30°	2.0778
80	7-25°	1.8887
85	10-45°	2.5517

$$\text{For } 15^\circ < \sigma < 45^\circ, \frac{\log \gamma_2 - \log \gamma_1}{\log (a_2-b) - \log (a_1-b)} \approx 0.5$$

$$\text{Therefore } \log\left(\frac{\gamma_2}{\gamma_1}\right) = \log\left(\frac{a_2-b}{a_1-b}\right)^{0.5},$$

$$\text{or } \gamma_2 = \frac{\gamma_1}{\sqrt{a_1-b}} \sqrt{a_2-b} = k \sqrt{a_2-b} .$$

Intersections of the curves with the tilted ring rotation angle axis determine k , the magnification or scaling factor.

For

$$\begin{aligned} \sigma &= 15^\circ & k &= 23.0 \\ \sigma &= 30^\circ & k &= 17.5 \\ \sigma &= 45^\circ & k &= 15.0 \end{aligned}$$

Essentially, then, a mechanism has been devised which will not only transmit information through a hermetically sealed chamber, but it will also magnify that information linearly and extract its square root. As used in this instrument, the angular displacement of the tilted ring indicates flow rate. The linear scale permits step-wise time integration of total flow.

Design of the Magnetic Crossover Assembly

The form of the magnetic crossover assembly will now be described. As shown in Figure 11, the permanent magnet is supported within the chamber by a horizontal pin, mounted at an angle of 30° to the horizontal when the diaphragm capsule is unstrained by a pressure differential across it. The crossover ring, which is also tilted at an angle of 30° with the horizontal, is mounted in a support bracket pivoted to the exterior face of the chamber. As the magnet excursion changes, the crossover ring and support frame rotate to keep the air gap at a minimum, thereby rotating the pointer mounted on the support frame, which gives an indication of the flow rate through the orifice.

To avoid that point on the ring of ambiguous direction of rotation, the ring is oriented in assembly through a γ of 22° , corresponding to an (a-b) excursion of 2° , and restrained from returning to the point of minimum reluctance for the zero flow rate condition. This suppression of the indicating scale does not allow instrument accuracy below 3 lpm, but is necessary for proper

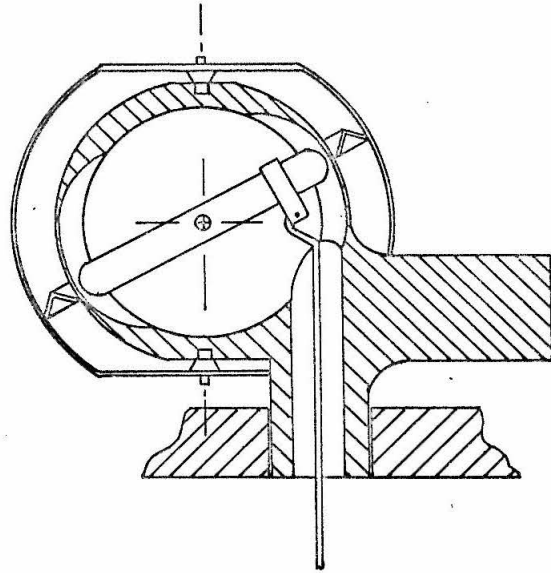


Fig. 11. The Magnetic Crossover Assembly.
(Scale = twice full size)

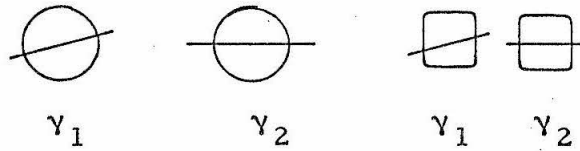


Fig. 12. Comparison of the Configurational Aspects
of the Tilted Ring to the Magnet for Circular
and Square Cross Sections.

design use of the curves in Figures 9 and 10.

Although any angle of tilt for the crossover ring between 15° and 45° would provide a rotational output approximately proportional to the square root of the magnet excursion angle, as shown by Table I, the angle 30° was chosen as it provides an adequate range of oscillation for the magnet and does not cause excessive nonlinearities to develop due to bending of the linkage pivoted at the magnet but rigidly joined to the bellows.

Alnico V was chosen as material for the magnet because of its high coercive intensity, which is about 870 ampere-turns per inch, almost twice that of 36% cobalt steel. Because of its higher maximum available energy, an Alnico V magnet can be designed with smaller volume than another magnet material for a given amount of energy in the air gap. It is also very stable as regards decrease in magnetization due to vibration, superposed alternating fields, or high temperatures. Although relatively weak and brittle, a cast or sintered Alnico V magnet can be ground to size and elox drilled. For production quantities, the magnet would either have necessary holes cored into the casting, or soft steel inserts cast in for further machining. The magnet cross-section is necessarily a body of revolution about its longitudinal axis, perpendicular to its pivot axis, so that the configuration seen by the tilted ring is constant for all γ . This aspect would not remain constant if the magnet cross-section were square, for example, as shown in Figure 12. The flux path

dimensions are obviously altered for the square cross-section, while the configuration remains the same for the circular cross-section.

The design and construction of the chamber, the crossover-ring, and the crossover-ring support frame show compromise between precise tolerances where necessary and concessions made for production machining and easy assembly of the components. Tolerances on the magnet length, magnet location within the chamber, the crossover ring, and its relation to the chamber, as determined by the pivots of the support frame, are held quite closely because any air gap variations directly affect the reluctance of the flux path and, therefore, the accuracy, or resolution of the instrument. The chamber design features a .002" "skin" in the pathway of the magnet rotation arc, requiring a fine-grained material such as tobin brass to insure that the special milling cutter does not gouge through the section. Brass is also non-magnetic and possesses the necessary strength to withstand 50 psig line pressure within the chamber despite the thin walled section.

The crossover ring is designed of a soft, ferro-magnetic steel, .005" in cross section and creased for strength. A swiss-die set, shown in Figure 13, was designed to maintain close tolerances and to allow for accurate reproduction of this component. The crossover ring is joined to its support frame by melted polyanide cement applied at 200°F.



Fig. 13. Swiss-Die Set Used in the Fabrication of the Tilted Ring.

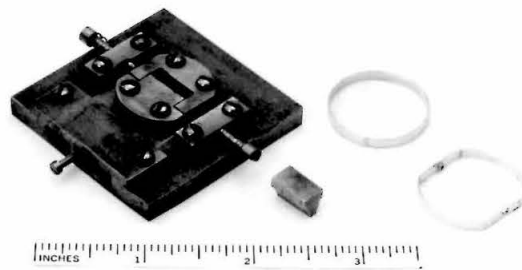


Fig. 14. Stretch Former Used in the Fabrication of the Support Frame of the Tilted Ring.

The crossover ring support is designed of non-magnetic, light weight aluminum, stretch-formed to shape for rigidity and close tolerance by another die set, shown in Figure 14. The pivot bearings are punched into the frame, and the pivot holes pierced through in the same die set. Jewelled bearings were considered for the pivots, but it was later felt that this added expense was unnecessary because only small oscillations of the tilted ring and its support frame occur. For hospital application, breathing flow rates are normally set and maintained without alteration. Aluminum against brass provides suitable bearing surfaces for these conditions.

It should be noticed that the magnetic crossover assembly adds several calibration features to the instrument. The variation in ring tilt, kinking the linkage to the magnet to alter its length, varying the connection point of the linkage on the magnet, and bending the flow rate pointer, all provide suitable methods of adjusting the linearity during different stages of assembly. Overall calibration of the instrument is made, however, by varying slightly the diameter of the orifice by reaming through the valve port after assembly. Suppression of the scale zero is necessary because zero flow rate can only be indicated by that position on the tilted ring which offers an ambiguous direction of subsequent rotation. The zero set adjustment, however, is not necessarily critical since calibration can be made at mid-scale where, due to the parabolic shape of the response curve, an error in zero setting causes a much smaller corresponding error for higher flow rates, which is clearly shown by Figure 15.

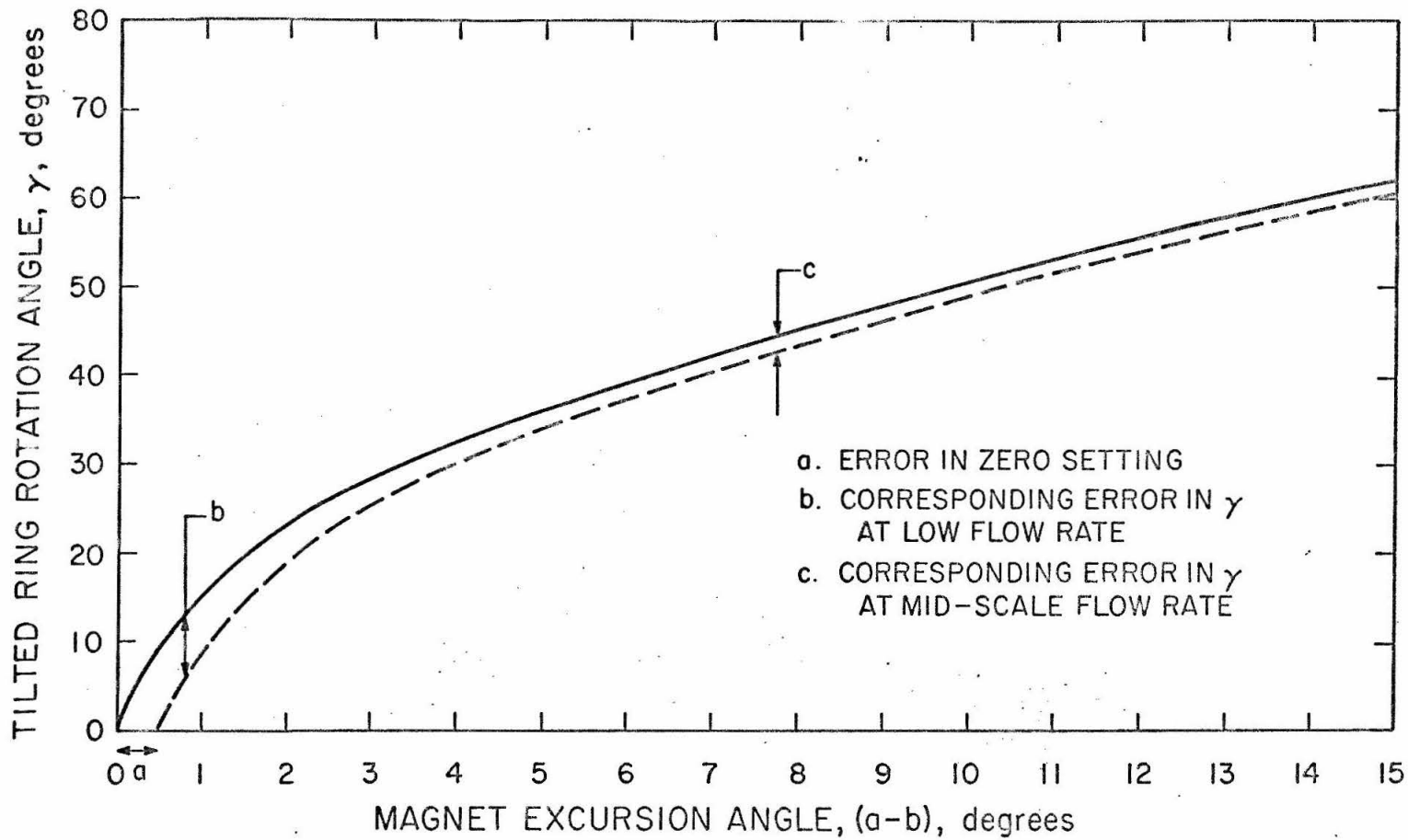


Fig. 15. Plot of Magnet Excursion Versus Tilted Ring Rotation, for $\sigma = 30^\circ$, Showing Comparison of Flow Rate Errors Developed by an Error in Zero-Setting of the Instrument.

CHAPTER V

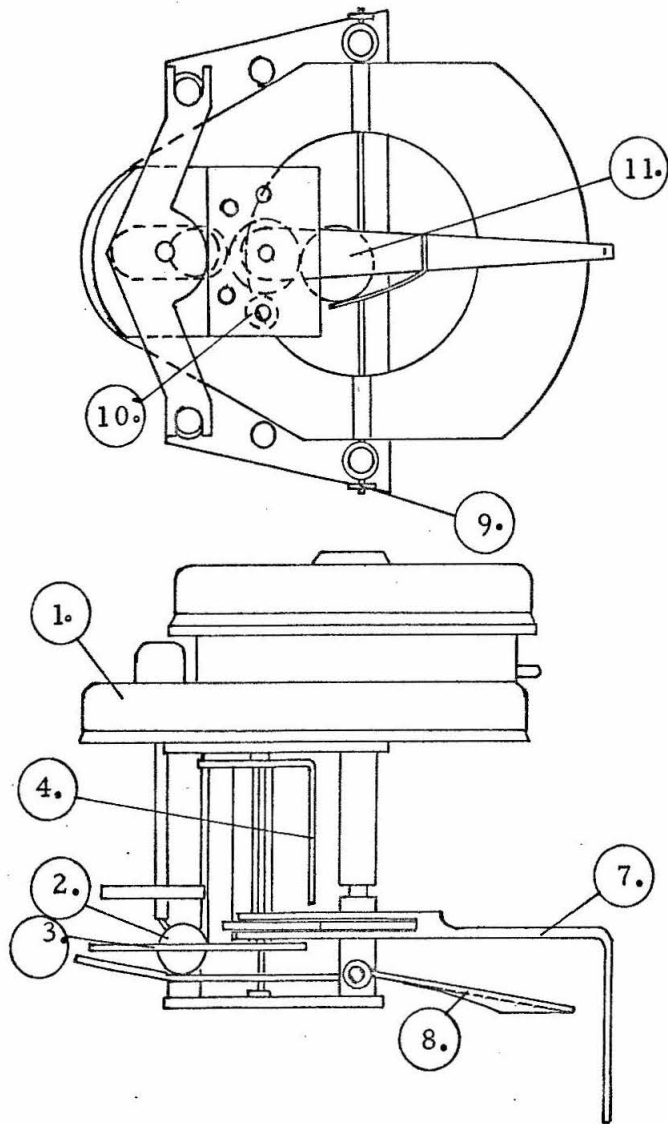
FLOW TOTALIZER ASSEMBLY SECTION

The purpose of the flow totalizer assembly is to provide an accurate count of the total number of liters of oxygen that have passed through the instrument. The indication of flow rate on the linearly calibrated anvil by the pointer, connected to the tilted-ring support frame, has already been described. The angular location of this pointer from a known zero point also permits stepwise time integration of the amount of through flow, i. e., the angular distance from true scale zero is directly related to the number of liters flowing through the orifice in a discrete length of time. Similar to other methods discussed in Chapter I, the magnetic crossover assembly produces insufficient power to accurately drive a mechanical counter; consequently, an auxiliary power source is necessary. The pertinent feature of this section of the instrument is, therefore, the design of a mechanism whereby the counter is driven only as much as is indicated by the position of the crossover assembly pointer.

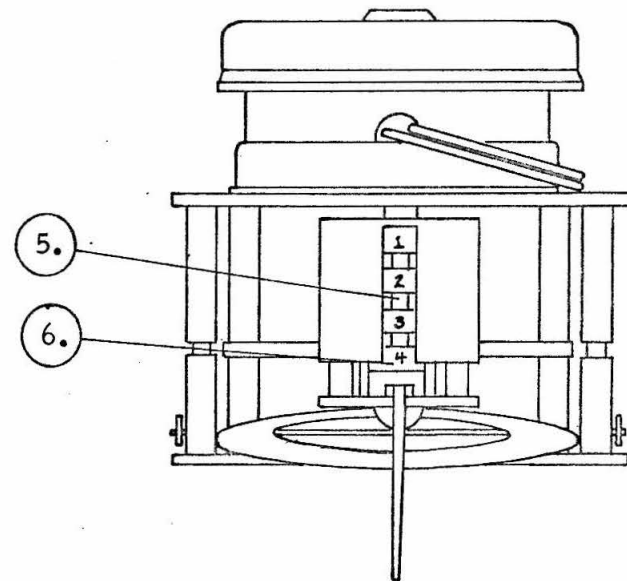
Operation of the Totalizer

A 110 volt, 60 cps, synchronous, AC timing motor provides a reliable method of driving a counter at a constant speed. Mounted atop the assembly, Figure 16, a Hayden gear motor (1), picked for its small size, rotates a crank, on which is mounted a ball cam (2)

Fig. 16. The Flow Totalizer Assembly.



1. gear motor
2. ball cam
3. counter housing baseplate
4. counter housing
5. counter disks
6. lowest counter disk
7. counter drive
8. clamp
9. hair spring
10. pawl
11. overrunning clutch



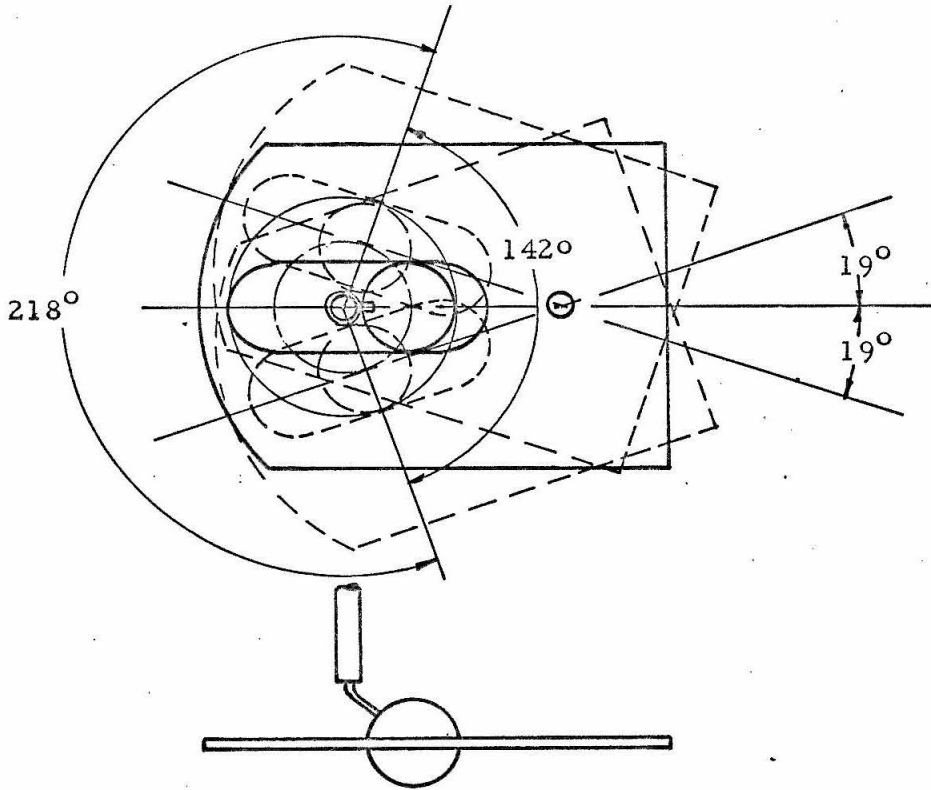


Fig. 17. Diagram of Quick-Return Mechanism. The ball crank rotates at a constant speed of 1 rpm producing 38° of scan for the slotted baseplate to the counter housing. The ratio of scan time to return time, determined by the length of the crank, is $142^\circ/218^\circ = 0.65$.

which travels in the slotted base plate of the counter housing (3) at 1 rpm. The slot is so designed as to provide a quick-return scan for the counter housing (4) of 40 degrees of the calibrated anvil, as explained by Figure 17. A slow scan rate is possible because the instrument is protected from any fluctuations in back pressure by the throttling valve; therefore, few changes in the indicating level will be experienced.

The motor is allowed to run continuously, driving the counter housing which contains the four counter disks (5). By stopping the lowest counter disk (6) with respect to the rotating housing, a count is put into the meter. This counter disk is stopped by linking it to the counter drive (7) which strikes the end of the crossover assembly pointer. To keep the pointer from moving on impact, a clamp (8) is held against it on the calibrated anvil for one-half cycle of the counter housing by two torsion springs (9), and is then released when the ball cam begins the quick return portion of its cycle. The other counter disks are actuated by pawls (10) driven in step by the lower counter disk in typical odometer operation.

An overrunning friction clutch (11), built into the counter drive, engages so that while the housing and other counter disks continue their rotation, the counter drive and lower counter disk remain stationary. As the scan reverses, however, the clutch slips so that the counter drive and the lower counter disk rotate along with the housing. Counter drive alignment with the housing is achieved at the end of the cycle by pin-stopping it against the casing. No further

count is put into the meter until the rotation again reverses, and the counter drive seeks out the position of the crossover assembly pointer on the anvil.

The motor fulfills another important function that has not heretofore been mentioned. Due to its 60 cps operation, slight vibrations are set up in the entire casing which help to reduce the friction coefficients in all pins and bearings, thereby increasing the accuracy of the instrument. This is just one more added convenience in using readily available AC power.

The totalizer assembly must be aligned in the instrument so that the counter shaft, on which the counter drive is mounted, has the same axis of rotation as the crossover frame assembly, on which the flow rate pointer is mounted. This permits both parts to use the same angular scale on the anvil.

Brass is used for the ball cam, the slotted base plate to the counter housing, and the clamp, because of the relative wear these parts endure with no forced lubrication. Brass and aluminum are also used elsewhere in the assembly because of their workability and non-magnetic properties. The counter disks and pawls are made of delrin and purchased commercially from Veeder-Root.

CHAPTER VI

INSTRUMENT EVALUATION

From the full scale design layout, Figure 1, a complete detail drawing was prepared for each component of the instrument. These drawings, located in Appendix IV, are up to date with respect to all design changes made and represent the instrument in its present form. The flow meter was evaluated during and after assembly with emphasis placed on determining the accuracy of the crossover ring assembly in indicating flow rate and the success of the orifice-drilled diaphragm capsule in actuating the magnet. The findings of these tests will now be presented.

Test of the Magnetic Crossover Assembly

A depth micrometer was attached to the magnet in such a way that the geometry between the attachment position and the location of the magnet pivot allowed accurate determination of the magnet excursion angle. By varying the micrometer setting, the magnet would rotate through a defined angle and a corresponding rotation of the tilted ring would be observed and measured. Figure 18 shows the result of this test, which illustrates that there is a definite relation existing between the magnet excursion angle, (a-b), and the tilted ring rotation angle, γ . The discrepancy between the theoretical and experimental curves may be attributed, in part, to the following prototype deficiencies:

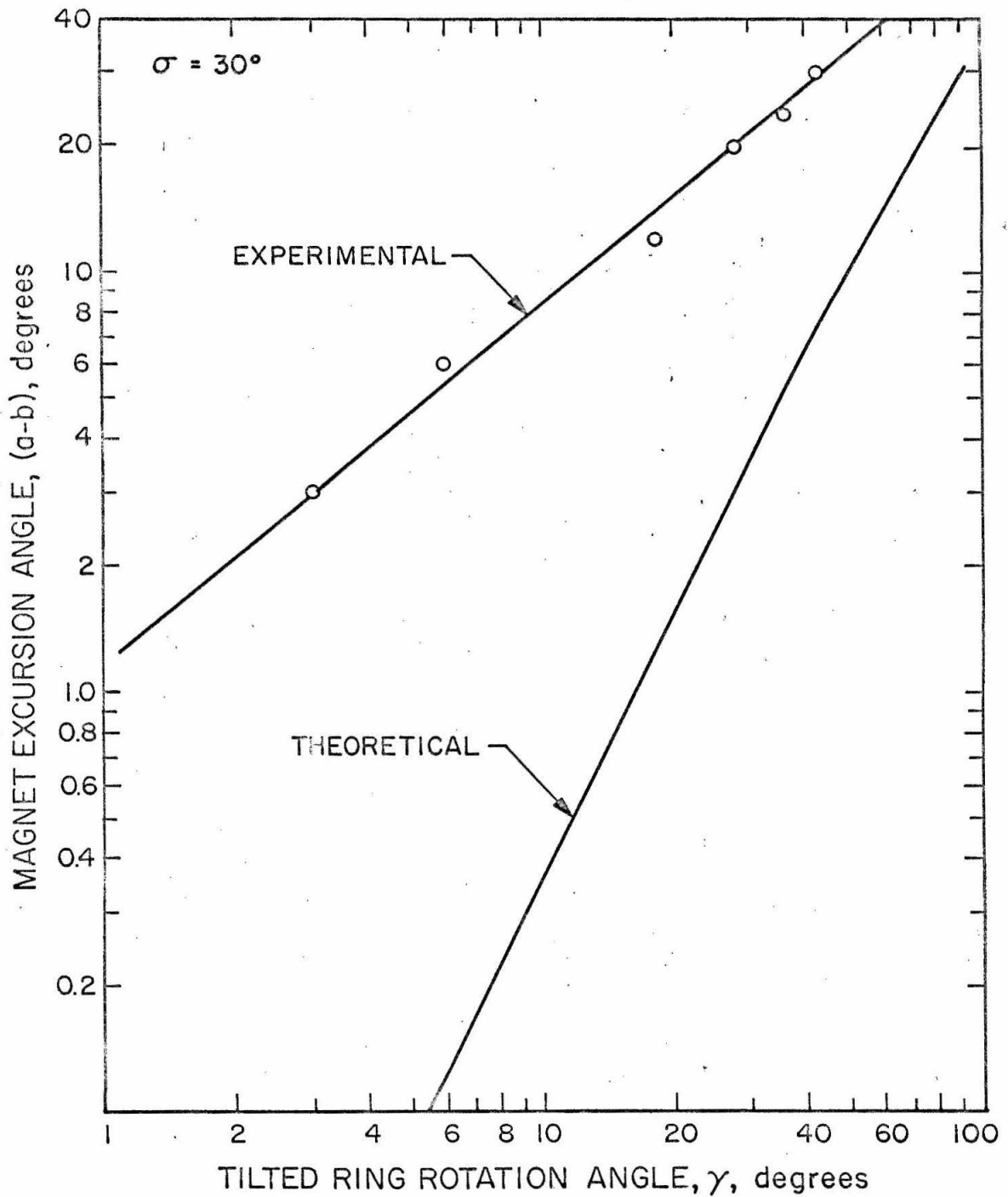


Fig. 18. Comparison of Theoretical and Experimental Results for Tilted Ring Rotation as a Function of Magnet Excursion.

1. The prototype tilted ring does not lie in an equatorial plane due to inaccurate location within the support frame. Sophisticated assembly jiggling will be necessary to properly locate the ring in the frame before gluing. Further experimentation with the cross-sectional configuration of the ring is also deemed necessary so that this component will not only provide the response required of the crossover assembly, but also can be blanked and handled without unreasonable fear of warpage.

2. Excess friction exists between the formed bearing surfaces of the support frame and the surfaces of the magnet chamber near the pivots. A redesign of the support frame may be necessary to facilitate easier assembly, eliminating the raising of burrs on these surfaces. The method of press fitting the pivots into the magnet chamber might be altered, and smaller diameter pins could be used. At the least, care must be taken to avoid scratching the bearing surfaces, even if this means using thin mylar washers for protection.

3. A further zero adjustment is needed to aid in the calibration of this assembly. Setting the zero magnet excursion angle accurately by means of a depth micrometer alone is a very laborious process which could be made easier by designing such an adjustment into the magnet chamber and/or the linkage.

Overall Test of the Instrument

The final instrument calibration has been delayed due to the abnormally long lead time required to procure the diaphragm capsule specified in Chapter III. The test procedure, however, has been established and a test run was made using, instead, an installed diaphragm capsule with insufficient stroke to rotate the magnet more than ten degrees. The tilted ring did respond to changes in flow rate, but no full-scale calibration could be made. The stepwise integrator performed as designed.

As shown in Figure 19, air passes through the flow meter and displaces water from the reservoir to a weighing tank. The weight of water collected in a specific time period is directly related to the flow of gas through the instrument in liters per minute.

Conclusions

1. The concept of passing information through a hermetically sealed wall by rotating a ring according to a monotonic function of the excursion of a magnet, mounted within the sealed chamber, has been explored and shown to be useful.

2. The flow meter design has been partially successful because all the components were built according to detailed drawings, and the instrument assembled as expected. The tooling for the ring and its support frame adequately provided prototype parts. Every indication points towards future success in calibrating the instrument when proper assembly jigging is devised and the specified diaphragm capsule is located.

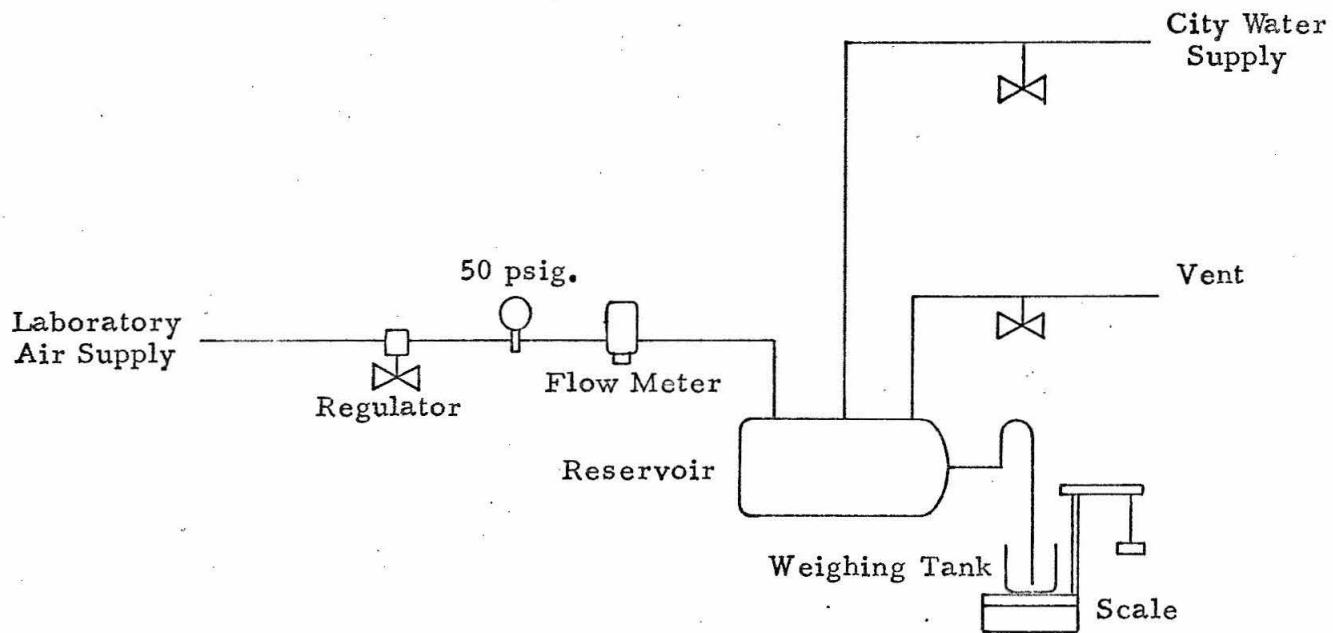


Fig. 19. Schematic Diagram of Flow Meter Calibration Equipment.

3. It should be noted that many outputs besides the square root of the magnet excursion could be obtained by altering the configuration of the high permeability component suspended exterior to the chamber. For example, if a helix is used, instead of a ring, a completely different response would be realized as it rotates to seek the point of minimum reluctance with the pivoted magnet. Care must be taken, however, to fabricate any such component so that the inside diameter tolerance is quite small and no warpage exists to destroy the desired instrument resolution.

APPENDIX I

ISENTROPIC GAS LAWS FOR ORIFICE FLOW

Frictionless, adiabatic, or isentropic, flow is an ideal that cannot be reached by flow of real gases, but it is approached, however, in flow through transitions where friction effects are minor owing to short distances traveled, and minor heat transfer losses because the changes that a particle undergoes are slow enough to keep the velocity and temperature gradients small.¹

For isentropic flow,

$$p = p_1 \rho_1^{-k} \rho^k \quad (1)$$

where k = ratio of the specific heats of the fluid

p_1 = reservoir pressure

ρ_1 = reservoir density

p = pressure at any other point

ρ = density at any other point

differentiating,

$$dp = k p_1 \frac{\rho^{k-1}}{p_1^k} d\rho \quad (2)$$

typing error

From Euler's equation

$$VdV + \frac{dp}{\rho} = 0 \quad (3)$$

¹H. W. Liepmann and A. Roshko, "Elements of Gas Dynamics", John Wiley & Sons, Inc., New York, 1957, p. 51.

where V = velocity of the fluid. Substituting and integrating,

$$\frac{V^2}{2} + \frac{k}{k-1} \frac{P_1}{\rho_1^k} \rho^{k-1} = \text{constant} \quad (4)$$

or

$$\frac{V_1^2}{2} + \frac{k}{k-1} \frac{P_1}{\rho_1^k} = \frac{V_2^2}{2} + \frac{k}{k-1} \frac{P_2}{\rho_2^k} \quad (5)$$

Combining with the perfect gas law,

$$p = \rho RT, \quad (6)$$

$$\frac{V_1^2}{2} + \frac{k}{k-1} RT_1 = \frac{V_2^2}{2} + \frac{k}{k-1} RT_2 \quad (7)$$

For adiabatic flow from a reservoir where conditions are given by P_1, ρ_1, T_1 , at any other section

$$\frac{V^2}{2} = \frac{kR}{k-1} (T_1 - T) \quad (8)$$

In terms of local Mach No., V/c , where $c^2 = kRT$,

$$M^2 = \frac{V^2}{C^2} = \frac{2kR(T_1 - T)}{(k-1)kRT} = \frac{2}{k-1} \left(\frac{T_1}{T} - 1 \right) \quad (9)$$

or

$$\frac{T_1}{T} = 1 + \frac{k-1}{2} M^2$$

But combining the isentropic flow equation with the perfect gas law yields

$$\frac{T_1}{T} = \left(\frac{P_1}{P} \right)^{k-1/k} = \left(\frac{\rho_1}{\rho} \right)^{k-1} \quad (10)$$

Therefore, for isentropic flow,

$$\frac{P_1}{P} = \left(1 + \frac{k-1}{2} M^2 \right)^{k/k-1} \quad (11)$$

Flow conditions are termed critical at the throat section of an orifice when the velocity there is sonic. Marking sonic conditions with an asterisk,

$$\frac{P^*}{P_1} = \left(\frac{2}{k+1} \right)^{k/k-1} = 0.528; \quad k = 1.40 \text{ for oxygen} \quad (12)$$

and for subsonic flow

$$\frac{P_{\text{orifice}}}{P_1} \geq \left(\frac{2}{k+1} \right)^{k/k-1} = 0.528 \quad (13)$$

Combining (1), (6), (8), the mass rate of flow, \dot{m} , is obtained for subsonic flow

$$\dot{m} = \rho VA = A \sqrt{2P_1 \rho_1 \frac{k}{k-1} \left(\frac{P}{P_1} \right)^{2/k} \left[1 - \left(\frac{P}{P_1} \right)^{k-1/k} \right]} \quad (14)$$

It is actually easier to develop a relation other than (14) for the mass flow rate because pressure differences are more easily measured than pressure ratios.

Writing Bernoulli's equation for incompressible flow between an upstream section and the downstream vena contracta without inserting head loss or elevation terms,

$$\frac{V_1^2}{2g} + \frac{P_1}{\gamma} = \frac{V_2^2}{2g} + \frac{P_2}{\gamma} \quad (15)$$

where the pressures at the upstream section and the vena contracta are actual pressures and the velocities, without a loss term, are theoretical velocities. The actual velocity is obtained by multiplying

by C_v , a velocity coefficient. By continuity,

$$V_1 D_1^2 = V_2 D_2^2 \quad (16)$$

or

$$\frac{V_1^2}{2g} = \frac{V_2^2}{2g} \left(\frac{D_2}{D_1} \right)^4$$

Substituting in (15) and solving at the vena contracta,

$$V_{2\text{ actual}} = C_v \sqrt{\frac{2g(p_1 - p_2)}{Y \left[1 - \left(\frac{D_2}{D_1} \right)^4 \right]}} \quad (17)$$

Since the contraction coefficient

$$C_c = A_2/A_0, \text{ where } A_0 \text{ is the orifice area, } (18)$$

$$\begin{aligned} Q &= C_v C_c A_0 \sqrt{\frac{2 \Delta p / \rho_1}{1 - C_c^2 (D_0/D_1)^4}} \quad (19) \\ &= C A_0 \sqrt{\frac{2 \Delta p}{\rho_1}} \end{aligned}$$

For compressible flow an expansion factor, Y , is inserted, which is a function of k , p_2/p_1 and A_2/A_1 :

$$Q_{\text{actual}} = C A_0 Y \sqrt{\frac{2 \Delta p}{\rho_1}} \quad (20)$$

or

$$\Delta p = 8 \rho_1 \left(\frac{Q}{\pi d_0^2 C Y} \right)^2 = 0.815 \rho_1 \left(\frac{Q}{C Y d_0^2} \right)^2 \quad (21)$$

where d_0 = orifice diameter.

APPENDIX II

CALCULATIONS FOR CURVES OF MAGNET EXCURSION ANGLE,
a-b, VERSUS TILTED RING ROTATION ANGLE, γ , FOR
VARIOUS FIXED ANGLES OF TILT, σ .

The following data is taken to satisfy the equation

$$\cos \gamma = \cot a \tan b$$

where $b = 90^{\circ} - \sigma$.

Figure 9 shows the resulting plot of maximum magnet excursion angle, (a-b) , versus tilted ring rotation angle, γ , for varied fixed angles of tilt from the horizontal equatorial plane, σ .

$$\text{Angle of tilt } \begin{cases} \sigma = 15^\circ \\ b = 75^\circ \end{cases}, \quad \tan b = 3.73205$$

a°	$\cot a$	$\cos \gamma$	γ°	$(a-b)^\circ$
75	0.26795	1.00000	0.0	0
75.1	0.26608	0.99302	6.983	0.1
75.2	0.26421	0.98604	9.950	0.2
75.5	0.25862	0.96891	15.833	0.5
76	0.24933	0.93051	21.483	1
77	0.23087	0.86161	30.500	2
78	0.21256	0.79333	37.500	3
79	0.19438	0.72543	43.483	4
80	0.17633	0.65807	48.850	5
81	0.15838	0.59108	53.766	6
82	0.14054	0.52450	58.366	7
83	0.12278	0.45822	62.716	8
84	0.10510	0.39223	66.900	9
85	0.08749	0.32651	70.950	10
86	0.06993	0.26098	74.883	11
87	0.05241	0.19559	78.716	12
88	0.03492	0.13032	82.516	13
89	0.01746	0.06516	86.266	14
90	0.0	0.0	90.0	15

$$\text{Angle of tilt } \left\{ \begin{array}{l} \sigma = 30^\circ \\ b = 60^\circ \end{array} \right. , \quad \tan b = 1.73205$$

a°	$\cot a$	$\cos \gamma$	γ°	$(a-b)^\circ$
60	0.57735	1.00000	0.0	0
60.1	0.57503	0.99598	5.416	0.1
60.2	0.57271	0.99196	6.800	0.2
60.5	0.56577	0.98994	11.666	0.5
61	0.55431	0.96009	16.250	1
62	0.53171	0.92094	22.933	2
63	0.50953	0.88253	28.050	3
64	0.48773	0.84477	32.350	4
65	0.46631	0.80767	36.133	5
66	0.44523	0.77116	39.550	6
67	0.42447	0.73520	42.666	7
68	0.40403	0.69980	45.583	8
69	0.38386	0.66486	48.333	9
70	0.36397	0.63041	50.916	10
75	0.26795	0.46410	62.350	15
80	0.17633	0.30541	72.216	20
85	0.08749	0.15153	81.283	25
90	0.0	0.0	90.0	30

$$\text{Angle of tilt } \begin{cases} \sigma = 45^\circ \\ b = 45^\circ \end{cases}, \quad \tan b = 1.00000$$

a°	$\cot a$	$\cos \gamma$	γ°	$(a-b)^\circ$
45	1.00000	1.00000	0.0	0
45.1	0.99652	0.99652	4.783	0.1
45.2	0.99362	0.99362	6.470	0.2
45.5	0.98270	0.98270	10.675	0.5
46	0.96569	0.96569	15.055	1
47	0.93252	0.93252	21.200	2
48	0.90040	0.90040	25.790	3
49	0.86929	0.86929	29.625	4
50	0.83910	0.83910	32.955	5
51	0.80978	0.80978	35.943	6
52	0.78129	0.78129	38.618	7
53	0.75355	0.75355	41.100	8
54	0.72654	0.72654	43.403	9
55	0.70021	0.70021	45.559	10
60	0.57735	0.57735	54.733	15
70	0.36397	0.36397	68.656	25
80	0.17633	0.17633	79.850	35
90	0.0	0.0	90.0	45

$$\text{Angle of tilt } \left\{ \begin{array}{l} \sigma = 60^\circ \\ b = 30^\circ \end{array} \right. , \quad \tan b = 0.57735$$

a°	$\cot a$	$\cos \gamma$	γ°	$(a-b)^\circ$
30	1.73205	0.99999	0.0	0
30.1	1.72512	0.99599	5.133	0.1
30.2	1.71824	0.99200	7.250	0.2
30.5	1.69776	0.98017	11.433	0.5
31	1.66428	0.96087	16.083	1
32	1.60033	0.92393	22.483	2
33	1.53986	0.88903	27.416	3
34	1.48256	0.85595	31.133	4
35	1.42815	0.82454	34.466	5
36	1.37638	0.79465	37.366	6
37	1.32704	0.76616	40.000	7
38	1.27994	0.73897	42.583	8
39	1.23490	0.71296	44.516	9
40	1.19175	0.68805	46.516	10
45	1.00000	0.57735	54.733	15
50	0.83910	0.48445	61.022	20
55	0.70021	0.40427	66.150	25
60	0.57735	0.33333	70.516	30
65	0.46631	0.26922	74.383	35
70	0.36397	0.21014	77.866	40
80	0.17633	0.10180	84.155	50
90	0.0	0.0	90.0	60

Angle of tilt $\left\{ \begin{array}{l} \sigma = 70^\circ \\ b = 20^\circ \end{array} \right.$, $\tan b = 0.36397$

a°	$\cot a$	$\cos \gamma$	γ°	$(a-b)^\circ$
20	2.74748	1.00000	0.0	0
20.1	2.73267	0.99458	5.966	0.1
20.2	2.71799	0.98923	8.416	0.2
20.5	2.67464	0.97347	13.233	0.5
21	2.60509	0.94817	18.533	1
22	2.47509	0.90085	25.716	2
23	2.35585	0.85745	30.966	3
24	2.24604	0.81749	35.166	4
25	2.14451	0.78053	38.683	5
26	2.05030	0.74624	41.733	6
27	1.96261	0.71433	44.416	7
28	1.88073	0.68452	46.800	8
29	1.80405	0.65662	48.950	9
30	1.73205	0.63041	50.916	10
35	1.42815	0.51980	58.683	15
40	1.19175	0.43376	64.300	20
45	1.00000	0.36397	68.666	25
50	0.83910	0.30541	72.216	30
55	0.70020	0.25485	75.233	35
60	0.57735	0.20285	78.300	40
65	0.46631	0.16972	80.216	45
70	0.36397	0.13247	82.383	50
80	0.17633	0.06418	86.342	60
90	0.0	0.0	90.0	70

$$\text{Angle of tilt } \begin{cases} \sigma = 75^\circ \\ b = 15^\circ \end{cases}, \quad \tan b = 0.26795$$

a°	$\cot a$	$\cos \gamma$	γ°	$(a-b)^\circ$
15	3.73205	1.00000	0.0	0
15.1	3.7062	0.99308	6.75	0.1
15.2	3.6806	0.98622	9.516	0.2
15.5	3.6059	0.96620	14.933	0.5
16	3.48741	0.93445	20.866	1
17	3.27085	0.87642	28.466	2
18	3.07768	0.82466	34.566	3
19	2.90421	0.77818	38.916	4
20	2.74748	0.73618	42.600	5
21	2.60509	0.69803	45.733	6
22	2.47509	0.66320	48.450	7
23	2.35585	0.63125	50.833	8
24	2.24604	0.60182	52.896	9
25	2.14451	0.57462	54.933	10
30	1.73205	0.46410	62.350	15
40	1.19175	0.31932	71.350	25
50	0.83910	0.22483	77.000	35
60	0.57735	0.14934	81.400	45
70	0.36397	0.09753	84.400	55
80	0.17633	0.04725	87.291	65
90	0.0	0.0	90.0	75

Angle of tilt $\left\{ \begin{array}{l} \sigma = 80^\circ \\ b = 10^\circ \end{array} \right.$, $\tan b = 0.17633$

a°	$\cot a$	$\cos \gamma$	γ°	$(a-b)^\circ$
10	5.67128	1.00000	0.0	0
10.1	5.61407	0.98992	8.140	0.1
10.2	5.56713	0.98165	10.994	0.2
10.5	5.39551	0.95139	17.933	0.5
11	5.14455	0.90713	24.883	1
12	4.70463	0.82956	33.950	2
13	4.33148	0.78140	39.600	3
14	4.01078	0.70722	45.008	4
15	3.73205	0.65807	48.850	5
16	3.48741	0.61493	52.050	6
17	3.27085	0.57674	54.783	7
18	3.07768	0.54268	57.133	8
19	2.90421	0.51209	59.200	9
20	2.74748	0.48446	61.033	10
25	2.14451	0.37814	67.783	15
30	1.73205	0.30541	72.216	20
35	1.42815	0.25182	75.416	25
40	1.19175	0.21014	77.866	30
45	1.00000	0.17633	79.850	35
50	0.83910	0.14795	81.483	40
60	0.57735	0.10180	84.150	50
70	0.36397	0.06417	86.316	60
80	0.17633	0.03109	88.216	70
90	0.0	0.0	90.0	80

Angle of tilt $\left\{ \begin{array}{l} \sigma = 85^\circ \\ b = 5^\circ \end{array} \right.$, $\tan b = 0.08749$

a°	$\cot a$	$\cos \gamma$	γ°	$(a-b)^\circ$
5	11.43010	1.00000	0.0	0
5.1	11.205	0.98033	11.383	0.1
5.2	10.988	0.96134	15.983	0.2
5.5	10.385	0.90858	24.689	0.5
6	9.51436	0.83241	33.650	1
7	8.14435	0.71254	44.550	2
8	7.11537	0.62252	51.500	3
9	6.31375	0.55238	56.466	4
10	5.67128	0.49618	60.253	5
11	5.14455	0.45009	63.251	6
12	4.70463	0.41160	65.683	7
13	4.33148	0.37896	67.733	8
14	4.01078	0.35090	69.450	9
15	3.73205	0.32651	70.933	10
20	2.74748	0.24037	76.100	15
25	2.14451	0.18762	79.183	20
30	1.73205	0.15153	81.283	25
35	1.42815	0.12494	82.816	30
40	1.19175	0.10426	84.016	35
45	1.00000	0.08749	84.983	40
50	0.83910	0.07341	85.783	45
60	0.57735	0.05051	87.100	55
70	0.36397	0.03184	88.166	65
80	0.17633	0.01542	89.116	75
90	0.0	0.0	90.0	85

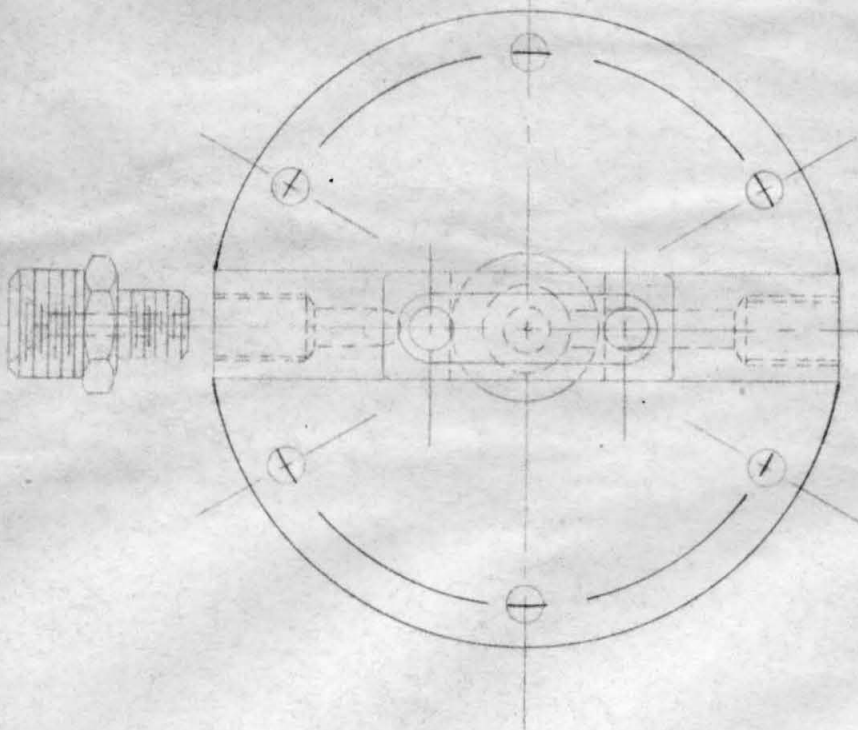
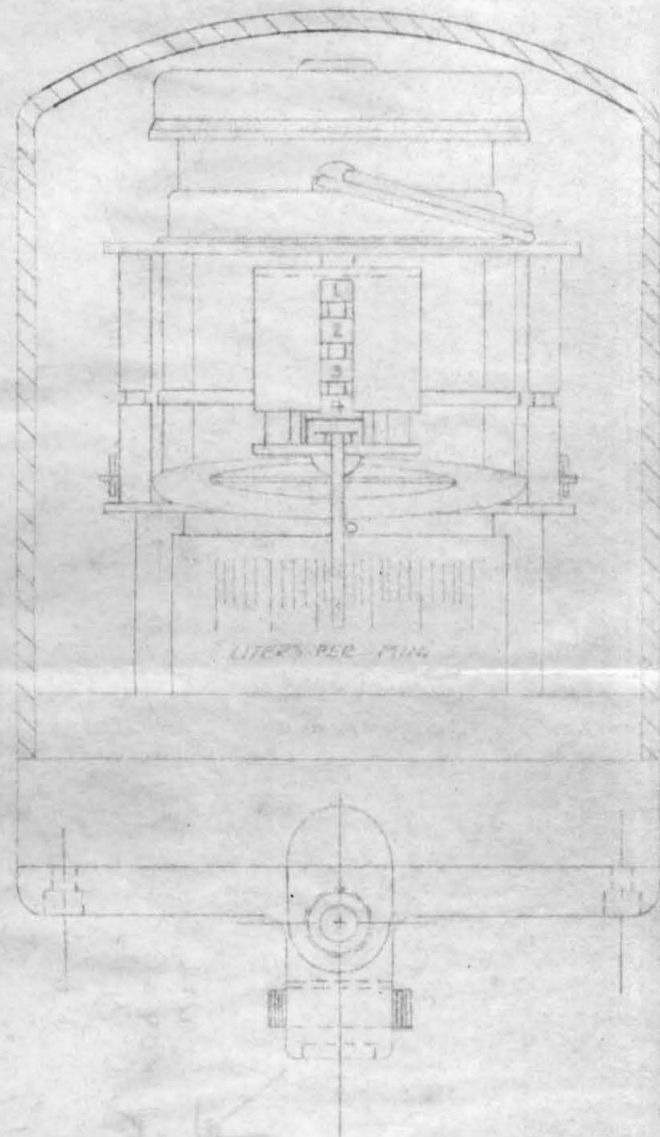
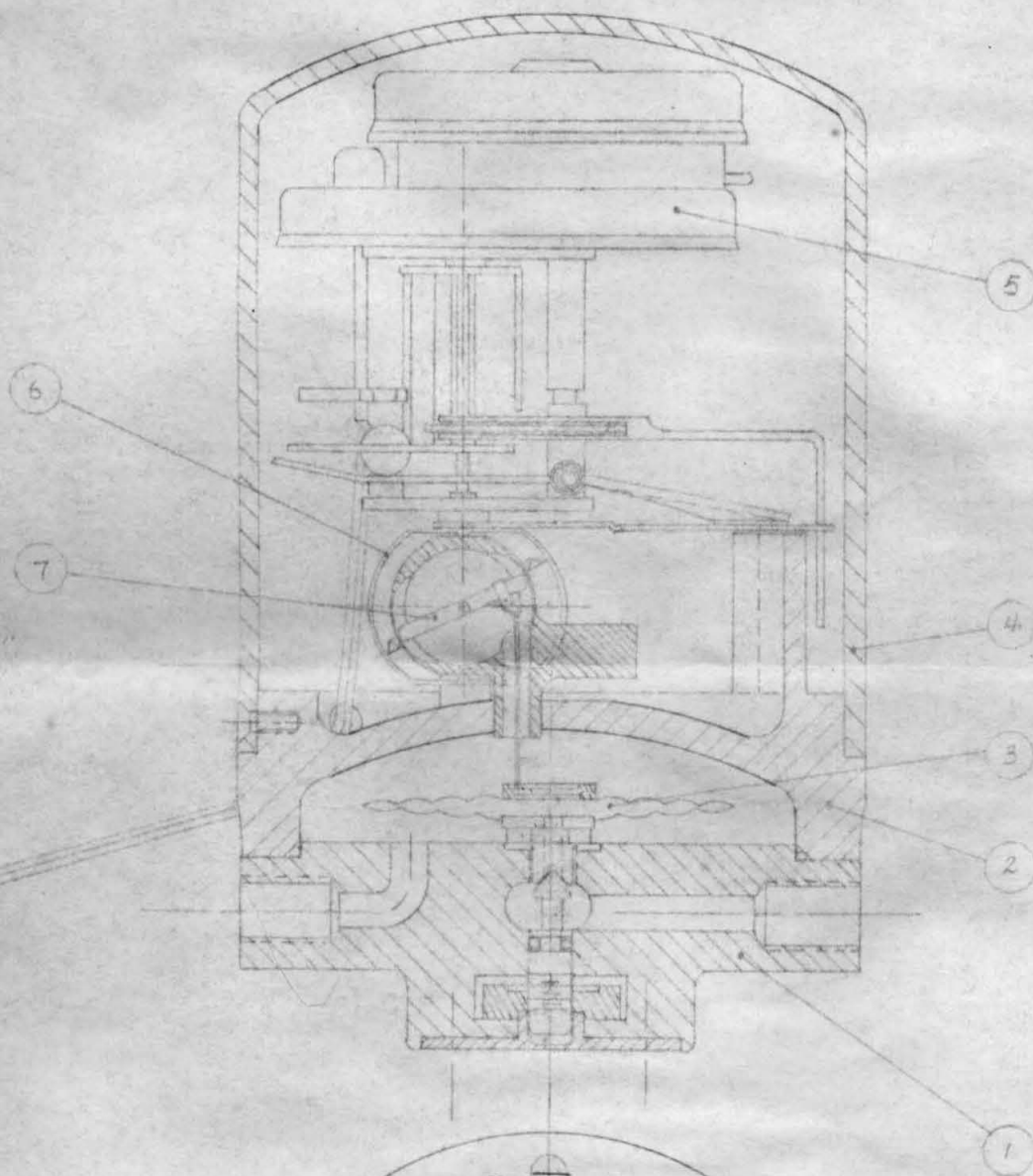
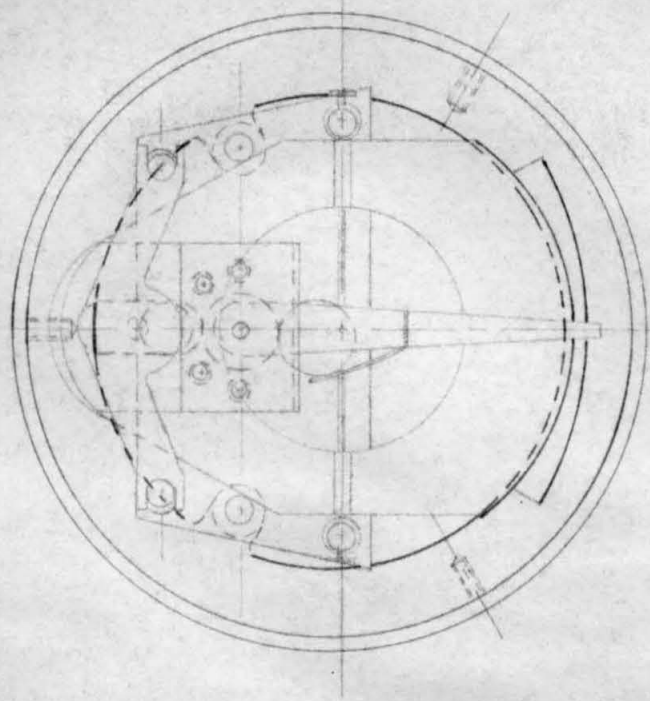
APPENDIX III

REFERENCES

1. American Society of Mechanical Engineers. Diaphragm Characteristics, Design and Terminology. New York, 1958.
2. American Society of Mechanical Engineers. Fluid Meters, Their Theory and Application, 5 ed. New York, 1959.
3. Bardell, P. R. Magnetic Materials in the Electrical Industry. New York: Philosophical Library, 1955.
4. Cambel, A. B., and Jennings, B. H. Gas Dynamics. New York: McGraw-Hill Book Co., Inc., 1958.
5. Christian, W. S. "Bellows-Type Orifice Meters." Instruments and Control Systems (March 1960), pp. 466-469.
6. Cooper, C. C. "Measuring Wet High Pressure Gas." Gas (September, 1959), pp. 117-118.
7. Dekker, A. J. Electrical Engineering Materials. Englewood Cliffs, N. J.: Prentice-Hall, Inc., 1959.
8. Elrod, H. G., and Fouse, R. R. "An Investigation of Electromagnetic Flowmeters." Trans. ASME (1952), vol. 19, pp. 589-594.
9. Filban, T. J., and Griffin, W. A. "Small-Diameter-Orifice Metering." Trans. ASME (1960), vol. 82-D, pp. 735-740.
10. Fitzgerald, A. E., and Kingsley, C. Electric Machinery. New York: McGraw-Hill Book Co., Inc., 1952.
11. Grace, H. P., and Lapple, C. E. "Discharge Coefficients of Small-Diameter Orifices and Flow Nozzles." Trans. ASME (1951), vol. 73, pp. 639-647.
12. Hodgson, J. L. "The Orifice as a Basis of Flow Measurement." Selected Engineering Paper No. 31, The Institution of Civil Engineers, London, 1925.

13. Iverson, H. W. "Orifice Coefficients for Reynolds Numbers from 4 to 50,000." Trans. ASME (1956), vol. 78, pp. 359-364.
14. Jorissen, A. L. "Discharge Measurements at Low Reynolds Numbers--Special Devices." Trans. ASME (1956), vol. 78, pp. 365-368.
15. Li, Y. T., and Lee, S. Y. "A Fast-Response True-Mass-Rate Flowmeter." Trans. ASME (1953), vol. 20, pp. 835-841.
16. Liepmann, H. W., and Roshko, A. Elements of Gas Dynamics. New York: John Wiley and Sons, Inc., 1957.
17. Loedel, W. "Core Magnets Versus External Magnets." Electronic Design News (January 1965), pp. 156-162.
18. National Advisory Committee for Aeronautics. Standards for Discharge Measurement with Standardized Nozzles and Orifices, 4 ed. Washington, 1940.
19. Rotors, H. C. Electromagnetic Devices. New York: John Wiley and Sons, Inc., 1941.
20. Sears, F. W. Principles of Physics II - Electricity and Magnetism. Cambridge: Addison Wesley Press, Inc., 1947.
21. Seeley, S. Introduction to Electromagnetic Fields. New York: McGraw-Hill Book Co., Inc., 1958.
22. Skilling, H. H. Electromechanics. New York: John Wiley and Sons, Inc., 1962.
23. Stanley, J. K. Electrical and Magnetic Properties of Metals. Metals Park, Ohio: American Society for Metals, 1963.
24. Streeter, V. L. Fluid Mechanics. New York: McGraw-Hill Book Co., Inc., 1962.
25. Swinney, G. W. "The Bellows Differential Guage in Orifice Measurement." Gas Age (October 15, 1959), pp. 41-44.

APPENDIX IV
MANUFACTURING DRAWINGS

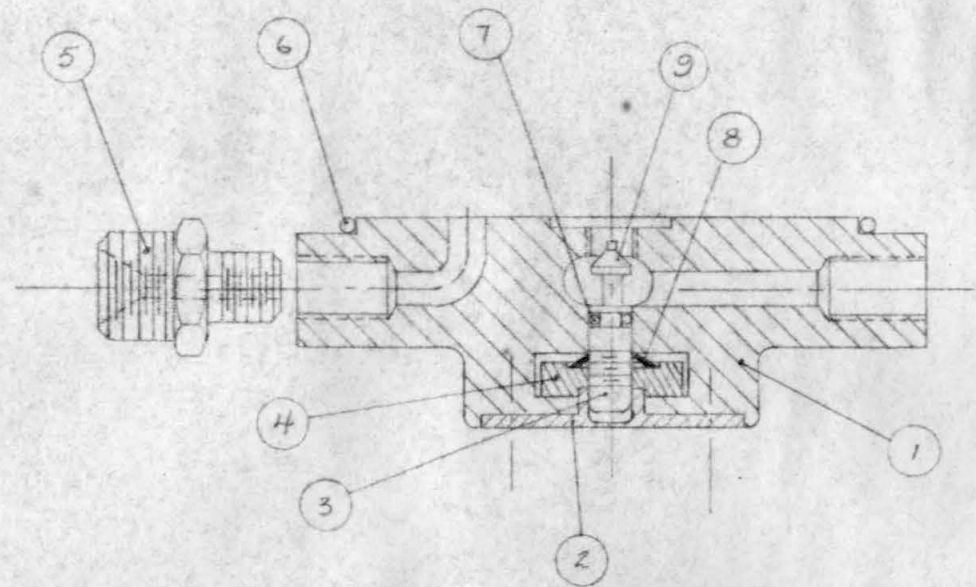


7	MAGNET	1	24
6	CROSSOVER RING	1	59
5	TOTALIZER	1	28
4	ENCLOSURE	1	11
3	DIAPHRAGM	1	
2	ANVIL CASING	1	9
1	VALVE CASING	1	4
NO.	ASSEMBLY NAME	REQ'D.	DETAIL DWG. NOS.

ENGINEERING DESIGN
CALIFORNIA INSTITUTE OF TECHNOLOGY

INTEGRATING FLOWMETER

DR. J.P. BARNES
APP'D:
SCALE: FULL
DATE: 7.26.65
TOLERANCES DWG. NO.



9	VALVE STEM CAP	1	13
8	KNOB SPRING	1	8
7	O-RING	1	PARKER 2-6 (BUTYL) OR EQUIV.
6	O-RING	1	PARKER 2-38 (BUTYL) OR EQUIV.
5	ADAPTER	2	18
4	KNOB	1	6
3	VALVE STEM	1	5
2	VALVE STOP	1	7
1	VALVE CASING	1	4
NO.	PART NAME	REQ'D	DETAIL DWG. NO.

ENGINEERING DESIGN
CALIFORNIA INSTITUTE OF TECHNOLOGY

VALVE CASING ASSEMBLY

DR: J. R. BARNES

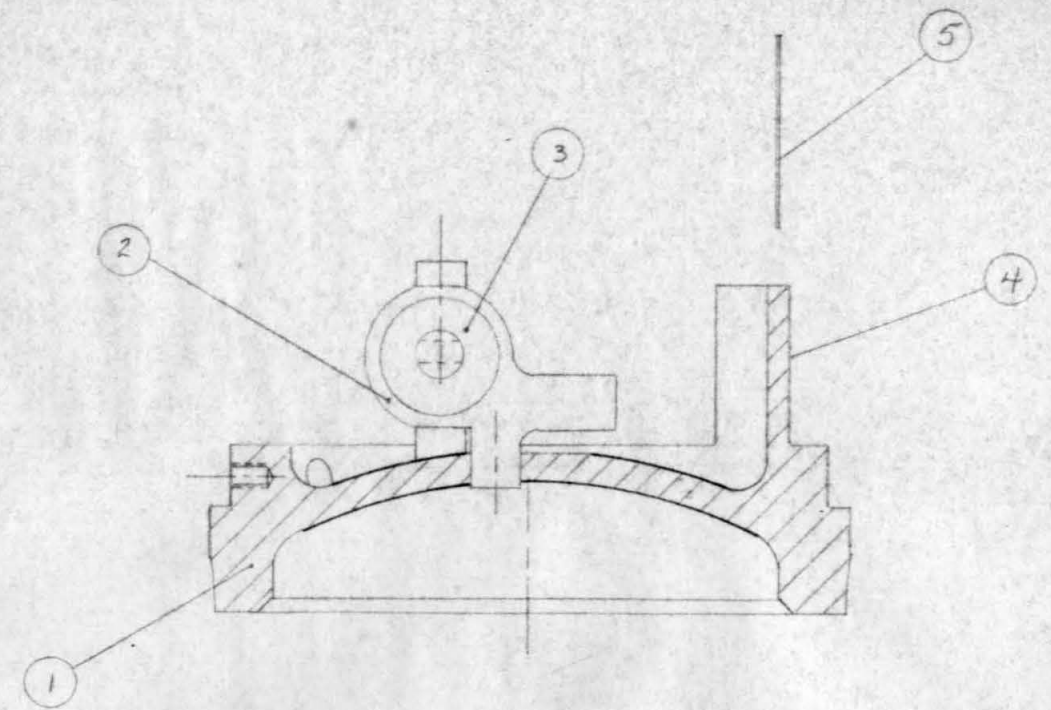
APPV'D:

SCALE: FULL

DATE: 7-27-65

TOLERANCES DWG. NO.

2



5	PIN STOP	1	.020 D. x 1" LONG S.S. WIRE
4	SCALE	1	
3	CLOSURE	1	12
2	MAG. SUP CHAMBER	1	10
1	ANVIL CASING	1	3
NO.	PART NAME	REQ'D	DETAIL DWG. NO.

ENGINEERING DESIGN
CALIFORNIA INSTITUTE OF TECHNOLOGY

ANVIL CASING ASSEMBLY

DR: J. R. BARNES

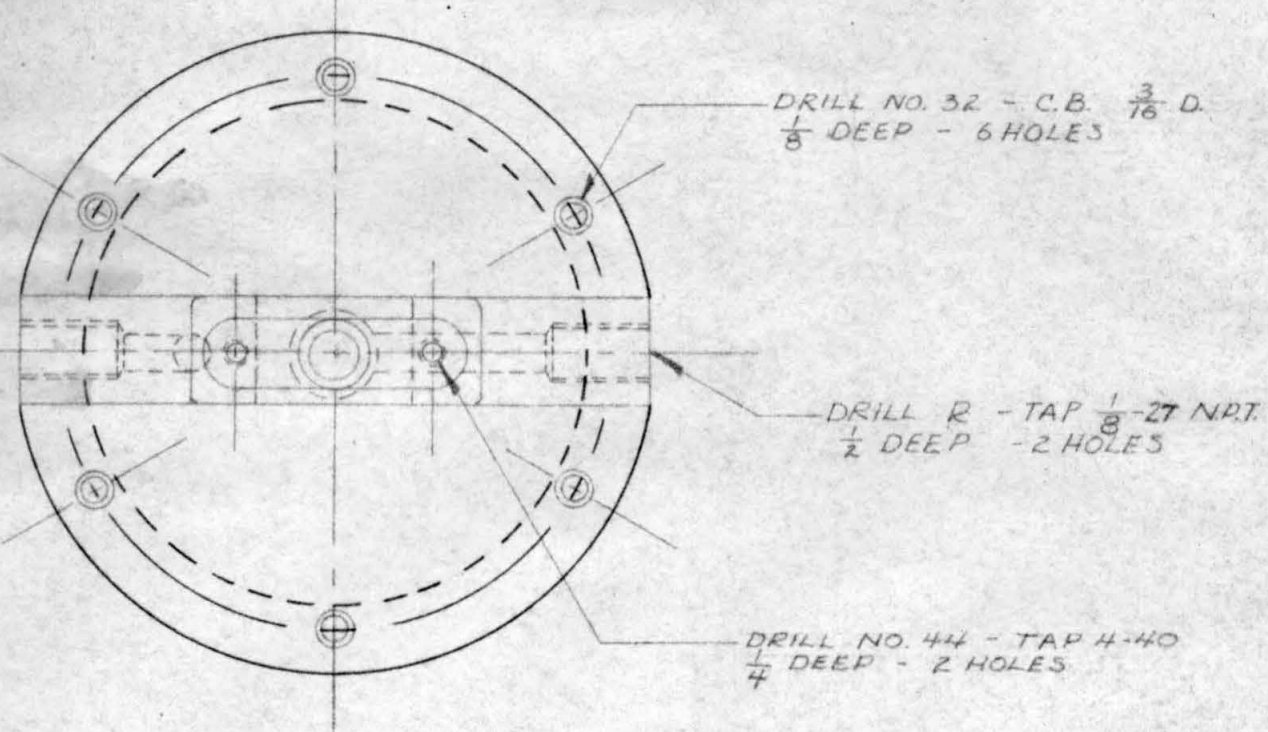
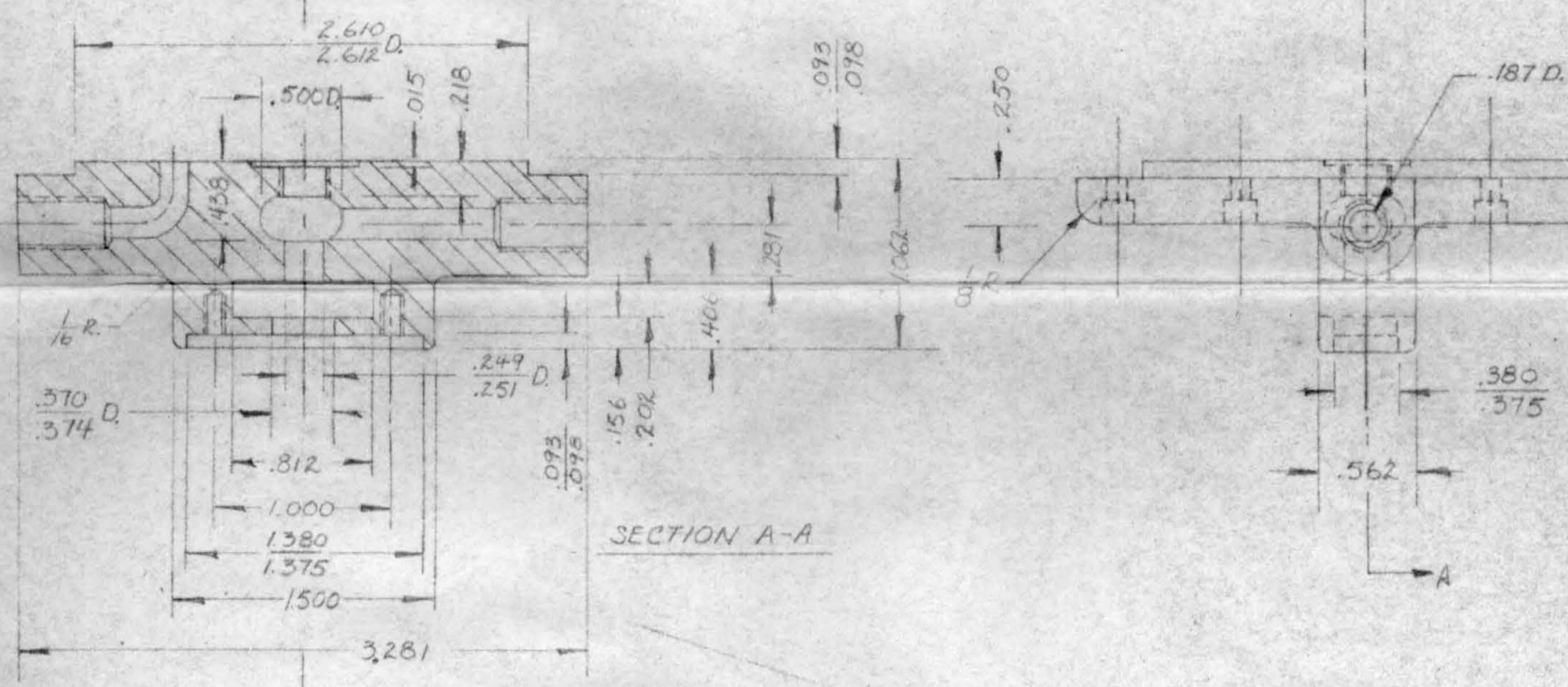
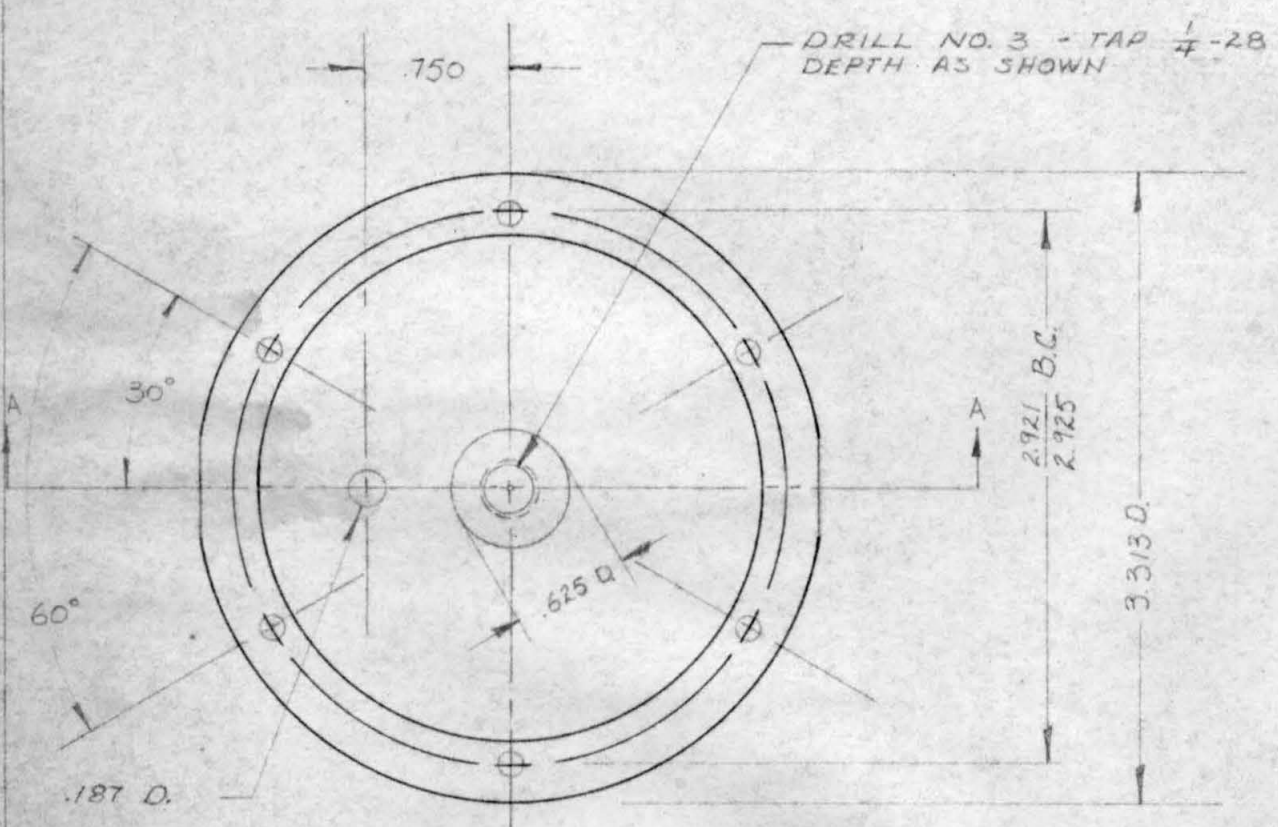
APPV'D:

SCALE: FULL

DATE: 7-27-65

TOLERANCES DWG. NO.

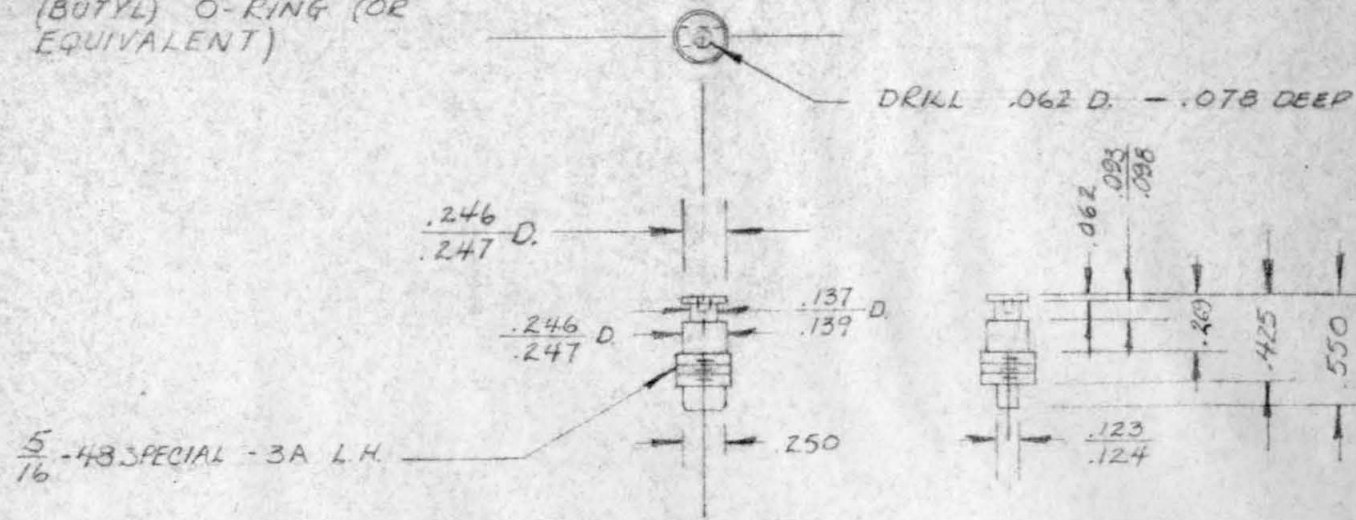
3



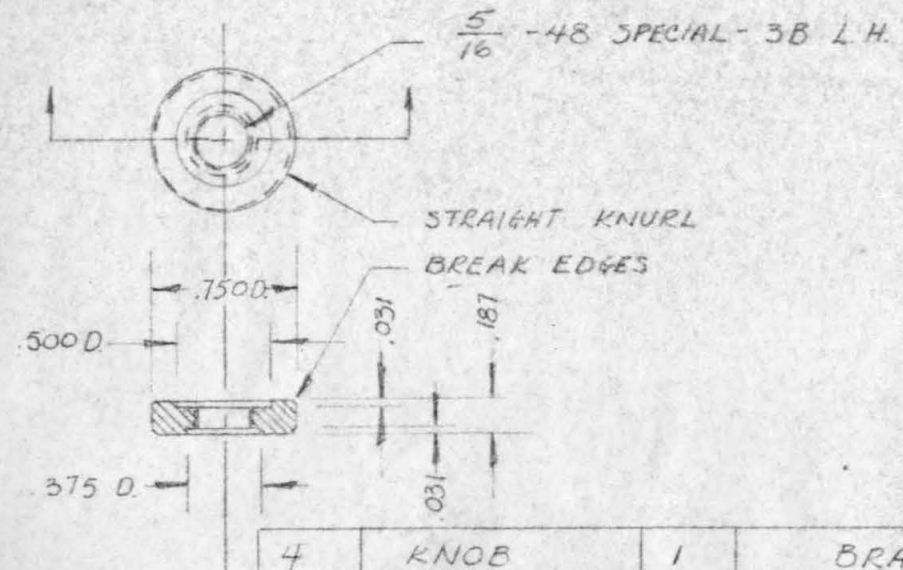
1	VALVE CASING	1	BRASS
NO.	PART NAME	REQ'D.	MATERIAL
ENGINEERING DESIGN CALIFORNIA INSTITUTE OF TECHNOLOGY			DR. J.R. BARNES
VALVE CASING ASSEMBLY			APP'D.
			SCALE: FULL
			DATE: 7-20-65
			TOLERANCES
			± .005"
			± .001"
			± 0.5°
			DWG. NO. 4

NOTE: DESIGNED FOR PARKER 2-38 (BUTYL) O-RING (OR EQUIVALENT)

NOTE: DESIGNED FOR PARKER 2-6
(BUTYL) O-RING (OR
EQUIVALENT)

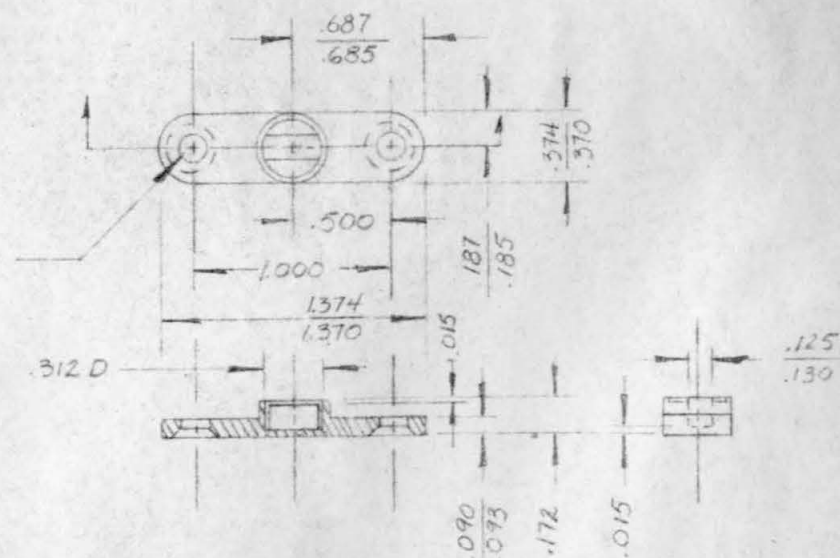


3	VALVE STEM	1	BRASS
NO	PART NAME	REQ'D	MATERIAL
ENGINEERING DESIGN CALIFORNIA INSTITUTE OF TECHNOLOGY			DR: J.R. BARNES
VALVE CASING ASSEMBLY			APP'D:
			SCALE: FULL
			DATE: 7-21-65
		TOLERANCES	DWG. NO.
		± .005"	5
		± 0.5°	

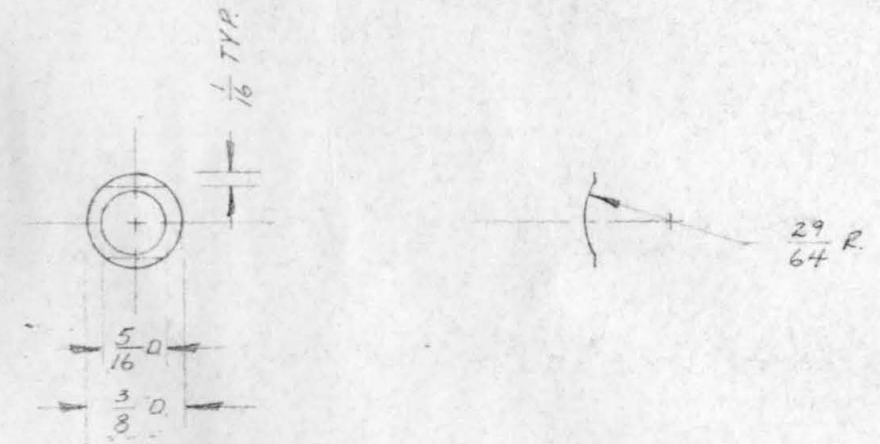


4	KNOB	1	BRASS
NO	PART NAME	REQ'D	MATERIAL
ENGINEERING DESIGN CALIFORNIA INSTITUTE OF TECHNOLOGY			DR: J.R. BARNES
VALVE CASING ASSEMBLY			APP'D:
			SCALE: FULL
			DATE: 7-21-65
		TOLERANCES	DWG. NO.
		± .005"	6

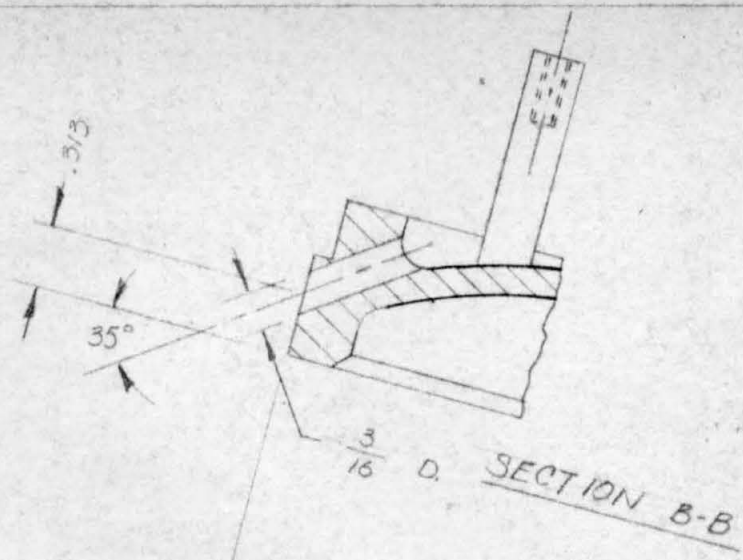
DRILL NO. 32 - C.S. 1/16 DR.
(FROM OTHER SIDE) -
2 HOLES



2	VALVE STOP	1	BRASS
NO	PART NAME	REQ'D	MATERIAL
ENGINEERING DESIGN CALIFORNIA INSTITUTE OF TECHNOLOGY			DR: J.R. BARNES
VALVE CASING ASSEMBLY			APP'D:
			SCALE: FULL
			DATE: 7-21-65
		TOLERANCES	DWG. NO.
		± .005"	7
		± 1/64"	



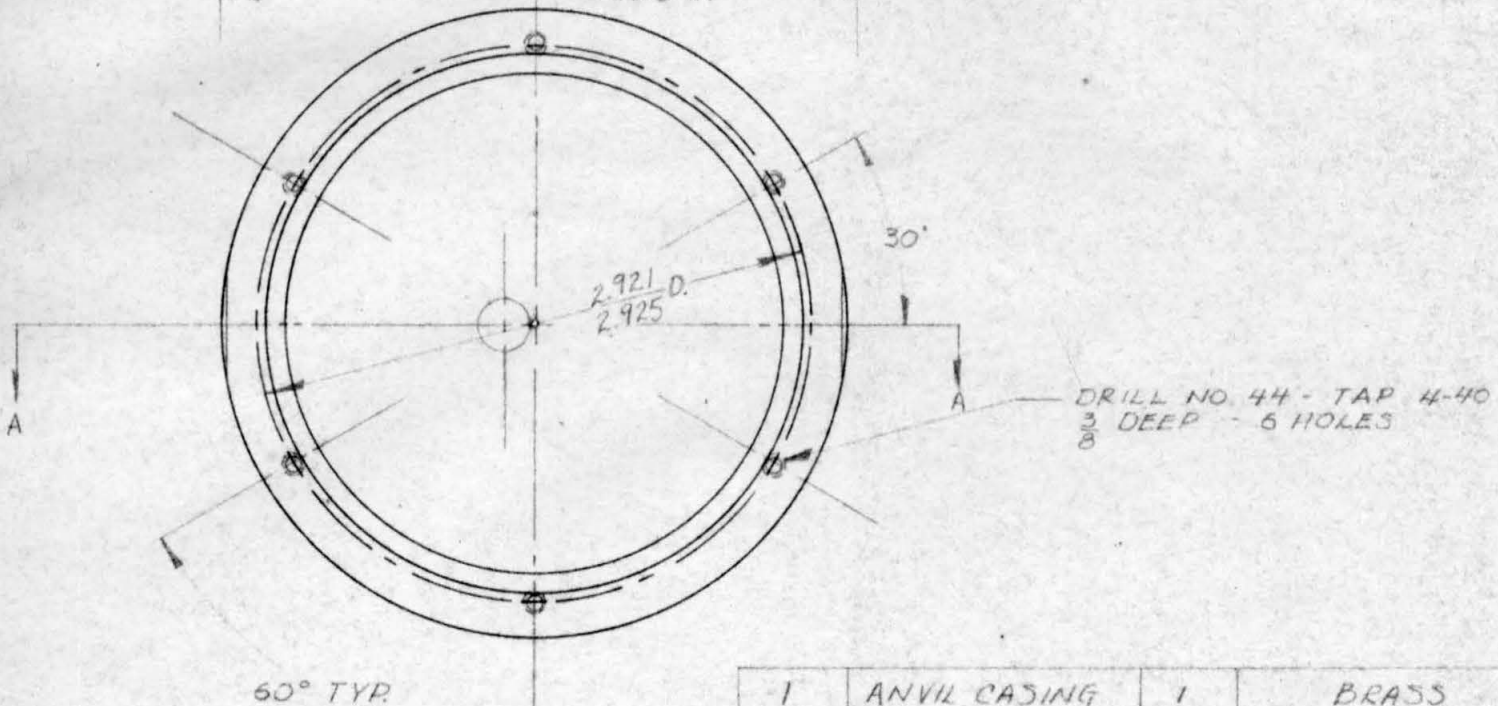
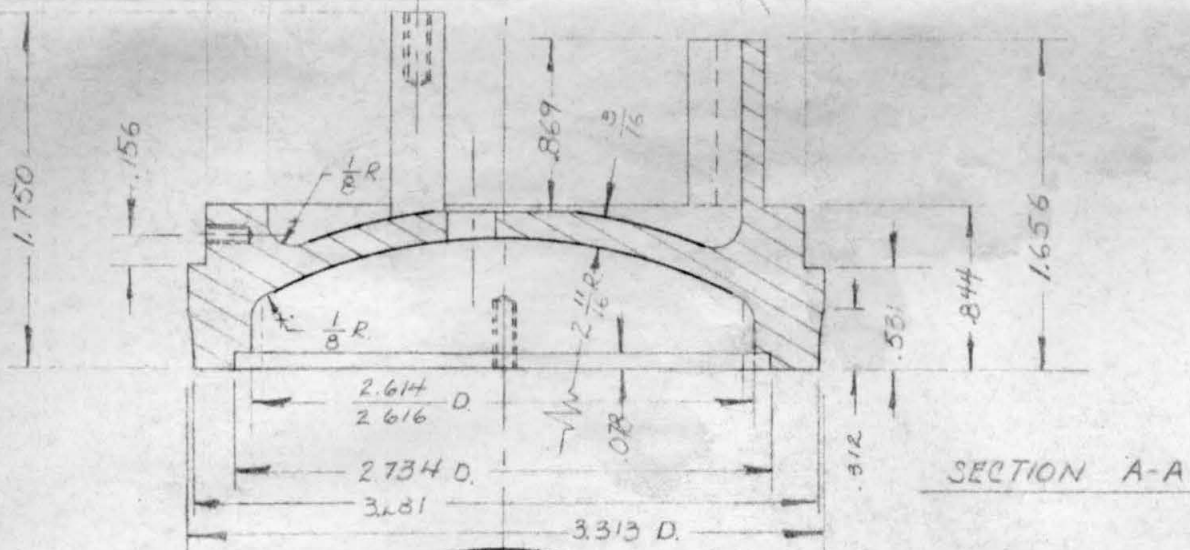
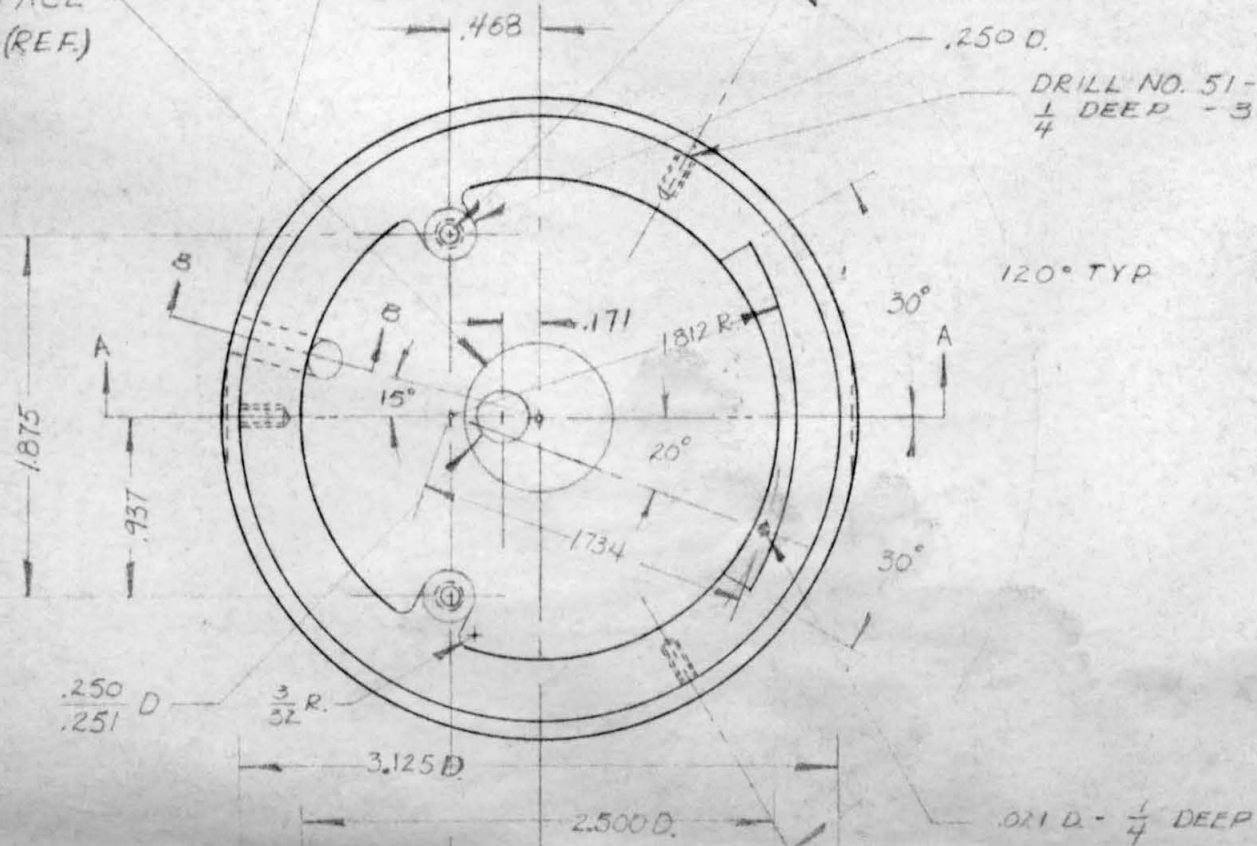
3	KNOB SPRING	1	.010 SHIM STOCK
NO	PART NAME	REQ'D	MATERIAL
ENGINEERING DESIGN CALIFORNIA INSTITUTE OF TECHNOLOGY			DR: J.R. BARNES
VALVE CASING ASSEMBLY			APP'D:
			SCALE: FULL
			DATE: 7-21-65
		TOLERANCES	DWG. NO.
		± .005"	8
		± 1/64"	



SPOTFACE
 $\frac{3}{4} D$ (REF.)

DRILL NO. 44 - TAP 4-40
 $\frac{3}{8}$ DEEP - 2 HOLES

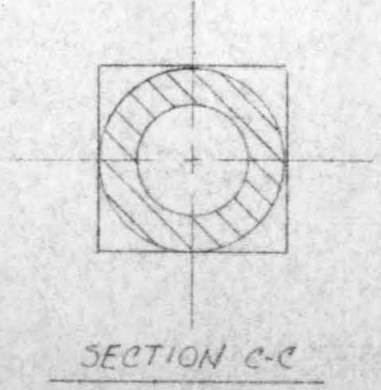
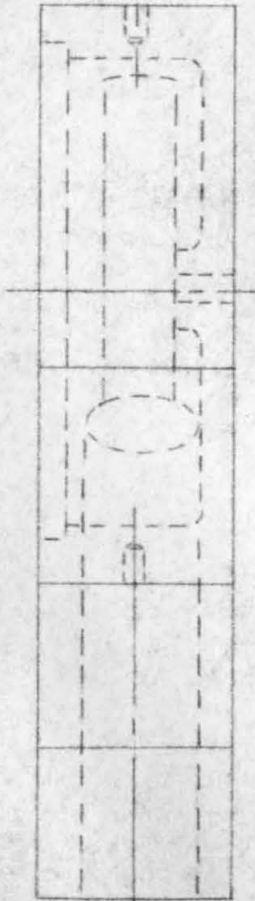
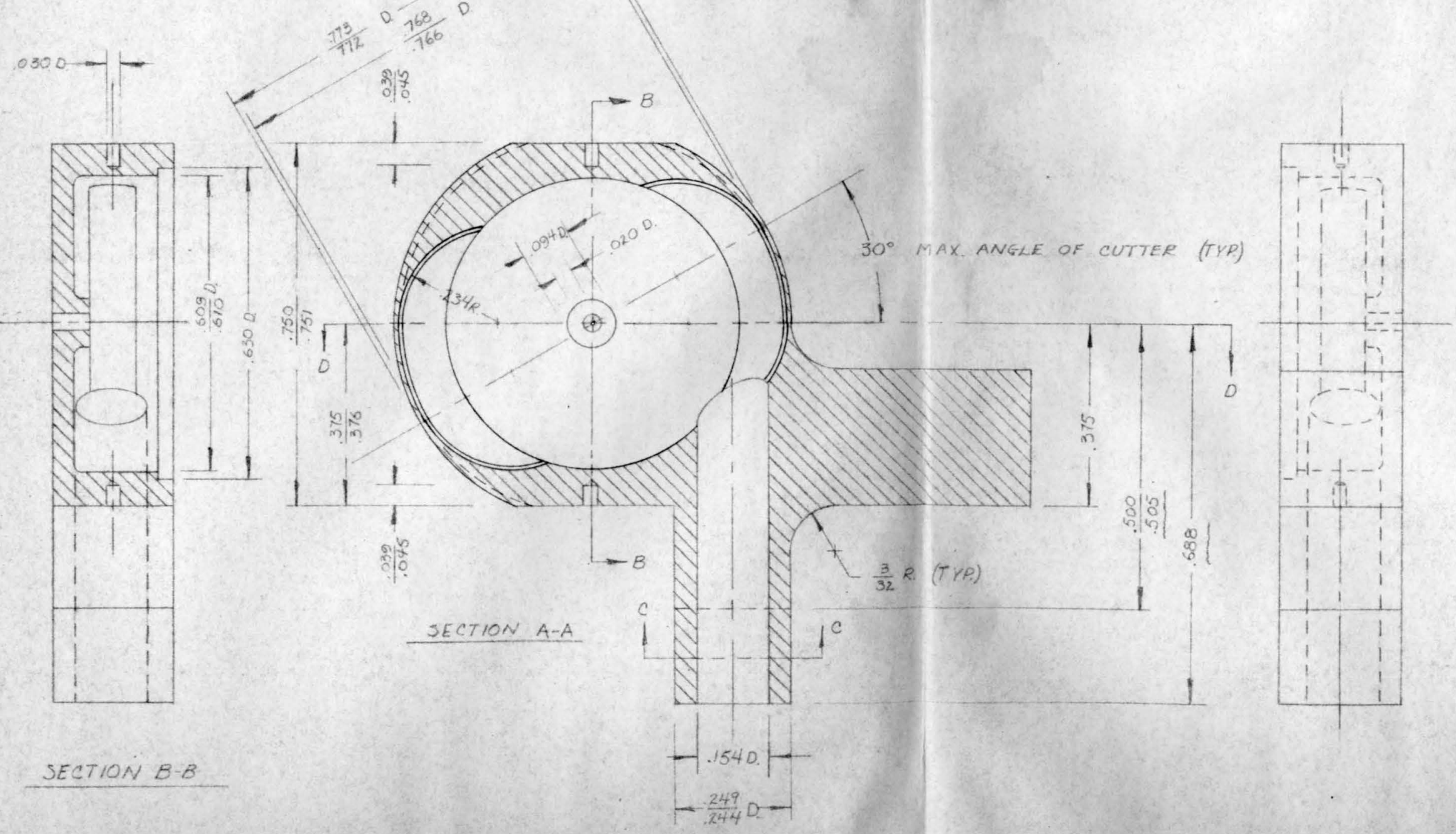
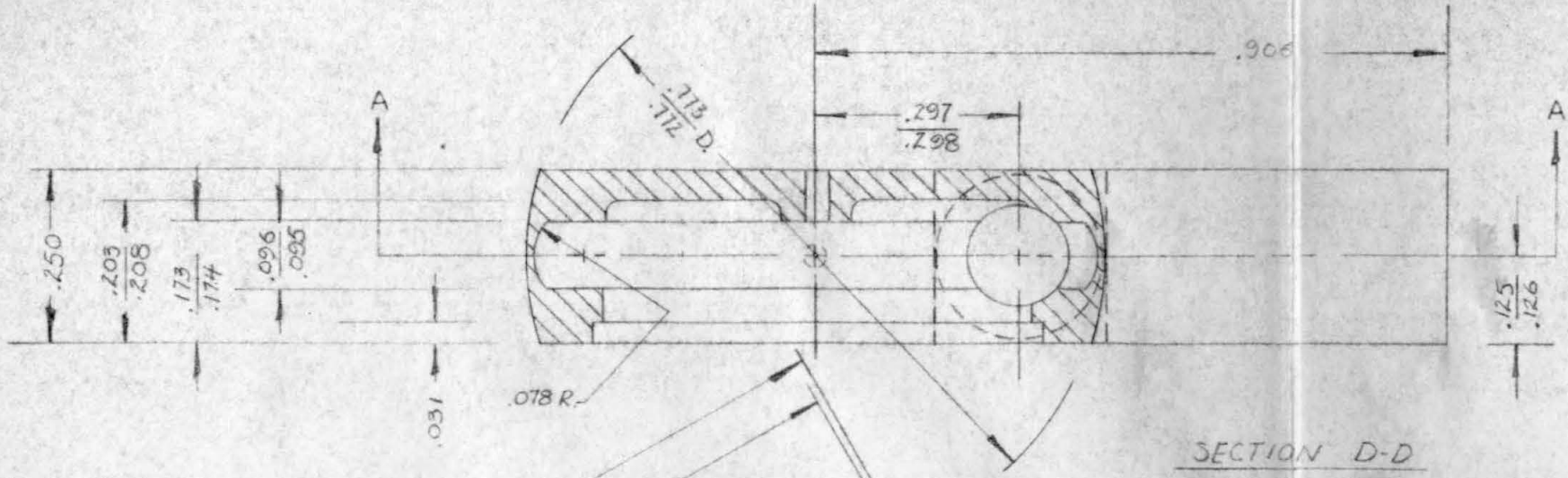
DRILL NO. 51 - TAP 2-56
 $\frac{1}{4}$ DEEP - 3 HOLES



NO.	PART NAME	REQ'D.	MATERIAL
1	ANVIL CASING	1	BRASS

ENGINEERING DESIGN CALIFORNIA INSTITUTE OF TECHNOLOGY		DR: J. R. BARNES
ANVIL CASING ASSEMBLY		APP'D:
		SCALE: FULL
		DATE: 7-16-65
		TOLERANCES DWG. NO.
		± .005"
		± 1/64"
		± .05°
		9

2	MAG SUP CHAMBER	1	BRONZE
NO	PART NAME	REQ'D	MATERIAL
CALIFORNIA INSTITUTE OF TECHNOLOGY ENGINEERING DESIGN			DR: J.R. BARNES
			APP'D:
			SCALE: 4x FULL
ANVIL CASING ASSEMBLY			DATE: 6-20-65
TOLERANCES		DWG. NO.	
± .005"		10	
± .0004"			
± 0.5°			

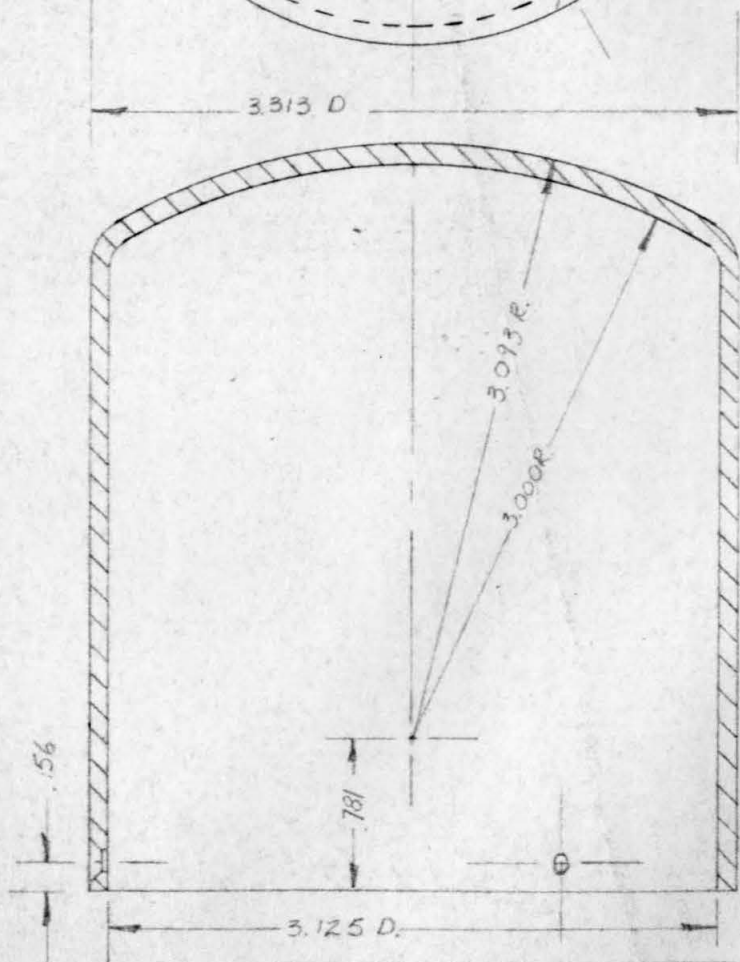
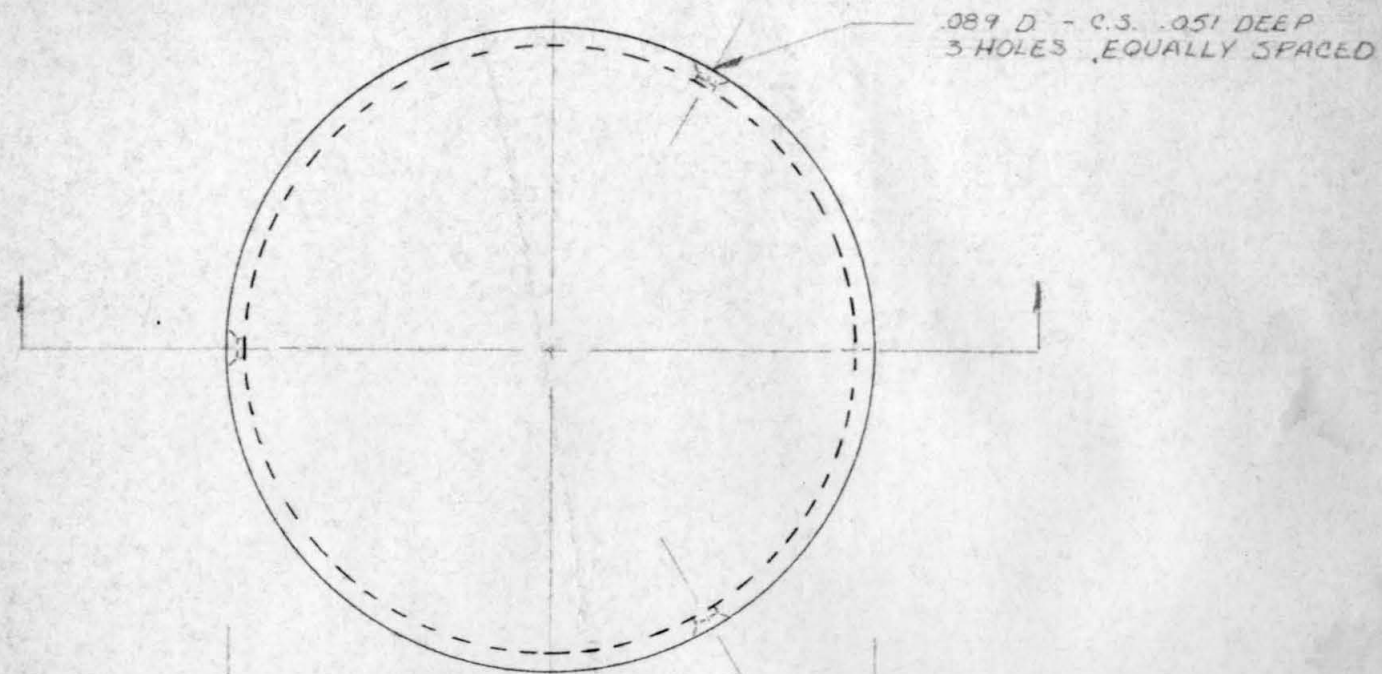


SECTION B-B

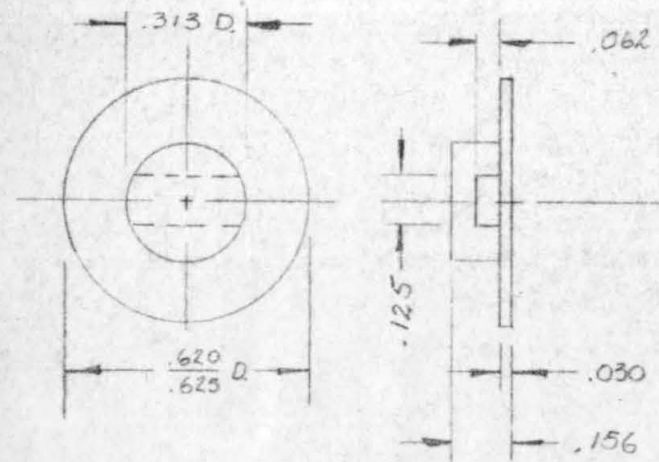
SECTION A-A

SECTION D-D

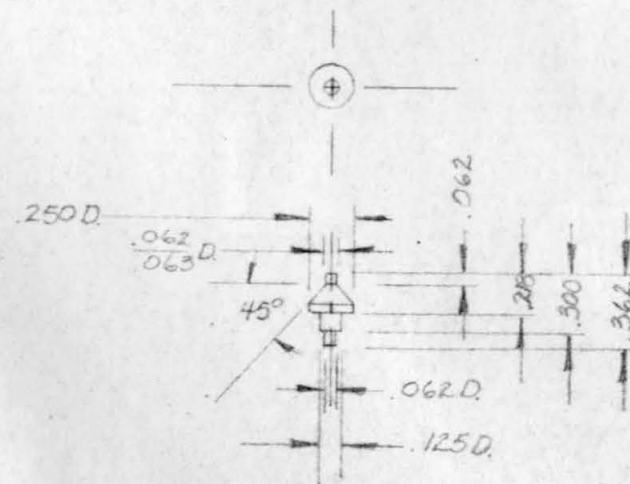
SECTION C-C



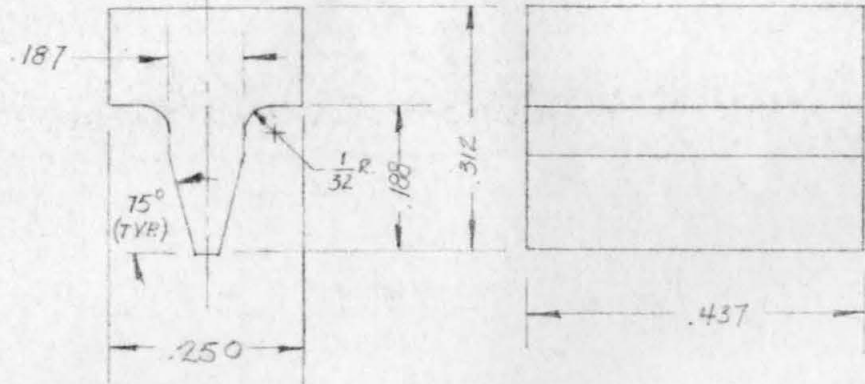
NO.	PART NAME	REQ'D	MATERIAL
		1	MOLDED LUCITE
ENGINEERING DESIGN CALIFORNIA INSTITUTE OF TECHNOLOGY			DR: J.R. BARNES
			APPV'D:
			SCALE: FULL
			DATE: 7-26-65
			TOLERANCES DWG NO.
			± .005" 11
<u>ENCLOSURE</u>			



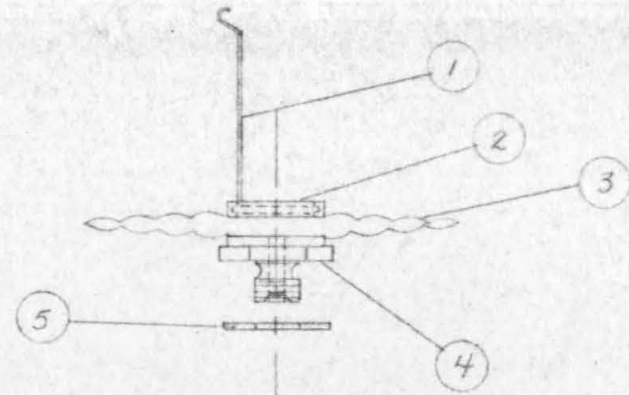
3	SUP. CHMBR. CLOS.	1	BRASS
NO.	PART NAME	REQ'D	MATERIAL
ENGINEERING DESIGN CALIFORNIA INSTITUTE OF TECHNOLOGY			DR: J.R. BARNES
			APPV'D:
			SCALE: 2x FULL
			DATE: 7-26-65
			TOLERANCES DWG NO.
			± .005" 12
<u>ANVIL CASING ASSEMBLY</u>			



9	VALVE STEM CAP	1	NYLON
NO.	PART NAME	REQ'D	MATERIAL
ENGINEERING DESIGN CALIFORNIA INSTITUTE OF TECHNOLOGY			DR: J.R. BARNES
			APPV'D:
			SCALE: FULL
			DATE: 8-25-65
			TOLERANCES DWG NO.
			± .005" ± 0.5° 13
<u>VALVE CASING ASSEMBLY</u>			



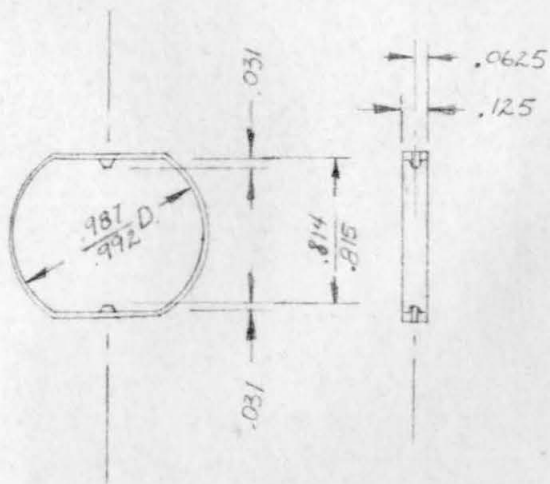
NO.	WEDGE	1	C 1020
ENGINEERING DESIGN CALIFORNIA INSTITUTE OF TECHNOLOGY			DR: J. R. BARNES
			APP'D:
			SCALE: 4X FULL
STRETCH FORMER ASSEMBLY			DATE: 7-26-65
TOLERANCES		DWG. NO.	
± .005		14	
± 1/64"			
± 0.5°			



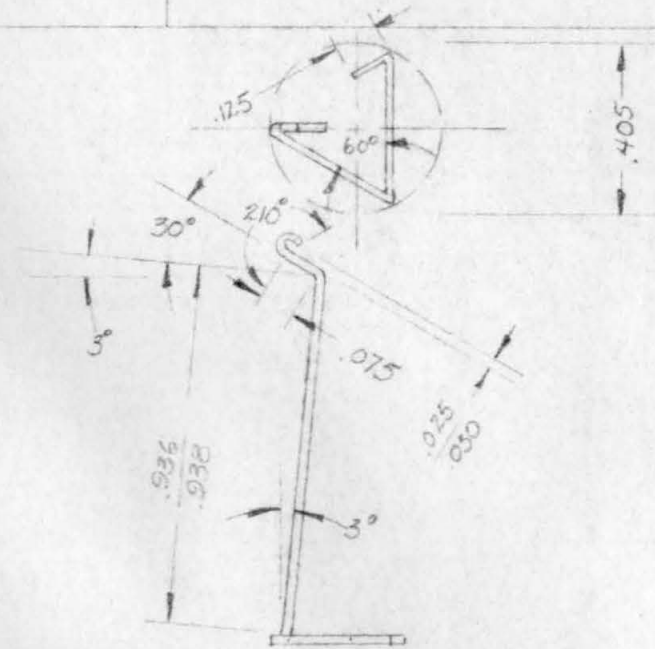
5	WASHER	1	CORK - .562 O.D. - .265 I.D. - .015 THK
4	VALVE SEAT	1	19
3	DIAPHRAGM	1	
2	LINK BRACKET	1	20
1	LINKAGE	1	17
NO.	PART NAME	REQ'D.	DETAIL DWG. NO.

ENGINEERING DESIGN CALIFORNIA INSTITUTE OF TECHNOLOGY			DR: J. R. BARNES
			APP'D:
			SCALE: FULL
DIAPHRAGM ASSEMBLY			DATE: 7-26-65
TOLERANCES		DWG. NO.	
± .005"		15	
± 0.5°			

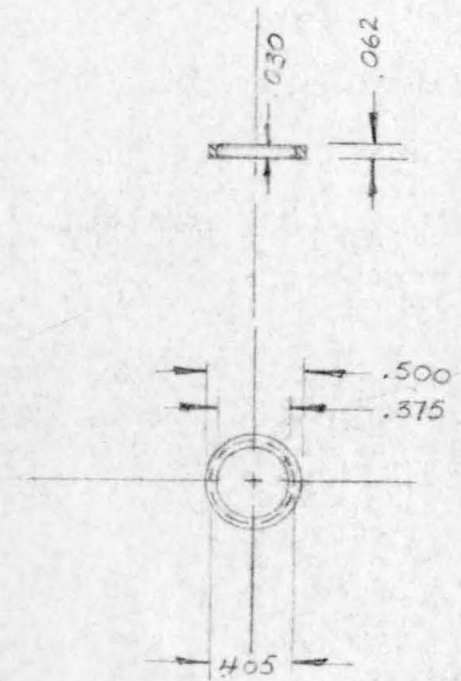
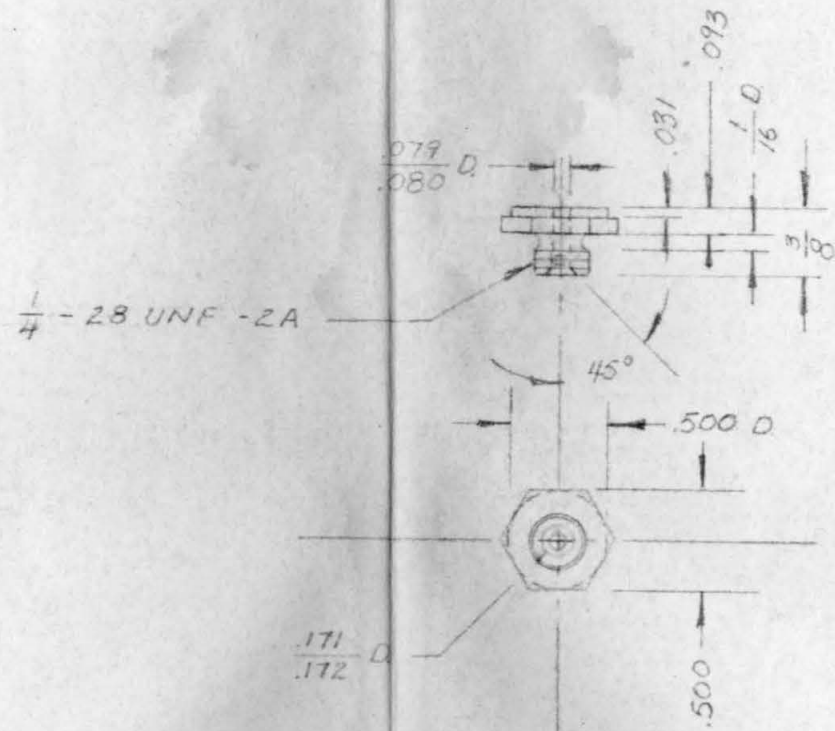
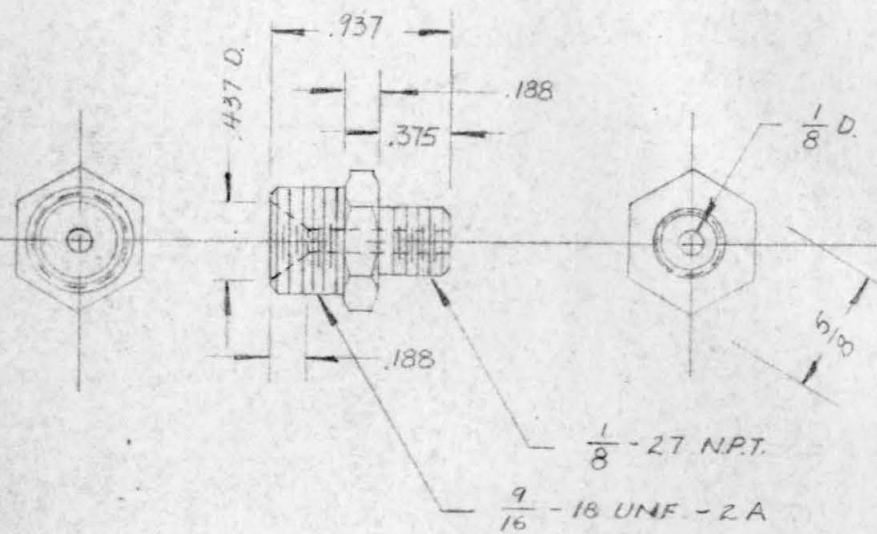
NOTE: FORM BY MEANS OF STRETCH FORMER ASSEMBLY.
DEVELOP FROM RING:
.960 I.D.
.990 O.D.
.015" THICK



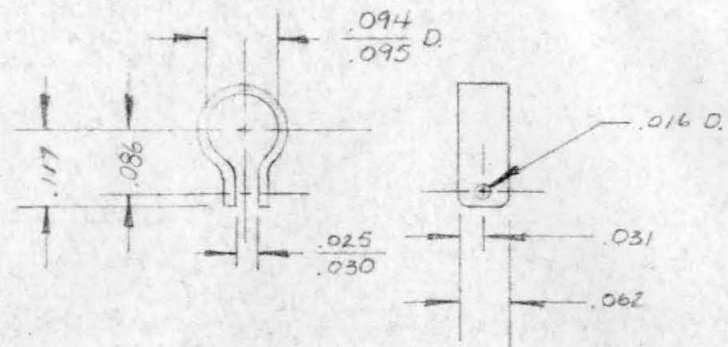
2	SUPPORT FRAME	1	ALUMINUM 6061-T6
NO.	PART NAME	REQ'D.	MATERIAL
ENGINEERING DESIGN CALIFORNIA INSTITUTE OF TECHNOLOGY			DR: J. R. BARNES
			APP'D:
			SCALE: FULL
CROSSOVER RING ASSEMBLY			DATE: 7-26-65
TOLERANCES		DWG. NO.	
± .005"		16	
± 0.5°			



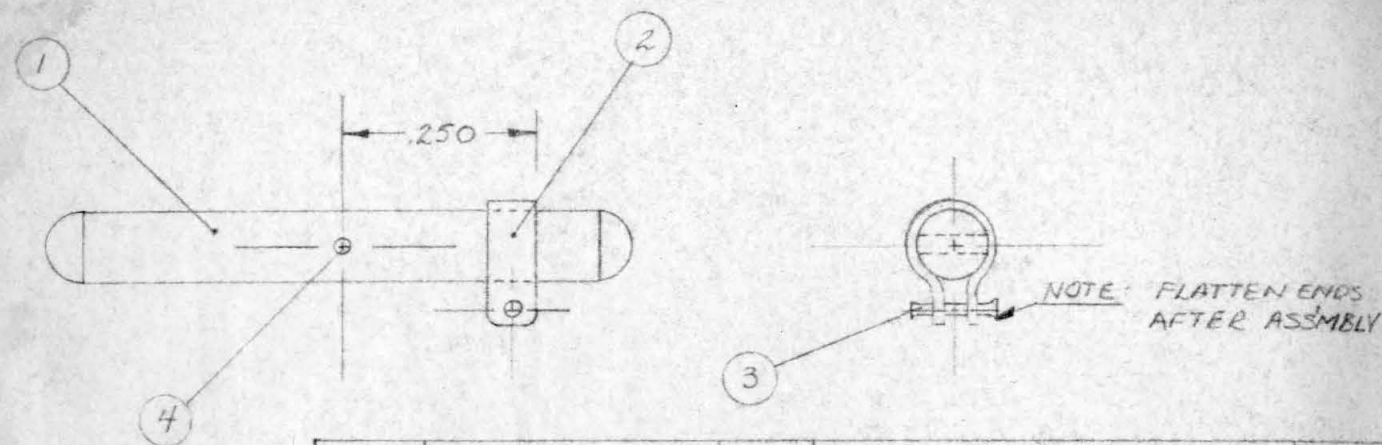
1	LINKAGE	1	.015" S.S. 303 WIRE
NO.	PART NAME	REQ'D.	MATERIAL
ENGINEERING DESIGN CALIFORNIA INSTITUTE OF TECHNOLOGY			DR: J. R. BARNES
			APP'D:
			SCALE: 2x FULL
DIAPHRAGM ASSEMBLY			DATE: 7-26-65
TOLERANCES		DWG. NO.	
± .005"		17	
± 0.5°			



NO.	PART NAME	REQ'D	MATERIAL	NO.	PART NAME	REQ'D	MATERIAL	NO.	PART NAME	REQ'D	MATERIAL
5	ADAPTER	2	BRASS	7	VALVE SEAT	1	1/2" BRASS HEX. STOCK	2	LINK. BRACKET	1	BRASS
ENGINEERING DESIGN CALIFORNIA INSTITUTE OF TECHNOLOGY				ENGINEERING DESIGN CALIFORNIA INSTITUTE OF TECHNOLOGY				ENGINEERING DESIGN CALIFORNIA INSTITUTE OF TECHNOLOGY			
DR: J.R. BARNES				DR: J.R. BARNES				DR: J.R. BARNES			
APPVD:				APPVD:				APPVD:			
SCALE: FULL				SCALE: FULL				SCALE: FULL			
DATE: 7-21-65				DATE: 7-21-65				DATE: 7-21-65			
TOLERANCES DWG. NO.				TOLERANCES DWG. NO.				TOLERANCES DWG. NO.			
± .005"				± .005"				± .005"			
± 1/64"				± 1/64"				± 1/64"			
18				19				20			
VALVE CASING ASSEMBLY				DIAPHRAGM ASSEMBLY				DIAPHRAGM ASSEMBLY			



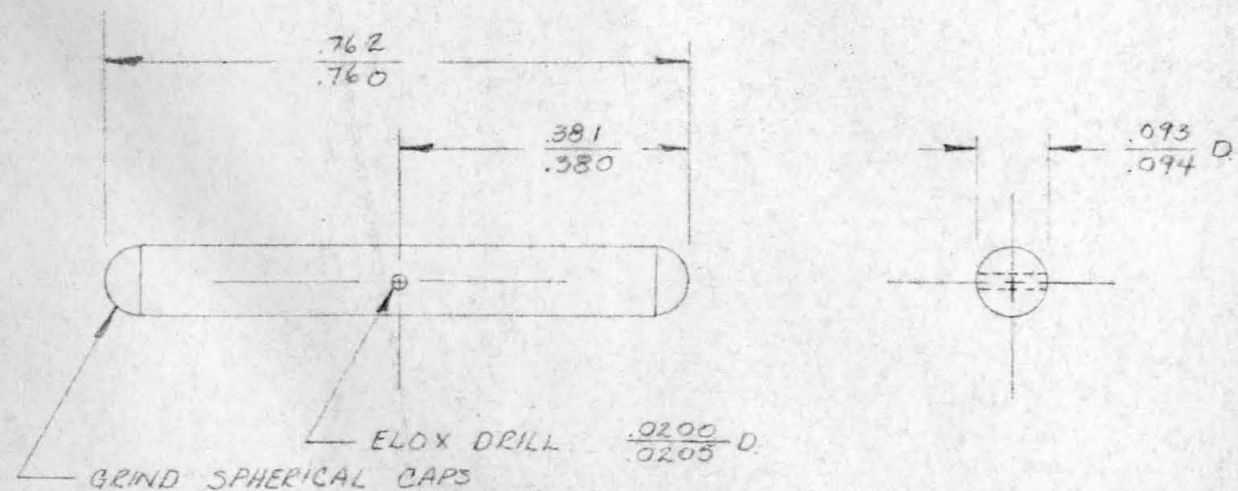
2	MAG BRACKET	1	.015" BRASS SHEET STK.
NO.	PART NAME	REQ'D	MATERIAL
ENGINEERING DESIGN CALIFORNIA INSTITUTE OF TECHNOLOGY			DR: J.R. BARNES
			APPV'D:
			SCALE: 4x FULL
			DATE: 7-26-65
MAGNET ASSEMBLY			TOLERANCES DWG. NO.
			± .005" 21



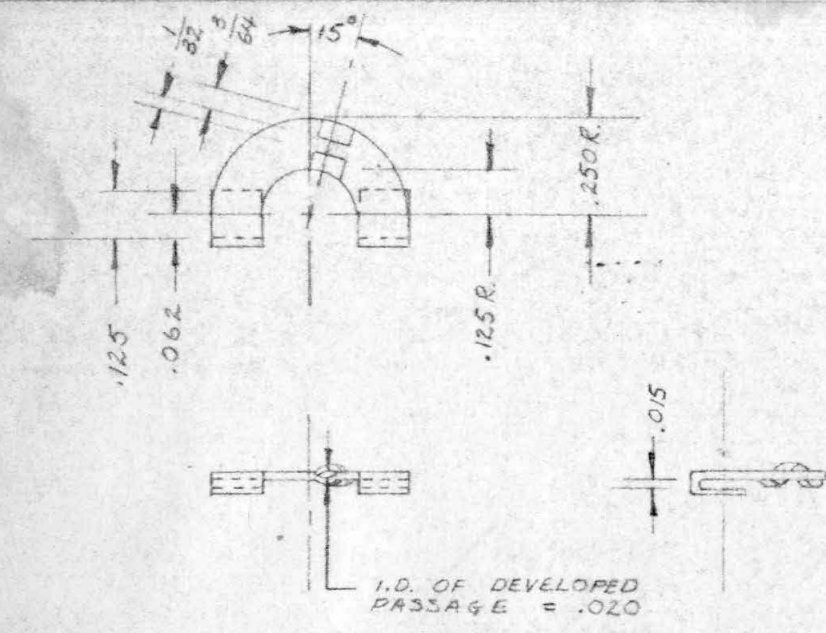
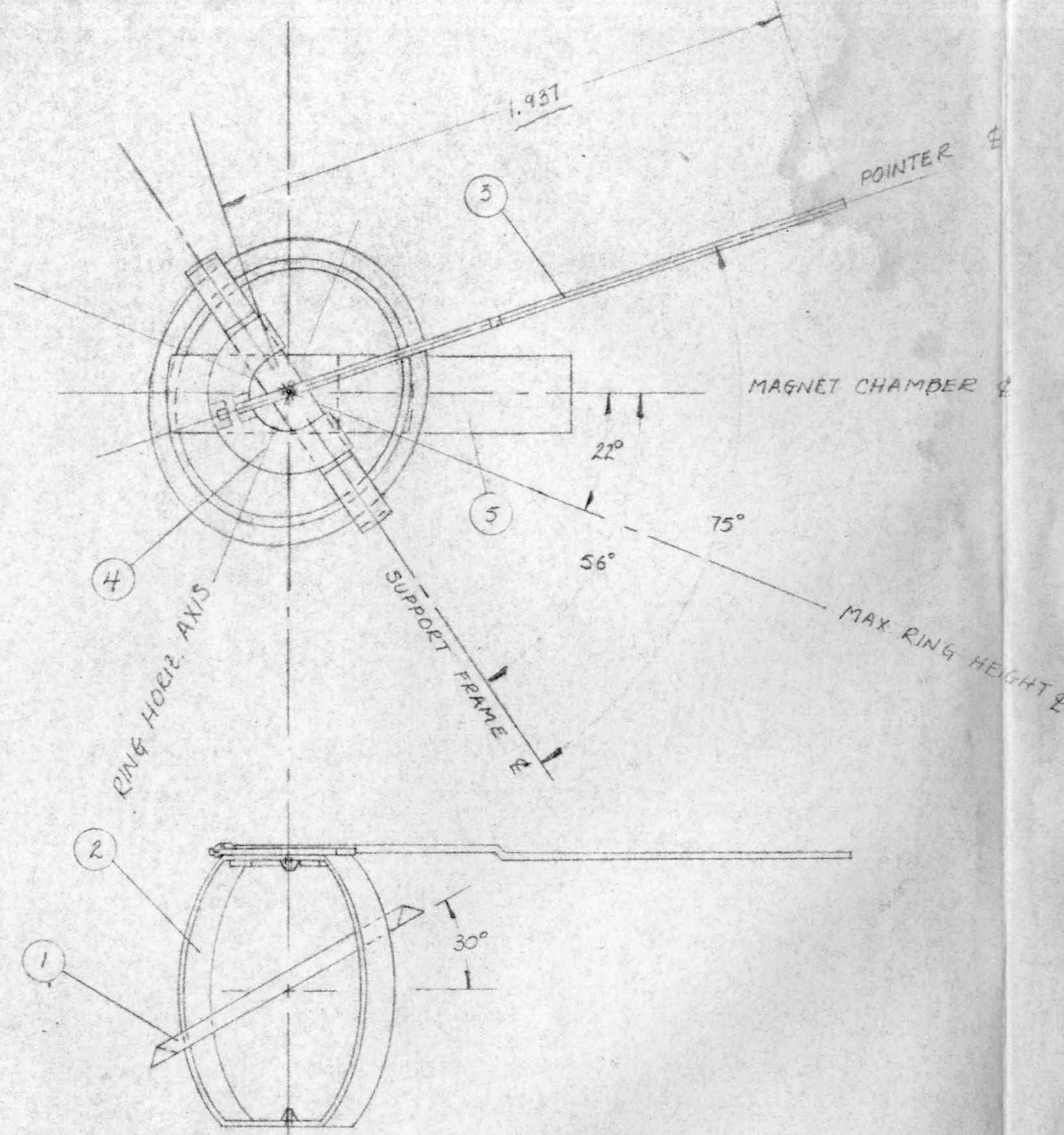
4	MAGNET PIN	1	23
3	MAG BRKT. PIN	1	.015" D BRASS
2	MAG. BRACKET	1	21
1	MAGNET	1	24
NO.	PART NAME	REQ'D	DETAIL DWG. NO.
ENGINEERING DESIGN CALIFORNIA INSTITUTE OF TECHNOLOGY			DR: J.R. BARNES
			APPV'D:
			SCALE: 4x FULL
			DATE: 7-26-65
MAGNET ASSEMBLY			TOLERANCES DWG. NO.
			± .005" 22



4	MAGNET PIN	1	S.S. 303
NO.	PART NAME	REQ'D	MATERIAL
ENGINEERING DESIGN CALIFORNIA INSTITUTE OF TECHNOLOGY			DR: J.R. BARNES
			APPV'D:
			SCALE: 4x FULL
			DATE: 7-26-65
MAGNET ASSEMBLY			TOLERANCES DWG. NO.
			± .005" 23 ± 1/64"



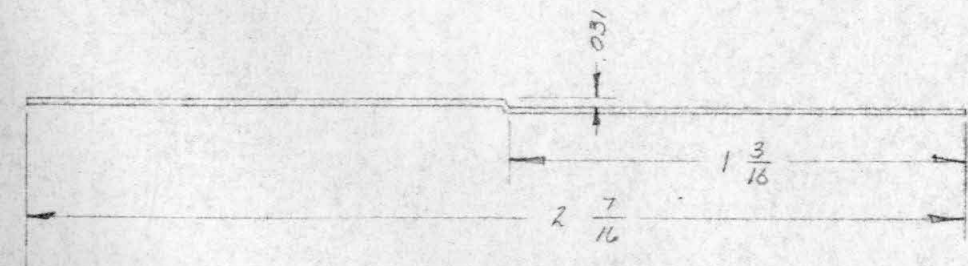
1	MAGNET	1	ALNICO V - STORCH SP-250
NO.	PART NAME	REQ'D	MATERIAL
ENGINEERING DESIGN CALIFORNIA INSTITUTE OF TECHNOLOGY			DR: J.R. BARNES
			APPV'D:
			SCALE: 4x FULL
			DATE: 7-26-65
MAGNET ASSEMBLY			TOLERANCES DWG. NO.
			± .005" 24



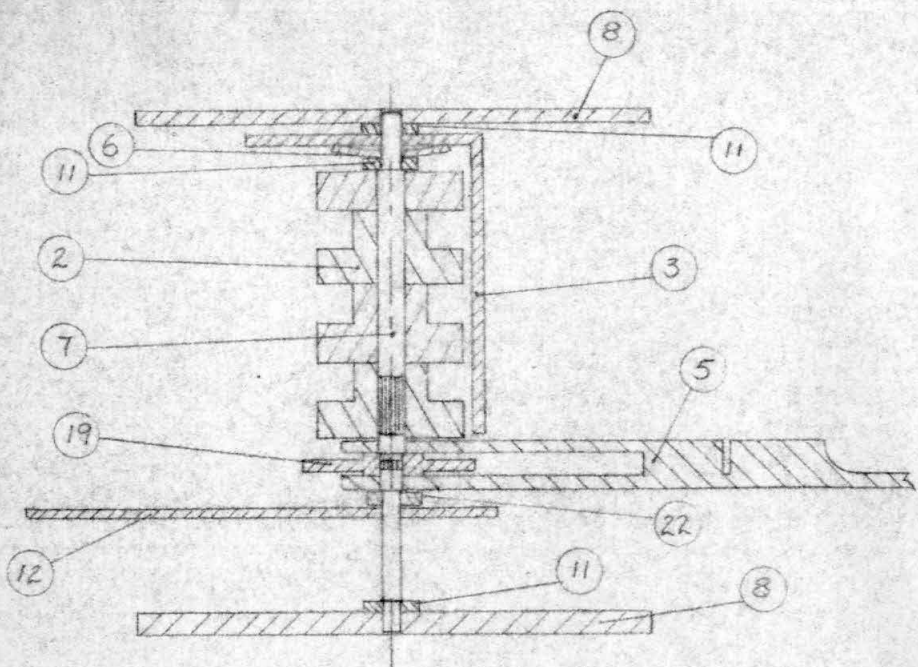
4	POINTER CLIP	1	.015" ALUM. 6061-T6
NO.	PART NAME	REQ'D	MATERIAL
ENGINEERING DESIGN CALIFORNIA INSTITUTE OF TECHNOLOGY			DR: J.R. BARNES
			APP'D:
			SCALE: 2x FULL
			DATE: 8-4-65
CROSSOVER RING ASSEMBLY			TOLERANCES DWG. NO.
			± .005" ± 1/64" ± .05°
			26

NOTE: JOIN RING TO SUPPORT FRAME POLYAMIDE CEMENT AT 200°F. TACK POINTER TO POINTER CLIP & POINTER CLIP TO SUPPORT FRAME WITH EPOXY RESIN.

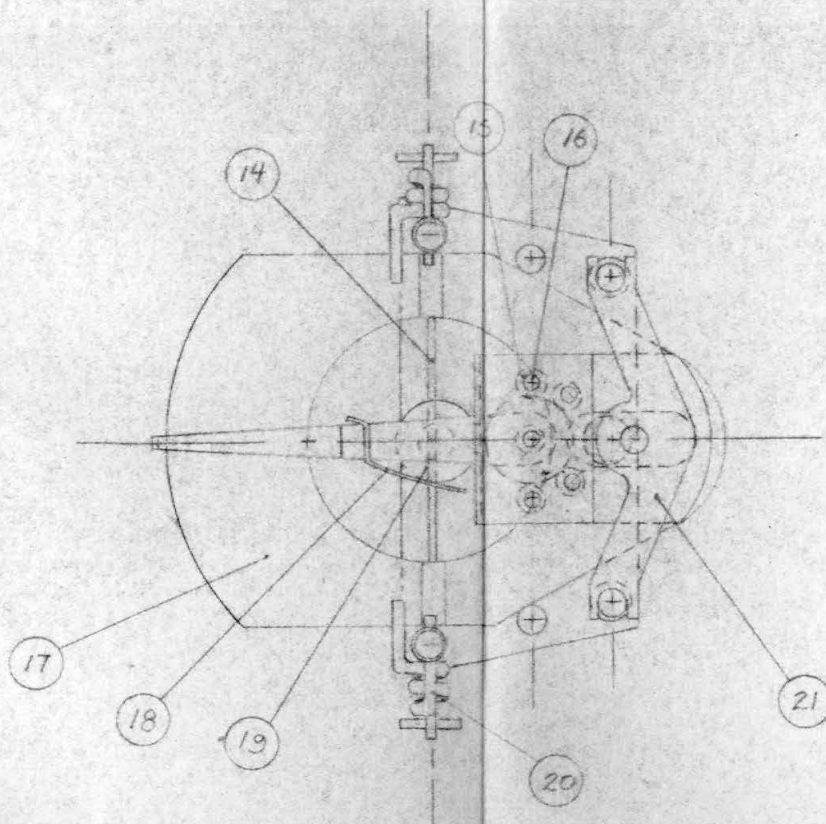
5	MAGNET CHAMBR	1	10
4	POINTER CLIP	1	26
3	POINTER	1	27
2	SUPPORT FRAME	1	16
1	RING	1	59
NO.	PART NAME	REQ'D	DETAIL DWG. NO.
ENGINEERING DESIGN CALIFORNIA INSTITUTE OF TECHNOLOGY			DR: J.R. BARNES
			APP'D:
			SCALE: 2x FULL
			DATE: 8-4-65
CROSSOVER RING ASSEMBLY			TOLERANCES DWG. NO.
			25



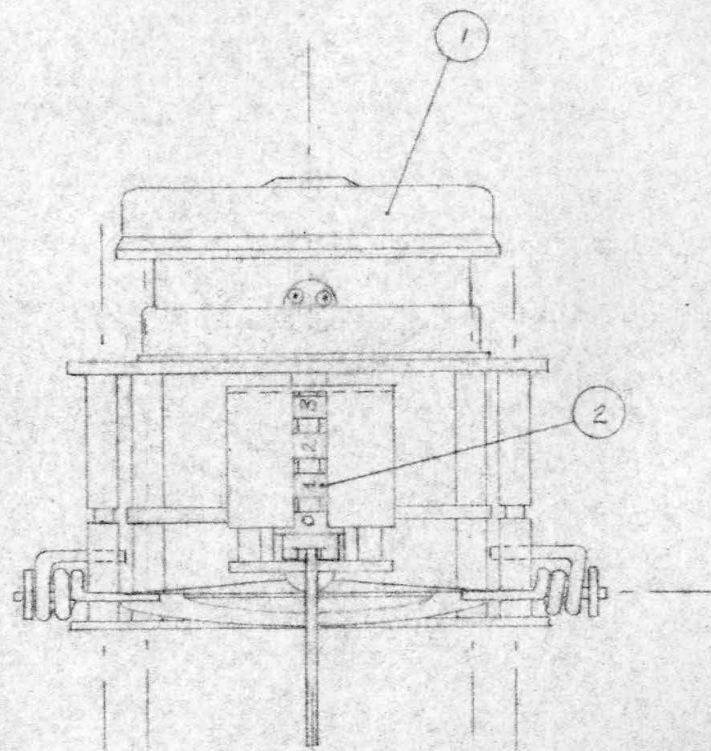
3	POINTER	1	.020 D. S.S. WIRE
NO.	PART NAME	REQ'D.	MATERIAL
ENGINEERING DESIGN CALIFORNIA INSTITUTE OF TECHNOLOGY			DR: J.R. BARNES
			APP'D:
			SCALE: 2x FULL
			DATE: 8-4-65
CROSSOVER RING ASSEMBLY			TOLERANCES DWG. NO.
			± .005" ± 1/64"
			27



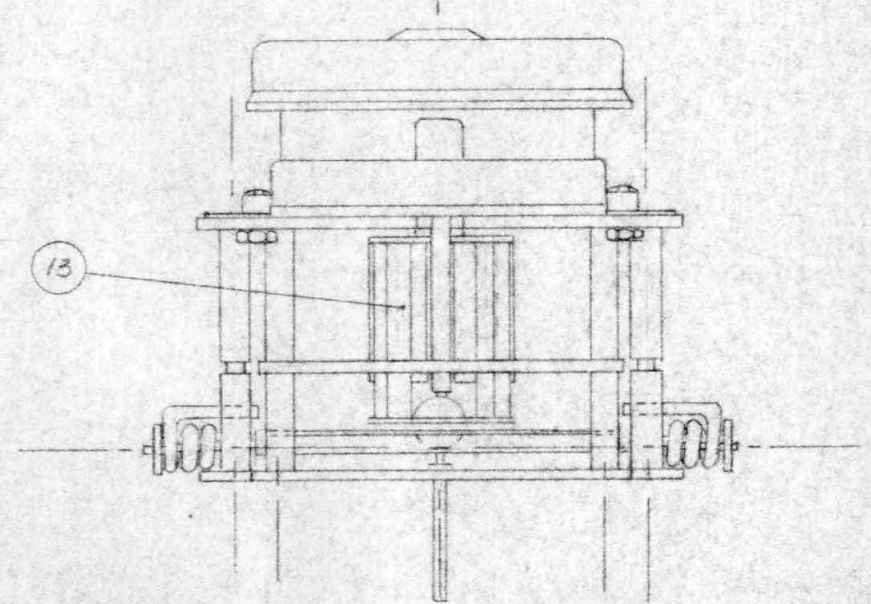
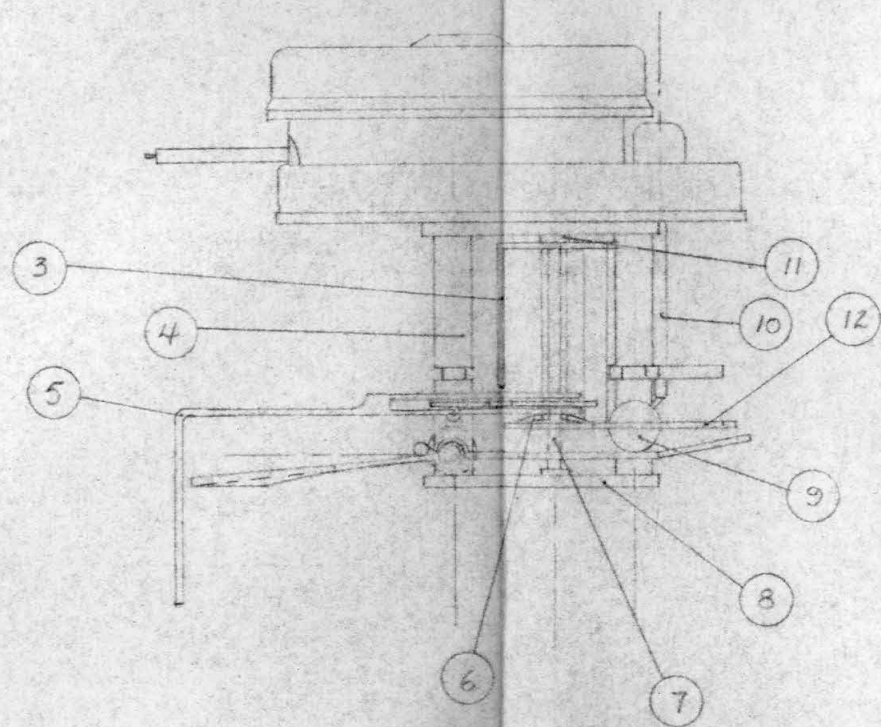
COUNTER HOUSING DETAIL (SCALE 2x FULL)
PARTS 4 & 13 NOT SHOWN



21	SHAFT GUIDE	1	43
20	TORSION SPRING	2	
19	CLUTCH PAWL	2	38
18	CLUTCH SPRING	1	32
17	CLAMP	1	40
16	CTR. PINION SHAFT	1	31
15	COUNTER PINION	3	VEEDER ROOT
14	CLAMP SHAFT	1	
13	PLATE POST	3	37
12	CTR. BOT. PLATE	1	35
11	WASHER	3	39
10	MOTOR SHAFT	1	
9	BALL CAM	1	34
8	MTG. PLATE	2	41
7	CTR. DISK SHAFT	1	33
6	PRELOAD WASHER	1	30
5	CTR. DRIVE POINTER	1	42
4	MTG. PLATE POST	4	29



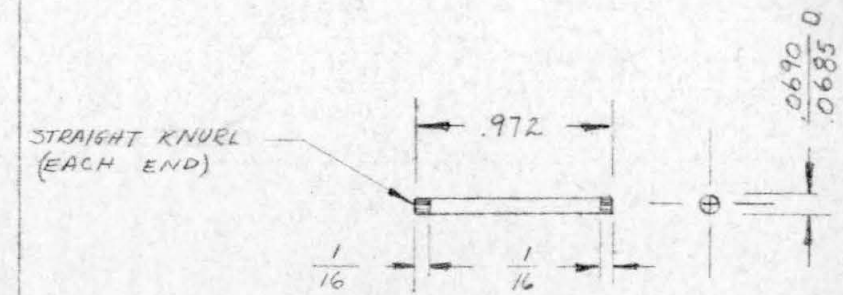
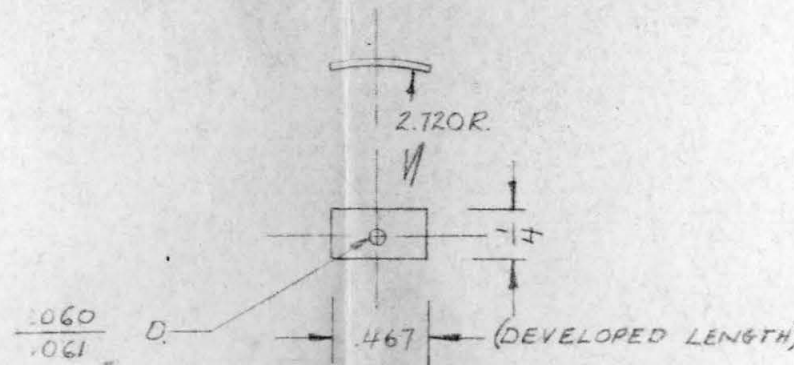
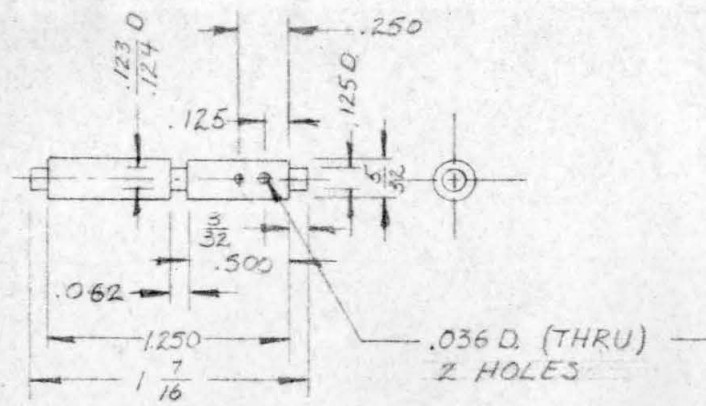
NOTE: COUNTER DISKS SHOWN
THIS VIEW ONLY



3	CTR. TOP PLATE	1	36
2	COUNTER DISK	4	VEEDER ROOT
1	GEAR MOTOR	1	HAYDON 22100
NO.	PART NAME	REQ'D	DETAIL DWG. NO.

ENGINEERING DESIGN		DR. J.R. BARNES	
CALIFORNIA INSTITUTE OF TECHNOLOGY		APP'D:	
TOTALIZER ASSEMBLY		SCALE: FULL	
		DATE: 7-14-65	
		TOLERANCES DWG. NO.	
		28	

22	WASHER	1	44
----	--------	---	----



4	MTE PLATE POST	4	BRASS
NO	PART NAME	REQ'D	MATERIAL

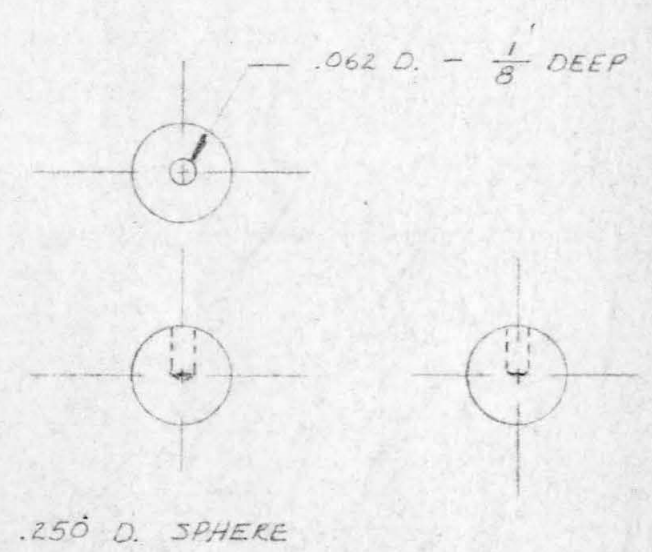
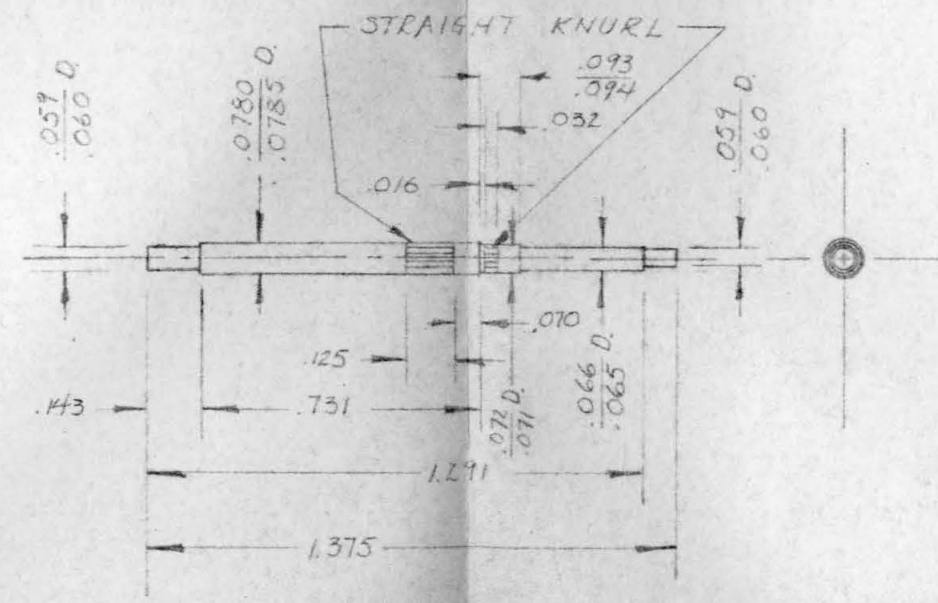
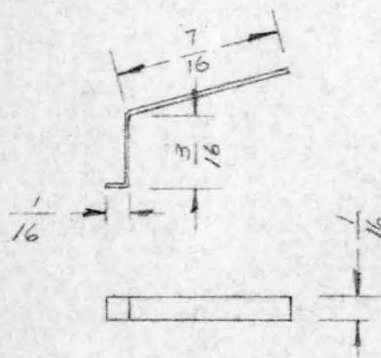
6	PRELOAD WASHER	1	005 PHOS. BRONZE
NO	PART NAME	REQ'D	MATERIAL

16	CTR PINION SHAFT	1	S.S. 303
NO	PART NAME	REQ'D	MATERIAL

ENGINEERING DESIGN CALIFORNIA INSTITUTE OF TECHNOLOGY	DR: J.R. BARNES
	APP'D:
	SCALE: FULL
	DATE: 7-27-65
TOTALIZER ASSEMBLY	TOLERANCES DWG. NO.
	± .005" ± 1/64" 29

ENGINEERING DESIGN CALIFORNIA INSTITUTE OF TECHNOLOGY	DR: J.R. BARNES
	APP'D:
	SCALE: FULL
	DATE: 7-27-65
TOTALIZER ASSEMBLY	TOLERANCES DWG. NO.
	± .005" ± 1/64" 30

ENGINEERING DESIGN CALIFORNIA INSTITUTE OF TECHNOLOGY	DR: J.R. BARNES
	APP'D:
	SCALE: FULL
	DATE: 7-27-65
TOTALIZER ASSEMBLY	TOLERANCES DWG. NO.
	± .005" ± 1/64" 31



18	CLUTCH SPRING	1	010 PHOS. BRONZE
NO	PART NAME	REQ'D	MATERIAL

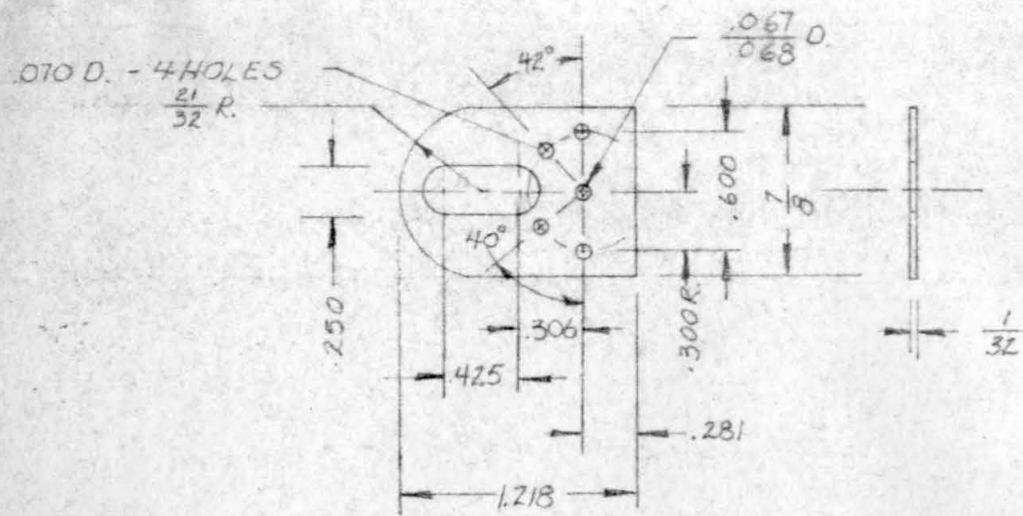
7	CTR. DRK. SHAFT	1	S.S. 303
NO	PART NAME	REQ'D	MATERIAL

9	BALL CAM	1	BRASS
NO	PART NAME	REQ'D	MATERIAL

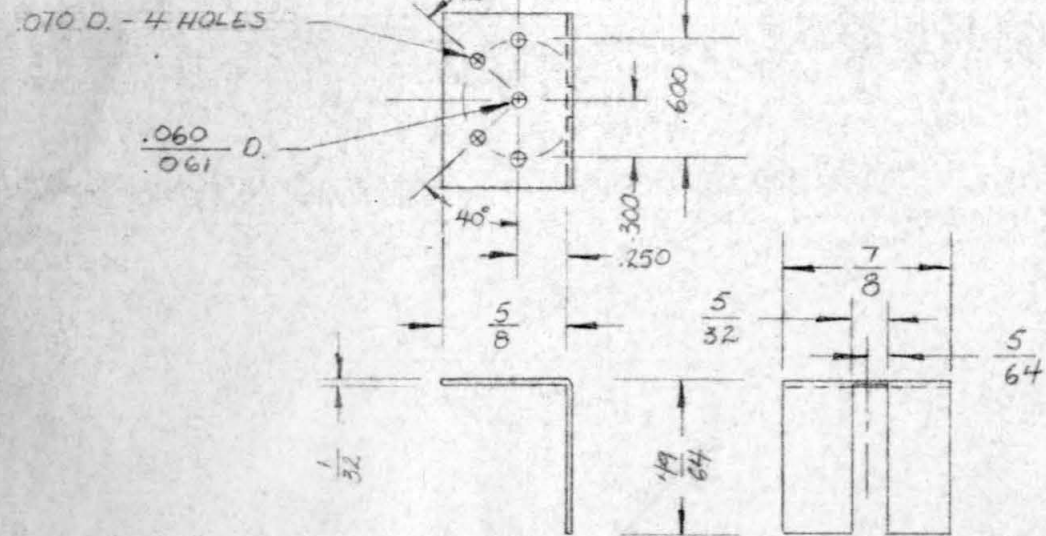
ENGINEERING DESIGN CALIFORNIA INSTITUTE OF TECHNOLOGY	DR: J.R. BARNES
	APP'D:
	SCALE: 2x FULL
	DATE: 7-27-65
TOTALIZER ASSEMBLY	TOLERANCES DWG. NO.
	± 1/64" 32

ENGINEERING DESIGN CALIFORNIA INSTITUTE OF TECHNOLOGY	DR: J.R. BARNES
	APP'D:
	SCALE: 2x FULL
	DATE: 8-3-65
TOTALIZER ASSEMBLY	TOLERANCES DWG. NO.
	± .005" 33

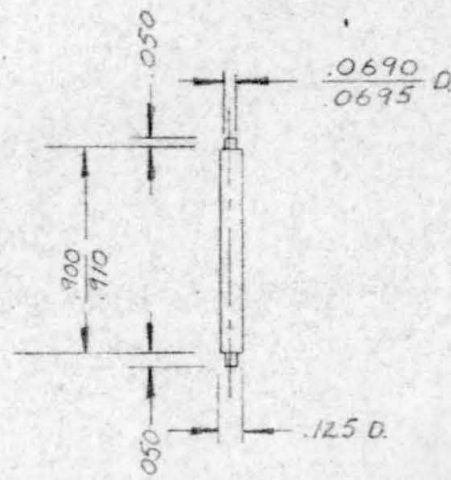
ENGINEERING DESIGN CALIFORNIA INSTITUTE OF TECHNOLOGY	DR: J.R. BARNES
	APP'D:
	SCALE: 2x FULL
	DATE: 8-3-65
TOTALIZER ASSEMBLY	TOLERANCES DWG. NO.
	± .005" ± 1/64" 34



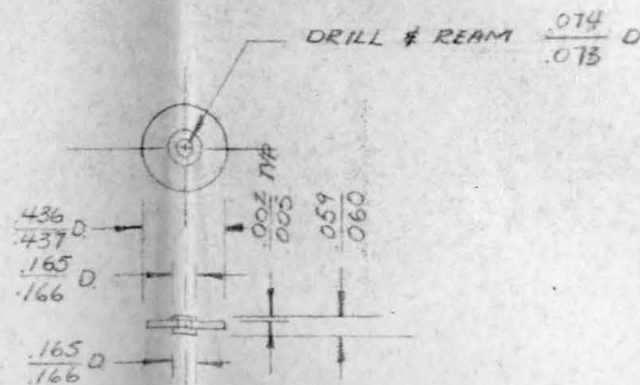
12	CTR. BOT. PLATE	1	BRASS
NO.	PART NAME	REQ'D	MATERIAL
ENGINEERING DESIGN CALIFORNIA INSTITUTE OF TECHNOLOGY			DR: J. R. BARNES
			APP'D:
			SCALE: FULL
			DATE: 7-27-65
TOTALIZER ASSEMBLY			TOLERANCES DWG. NO.
			± .005" ± 1/64" ± 0.5° 35



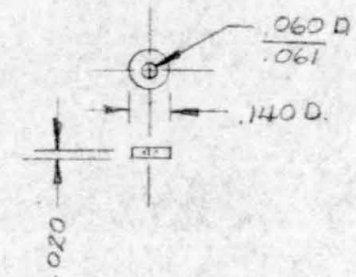
3	CTR. TOP PLATE	1	BRASS
NO.	PART NAME	REQ'D	MATERIAL
ENGINEERING DESIGN CALIFORNIA INSTITUTE OF TECHNOLOGY			DR: J. R. BARNES
			APP'D:
			SCALE: FULL
			DATE: 7-27-65
TOTALIZER ASSEMBLY			TOLERANCES DWG. NO.
			± .005" ± 1/64" ± 0.5° 36



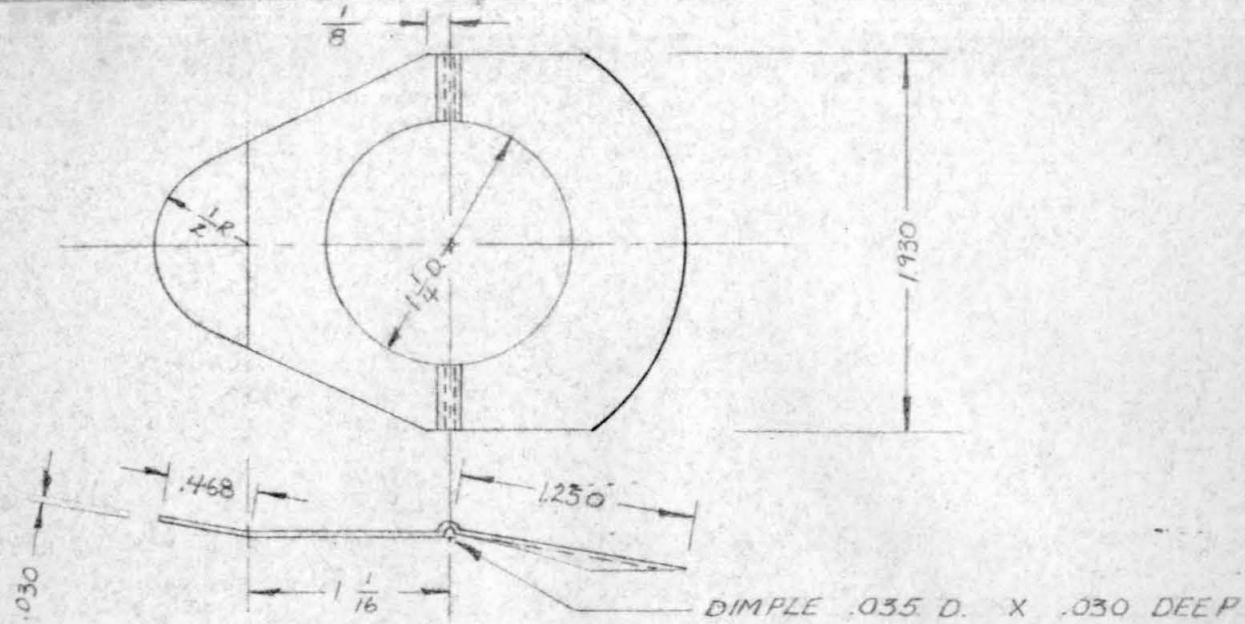
13	PLATE POST	3	BRASS
NO.	PART NAME	REQ'D	MATERIAL
ENGINEERING DESIGN CALIFORNIA INSTITUTE OF TECHNOLOGY			DR: J. R. BARNES
			APP'D:
			SCALE: FULL
			DATE: 7-27-65
TOTALIZER ASSEMBLY			TOLERANCES DWG. NO.
			± .005" 37



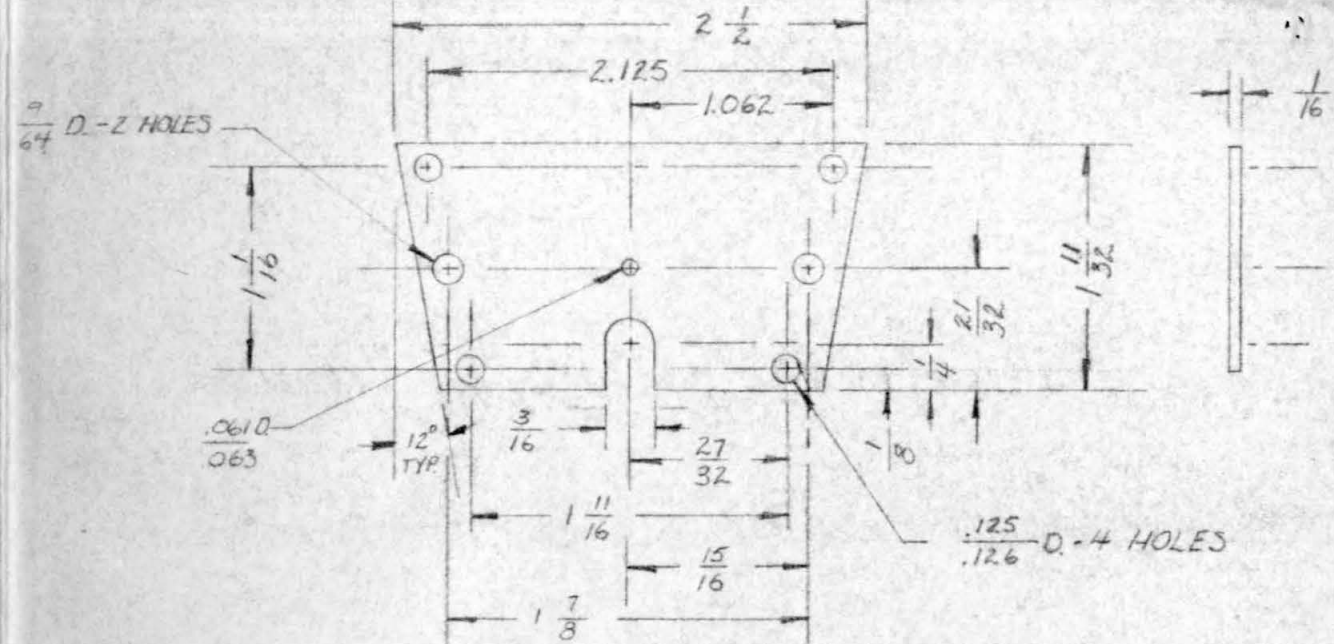
19	CLUTCH PAWL	2	ALUMINUM 2024
NO.	PART NAME	REQ'D	MATERIAL
ENGINEERING DESIGN CALIFORNIA INSTITUTE OF TECHNOLOGY			DR: J. R. BARNES
			APP'D:
			SCALE: FULL
			DATE: 7-27-65
TOTALIZER ASSEMBLY			TOLERANCES DWG. NO.
			± .005" 38



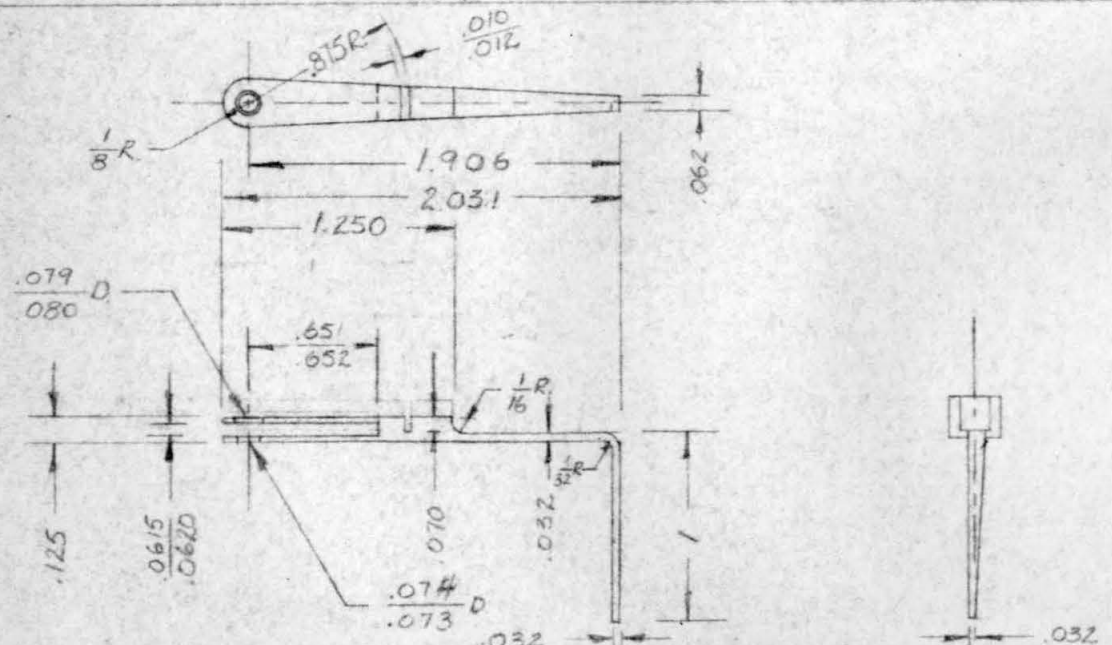
11	WASHER	3	BRASS
NO.	PART NAME	REQ'D	MATERIAL
ENGINEERING DESIGN CALIFORNIA INSTITUTE OF TECHNOLOGY			DR: J. R. BARNES
			APP'D:
			SCALE: FULL
			DATE: 7-27-65
TOTALIZER ASSEMBLY			TOLERANCES DWG. NO.
			± .005" 39



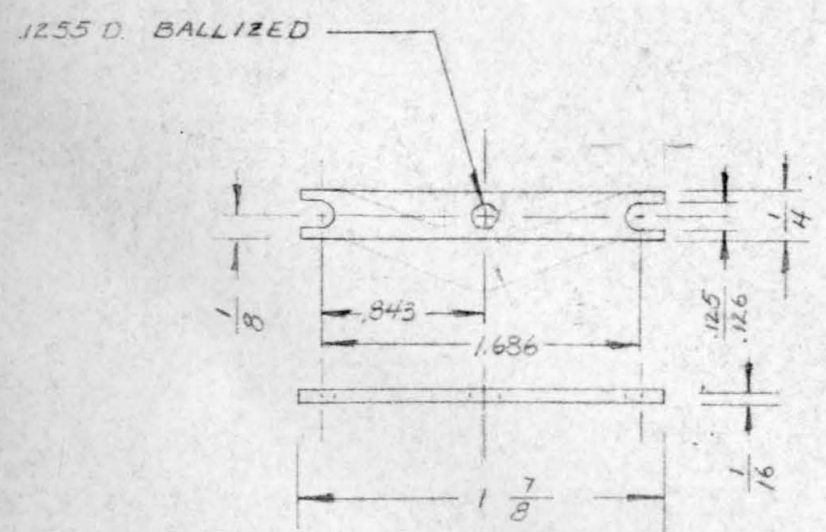
17	CLAMP	1	HALF HARD BRASS
NO.	PART NAME	REQ'D	MATERIAL
ENGINEERING DESIGN CALIFORNIA INSTITUTE OF TECHNOLOGY			DR: J. R. BARNES APPV'D: SCALE: FULL DATE: 7-27-65 TOLERANCES DWG NO. ± .005" ± 1/64" ± 0.5°
TOTALIZER ASSEMBLY			40



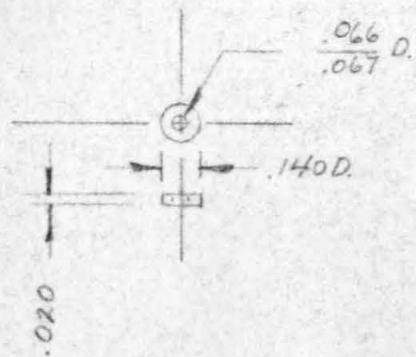
8	MTG. PLATE	2	BRASS
NO.	PART NAME	REQ'D	MATERIAL
ENGINEERING DESIGN CALIFORNIA INSTITUTE OF TECHNOLOGY			DR: J. R. BARNES APPV'D: SCALE: FULL DATE: 7-27-65 TOLERANCES DWG NO. ± .005" ± 1/64" ± 0.5°
TOTALIZER ASSEMBLY			41



5	CNTR. DRIVE POINTER	1	ALUM 6061-T6
NO.	PART NAME	REQ'D	MATERIAL
ENGINEERING DESIGN CALIFORNIA INSTITUTE OF TECHNOLOGY			DR: J. R. BARNES APPV'D: SCALE: FULL DATE: 7-27-65 TOLERANCES DWG NO. ± .005" ± 1/64"
TOTALIZER ASSEMBLY			42



21	SHAFT GUIDE	1	BRASS
NO.	PART NAME	REQ'D	MATERIAL
ENGINEERING DESIGN CALIFORNIA INSTITUTE OF TECHNOLOGY			DR: J. R. BARNES APPV'D: SCALE: FULL DATE: 7-27-65 TOLERANCES DWG NO. ± .005" ± 1/64" ± 0.5°
TOTALIZER ASSEMBLY			43



22	WASHER	1	BRASS																
NO	PART NAME	REQ'D	MATERIAL																

ENGINEERING DESIGN
CALIFORNIA INSTITUTE OF TECHNOLOGY

TOTALIZER ASSEMBLY

DR. J.R. BARNES
APVD
SCALE: FULL
DATE: 8-21-65
TOLERANCES DWG. NO.
 $\pm .005"$ 44

ENGINEERING DESIGN
CALIFORNIA INSTITUTE OF TECHNOLOGY

45

ENGINEERING DESIGN
CALIFORNIA INSTITUTE OF TECHNOLOGY

46

ENGINEERING DESIGN
CALIFORNIA INSTITUTE OF TECHNOLOGY

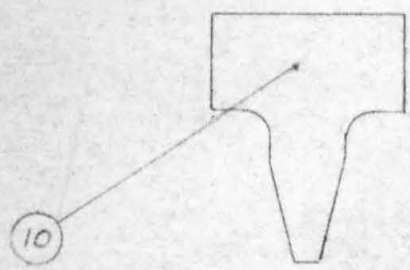
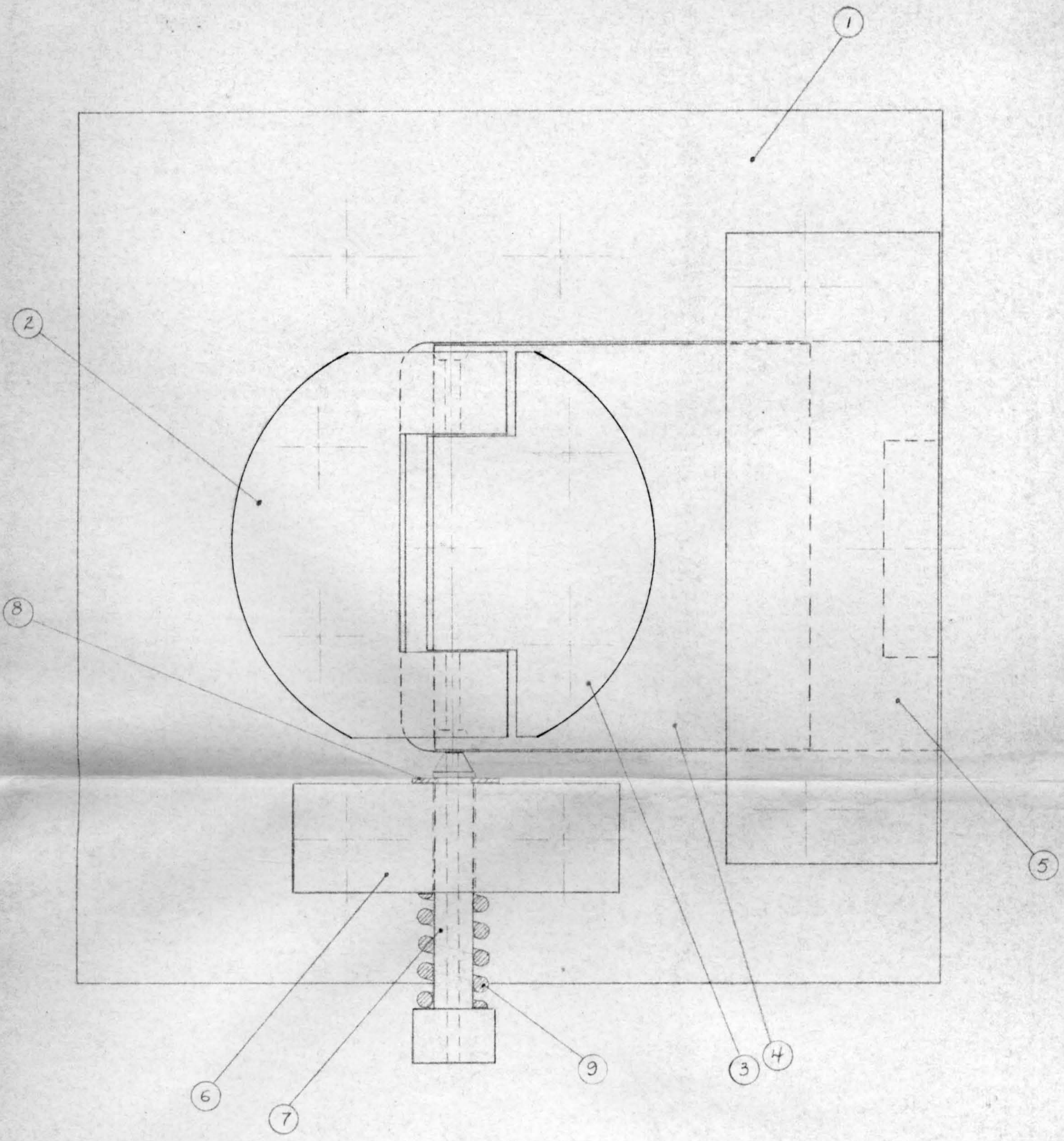
47

ENGINEERING DESIGN
CALIFORNIA INSTITUTE OF TECHNOLOGY

48

ENGINEERING DESIGN
CALIFORNIA INSTITUTE OF TECHNOLOGY

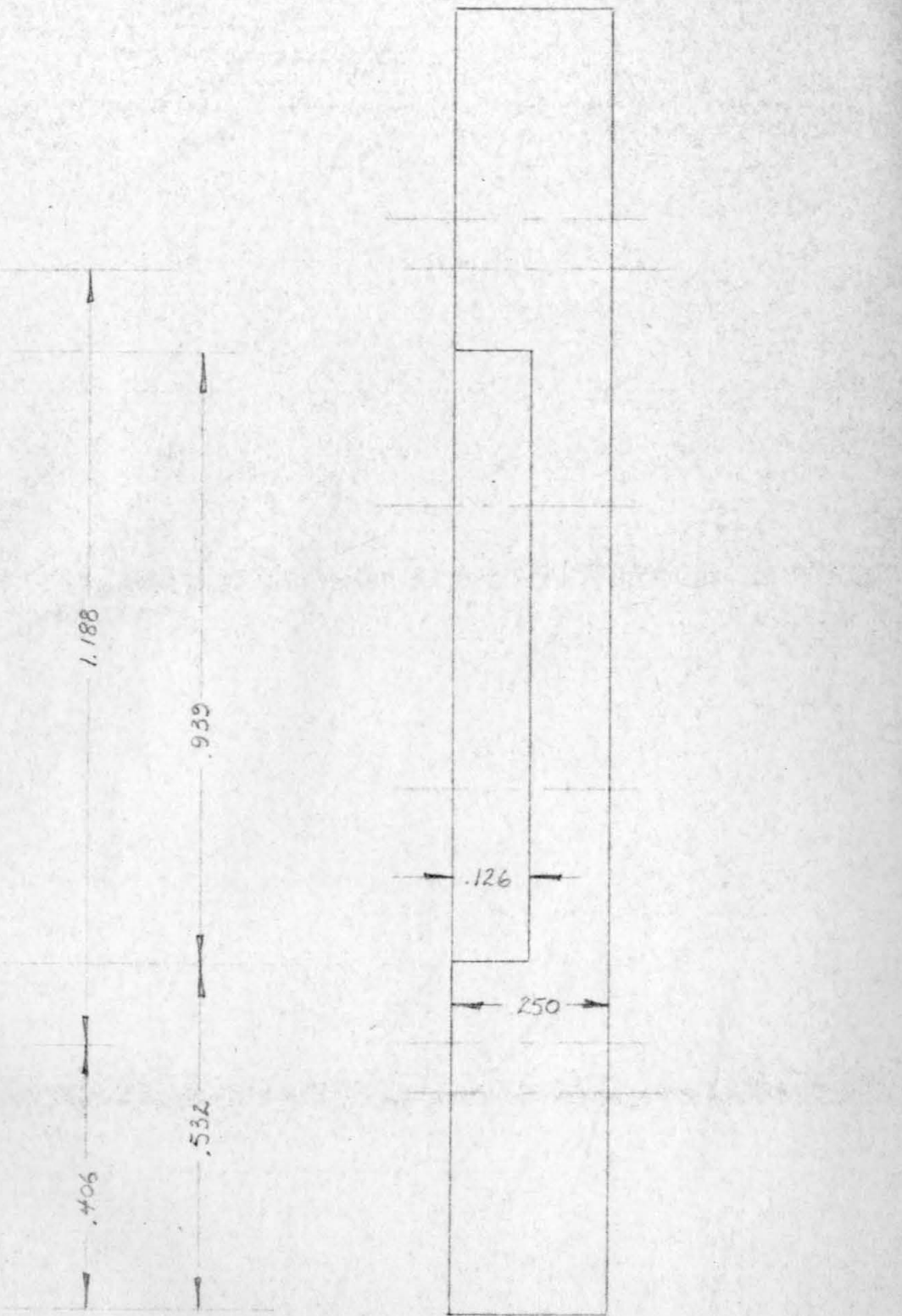
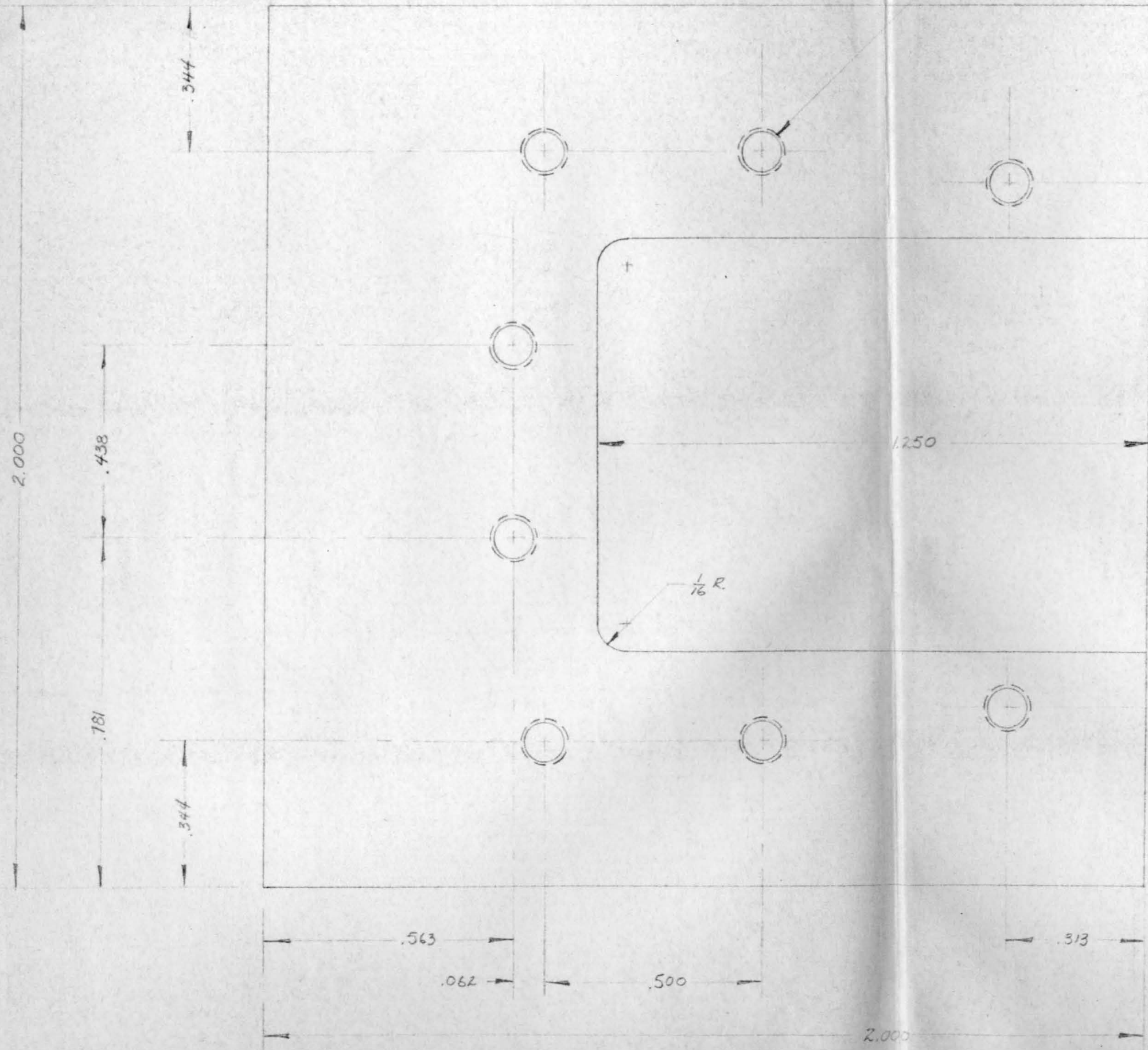
49



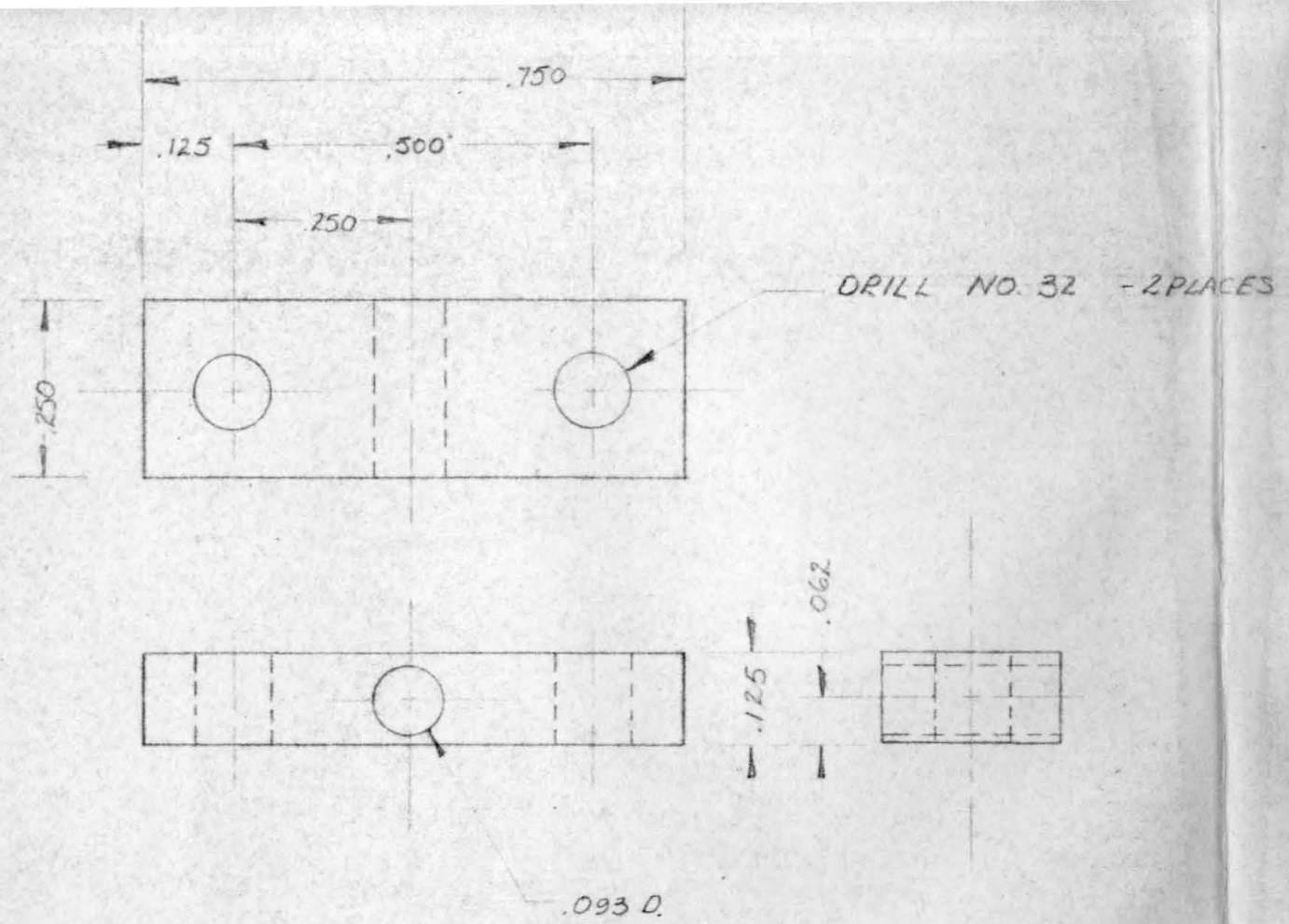
10	WEDGE	1	14	
9	SPRING	2	AS AVAILABLE	
8	SNAP RING	2	WALDES 5144-9	
7	PUNCH	2	57	
6	PUNCH HOLDER	2	56	
5	STOP PLATE	1	53	
4	SLIDE	1	54	
3	R.H. FORM	1	52	
2	L.H. FORM	1	51	
1	BASE PLATE	1	55	
NO.	PART NAME	REQ'D	DETAIL DWG. NO.	

ENGINEERING DESIGN CALIFORNIA INSTITUTE OF TECHNOLOGY	DR: J. R. BARNES
	APPVD:
STRETCH FORMER ASSEMBLY	SCALE: 4 X FULL
	DATE: 7-1-69
	DWG. NO. 50

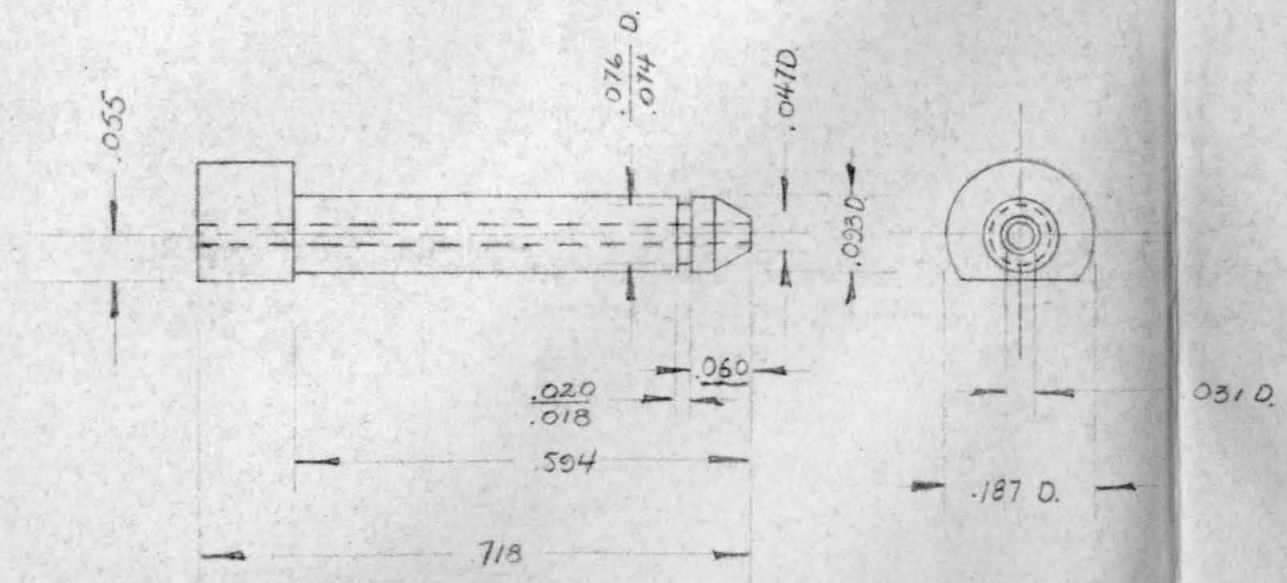
DRILL NO.44 - TAP 4-40 (THRU) - 8 PLACES



1	BASE PLATE	1	C1020
NO.	PART NAME	REQ'D	MATERIAL
ENGINEERING DESIGN CALIFORNIA INSTITUTE OF TECHNOLOGY			DR: J.R. BARNES
STRETCH FORMER ASSEMBLY			APP'D:
			SCALE: 4 X FULL
			DATE: 7-1-65
			TOLEANCES
			± .005"
			± 1/64"
			DWG NO. 55

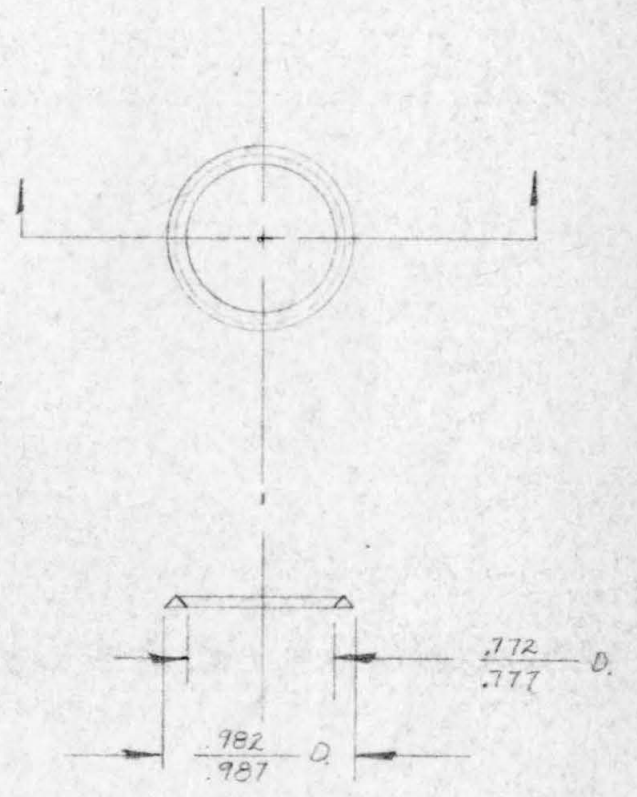
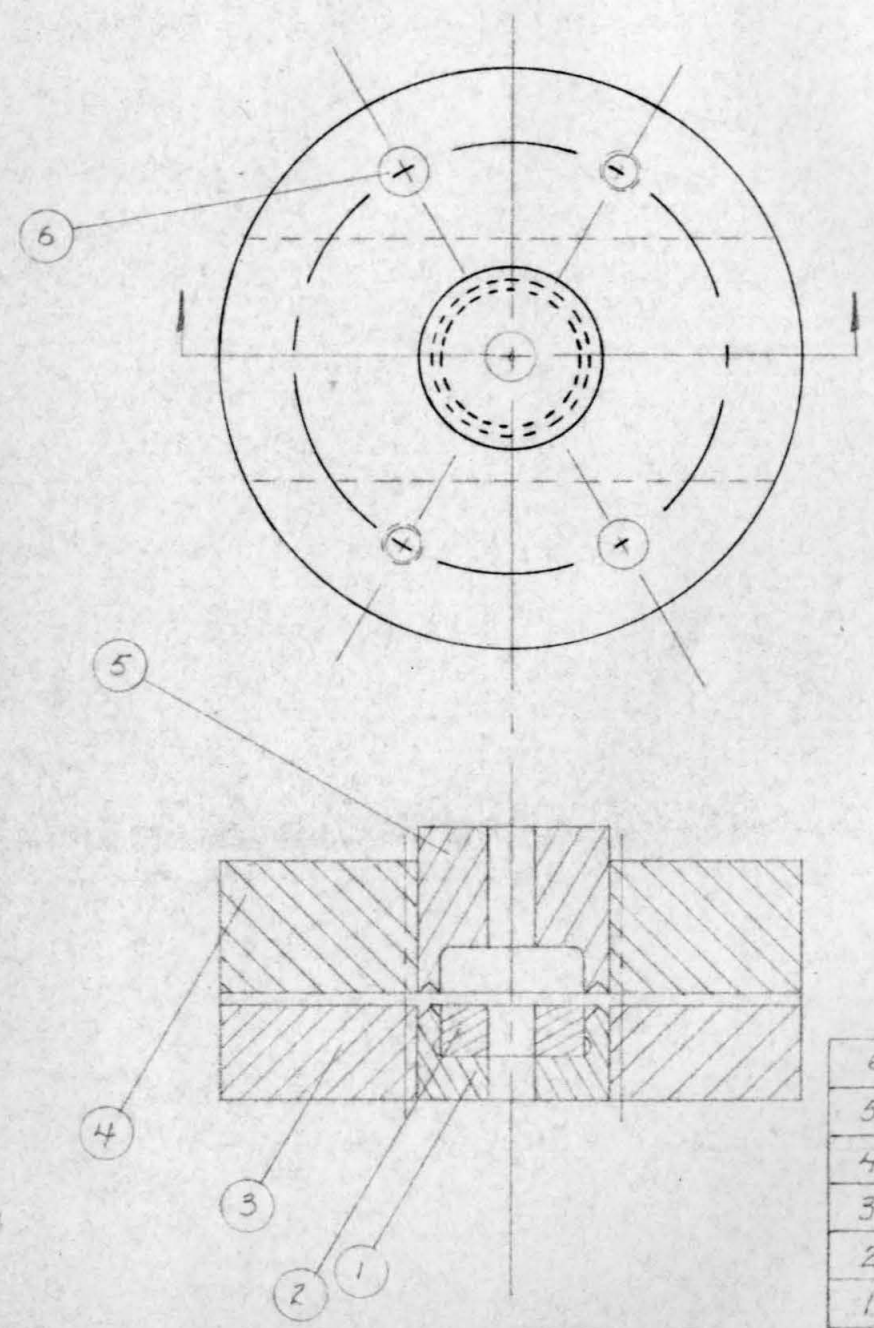


6	PUNCH HOLDER	2	C 1020
NO.	PART NAME	REQ'D	MATERIAL
ENGINEERING DESIGN CALIFORNIA INSTITUTE OF TECHNOLOGY			DR: J.R. BARNES
STRETCH - FORMER ASSEMBLY			APP'D:
			SCALE: 4x FULL
			DATE: 7-1-65
			TOLERANCES
			DWG. NO.
			± .005
			56



7	PUNCH	2	C 1020
NO.	PART NAME	REQ'D	MATERIAL
ENGINEERING DESIGN CALIFORNIA INSTITUTE OF TECHNOLOGY			DR: J.R. BARNES
STRETCH - FORMER ASSEMBLY			APP'D:
			SCALE: 4x FULL
			DATE: 7-1-65
			TOLERANCES
			DWG. NO.
			± .005
			57

NOTE: FORM BY MEANS OF RING DIE ASSEMBLY



6	DOWELL PIN	2	.250 D. x 1.250 DOWELL PIN
5	FEMALE DIE	1	63
4	FEM. DIE HOLDER	1	61
3	MALE DIE HOLDER	1	64
2	MALE CUTTER	1	60
1	MALE DIE	1	62
NO.	PART NAME	REQ'D	DETAIL DWG. NO.

1	RING	1	.005 STEEL SHIM STK.
NO.	PART NAME	REQ'D	MATERIAL

ENGINEERING DESIGN
CALIFORNIA INSTITUTE OF TECHNOLOGY

RING DIE ASSEMBLY

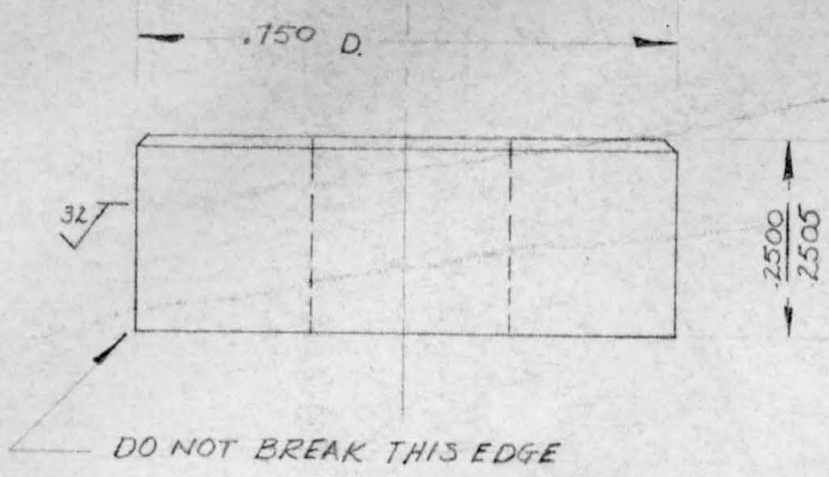
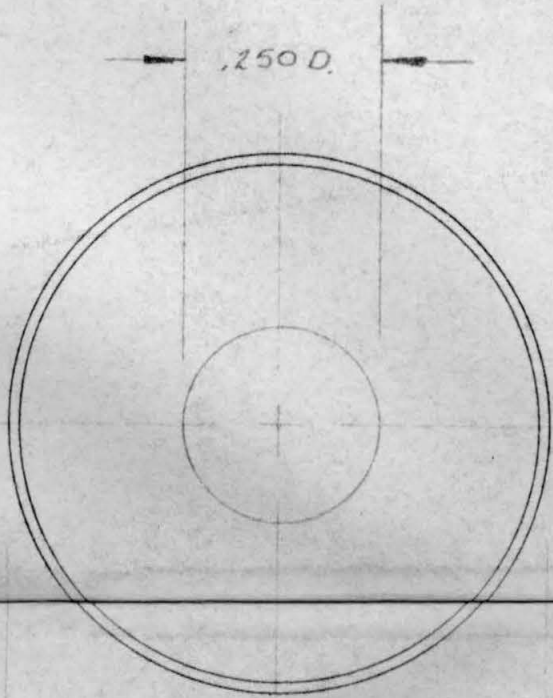
DR: J.R. BARNES
APP'D:
SCALE: FULL
DATE: 7-23-65
TOLERANCES DWG. NO.
± .005" 58

ENGINEERING DESIGN
CALIFORNIA INSTITUTE OF TECHNOLOGY

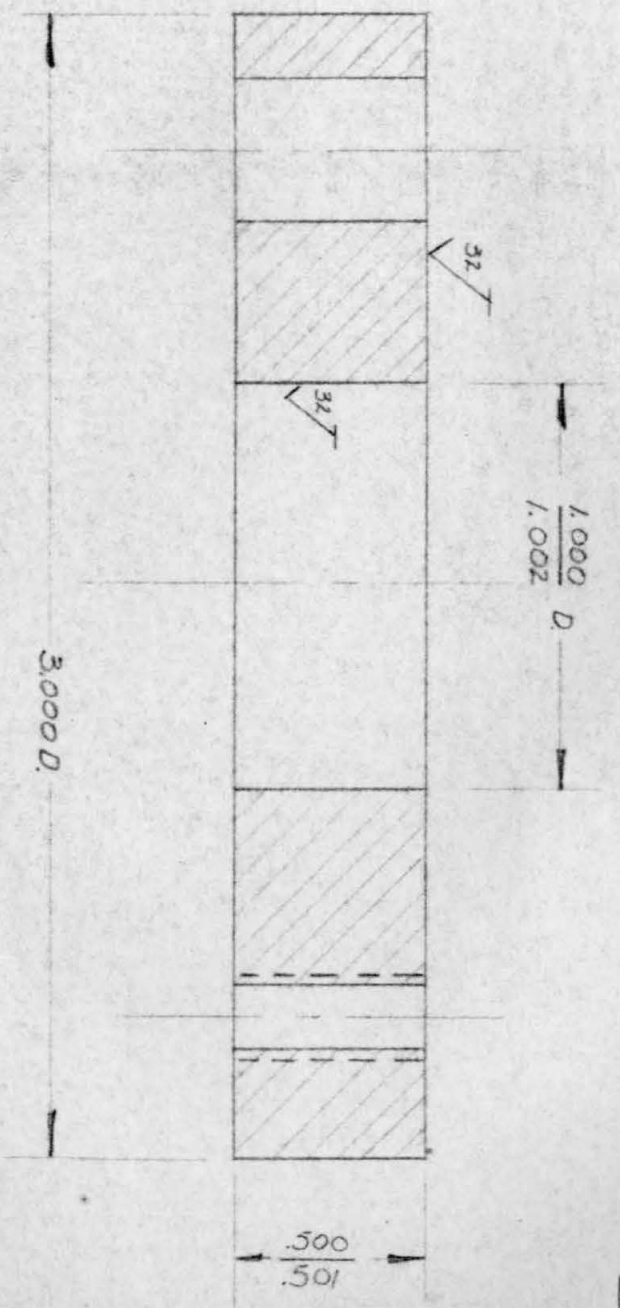
CROSSOVER RING ASSEMBLY

DR: J.R. BARNES
APP'D:
SCALE: FULL
DATE: 7-23-65
TOLERANCES DWG. NO.
± .005" 59

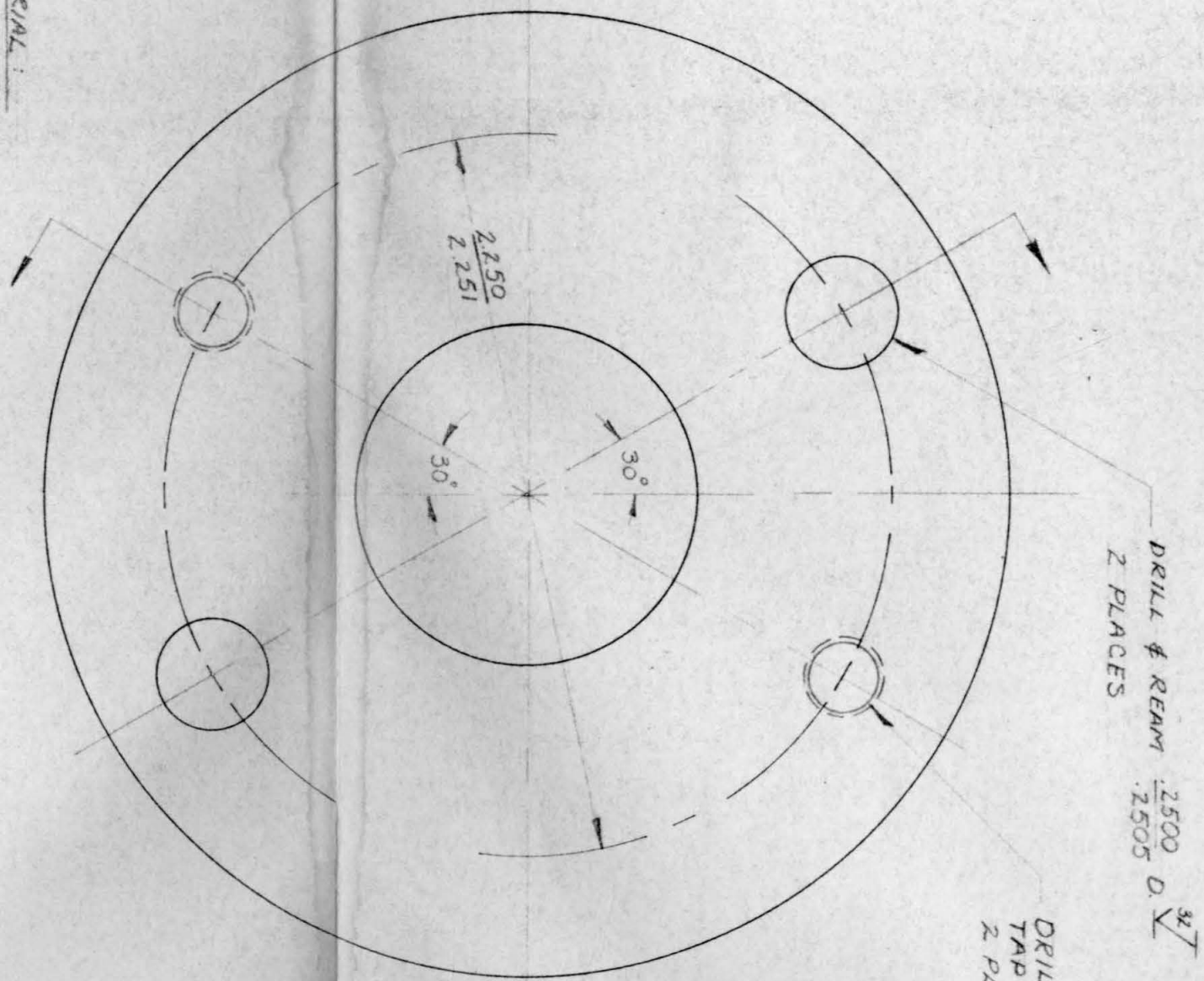
MATERIAL
 AISI 4340 (c) STEEL
 (HEAT TREATED)
 OR EQUIV.



MALE CUTTER	2	1	NOTED	60
NAME	NO.	REQ'D	MAT'L.	DRWG NO.
CALIF. INST. OF TECH.			DR. : J. R. BARNES	
RING DIE ASSEMBLY			APPV'D:	
TOLERANCES			DATE : 6-21-65	
AS SHOWN			SCALE : 4 x FULL	



MATERIAL:
 AISI 4340(E)
 (HEAT TREATED)
 OR EQUIV.



TOLERANCES	
ANGULAR :	± 0.1°
FRACTIONAL :	± 1/64"
DECIMAL :	± 0.005

3	MALE DIE HOLDER	1	NOTED	61
NO.	NAME	REQ'D.	MAT'L.	DRW'G. NO.
CALIF. INST. OF TECH.			DR. : J.R. BARNES	
RING DIE ASSEMBLY			APPVD.:	
			DATE : 6-21-65	
			SCALE : 2x FULL	

TOLERANCES	MALE DIE	1	1	NOTED	62
ANGULAR : $\pm 0.1^\circ$	NAME	NO. REQ'D		MAT'L :	DRW'G. NO.
FRACTIONAL : $\pm 1/64$	CALIF. INST. OF TECH.			DR. : J. R. BARNES	
DECIMAL : ± 0.005	RING DIE ASSEMBLY			APPV'D:	
				DATE : 6-21-65	
				SCALE : 4x FULL	

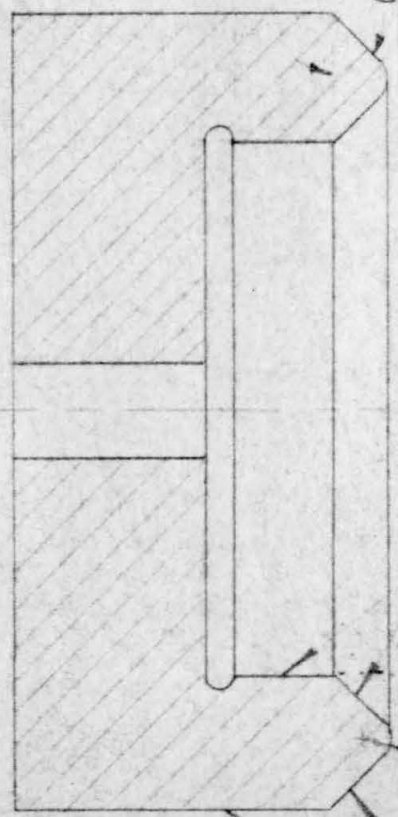
500 REF

.412
 .417

.2500
 .2505

1/32

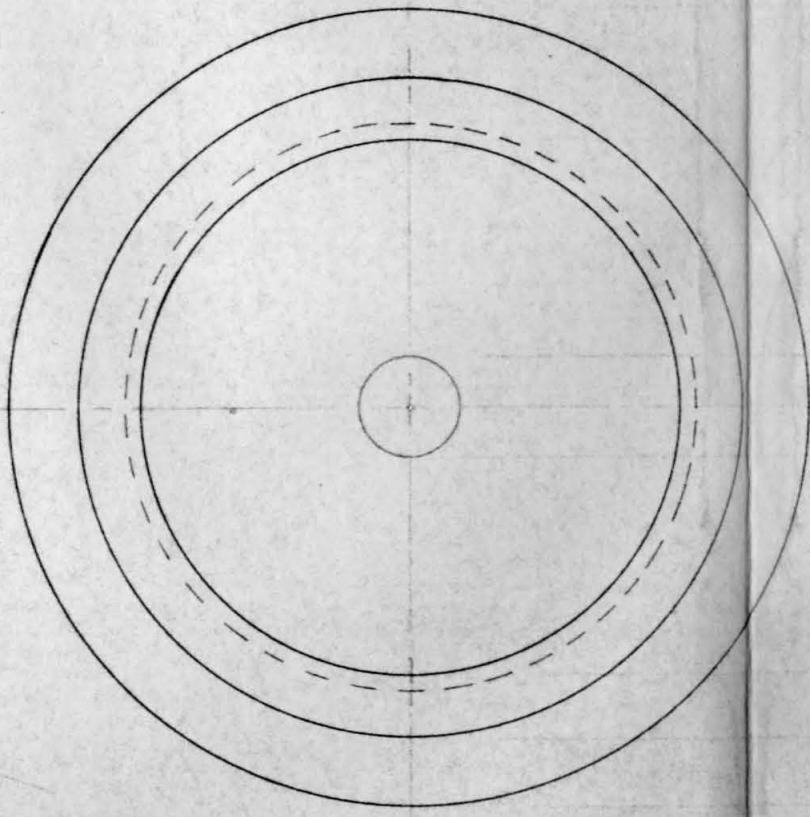
45° (TYP)



3/32

BREAK
 EDGE

3/32



3/8 D

.750 D

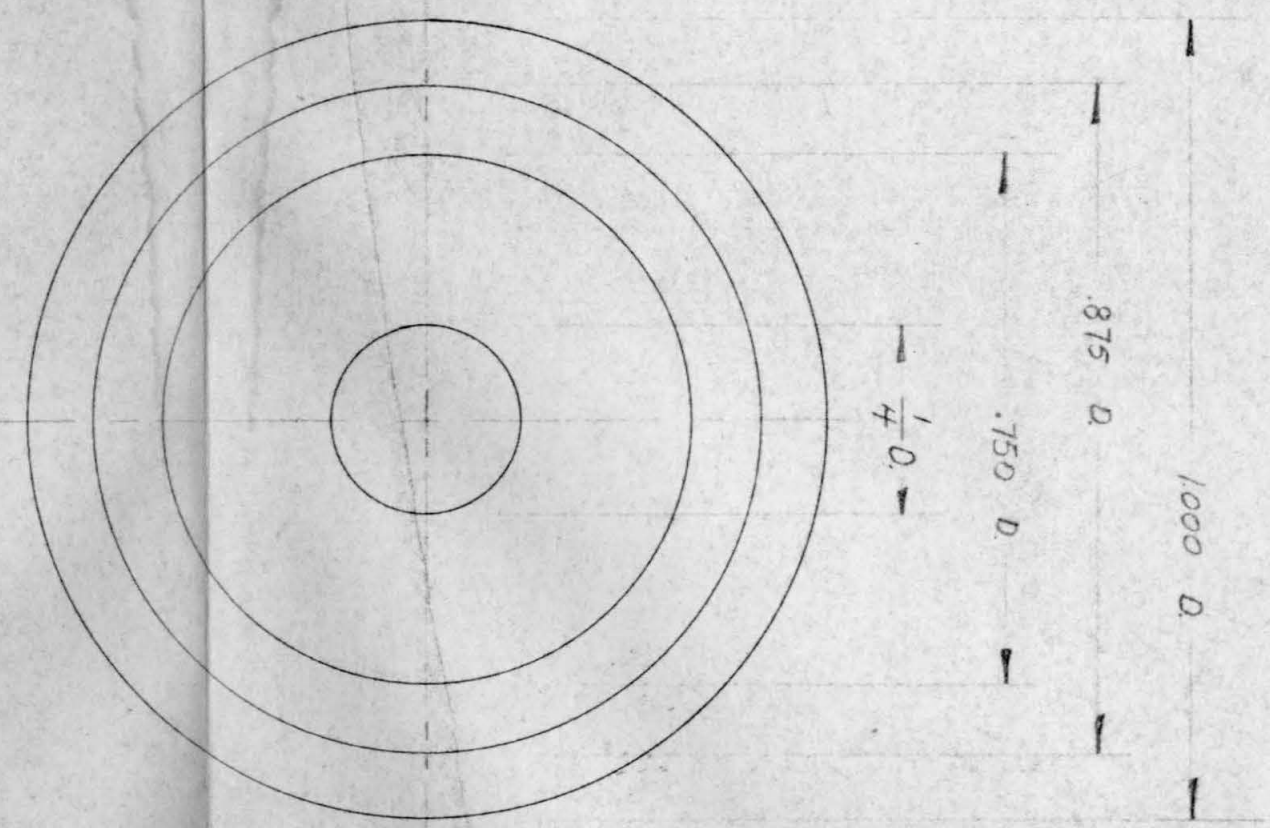
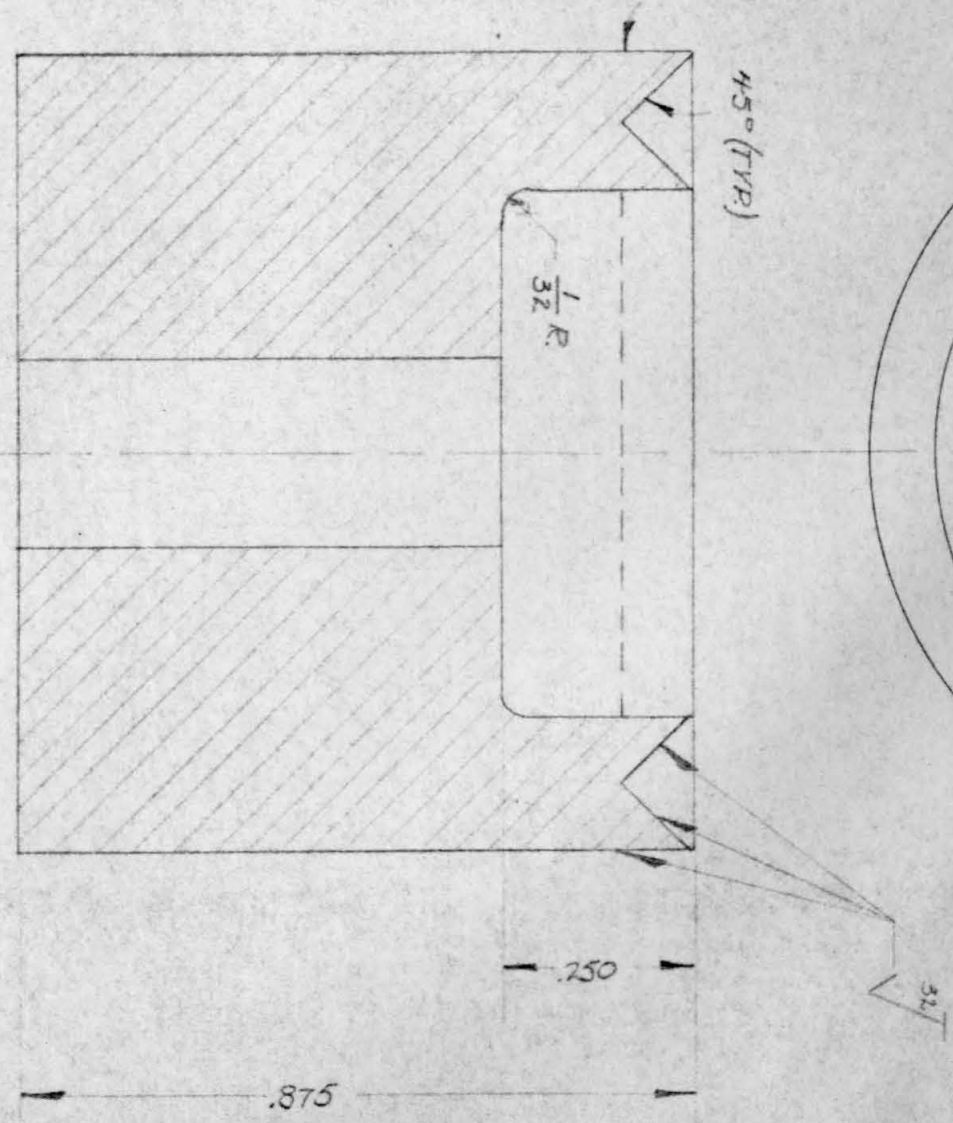
.875 D

1.000 D

MATERIAL :
 AISI 4340 (e)
 OR EQUIV.

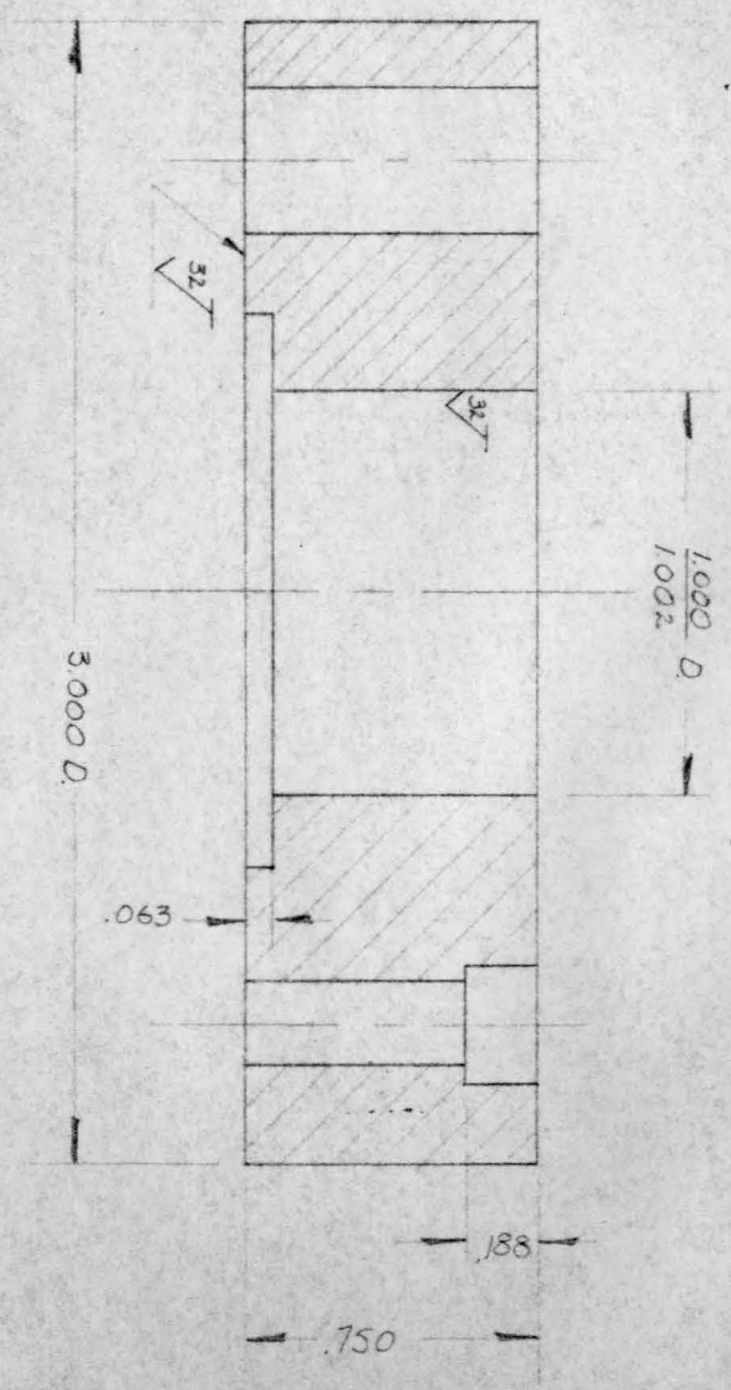
TOLERANCES
 ANGULAR : $\pm 0.1^\circ$
 FRACTIONAL : $\pm 1/64$
 DECIMAL : ± 0.005

FEMALE DIE	5	1	NOTED	63
NAME	NO.	REQ'D	MAT'L	DRW'G. NO
CALIF. INST. OF TECH.			DR: J.R. BARNES	
RING DIE ASSEMBLY			APPV'D.:	
			DATE: 6-21-65	
			SCALE: 4x FULL	

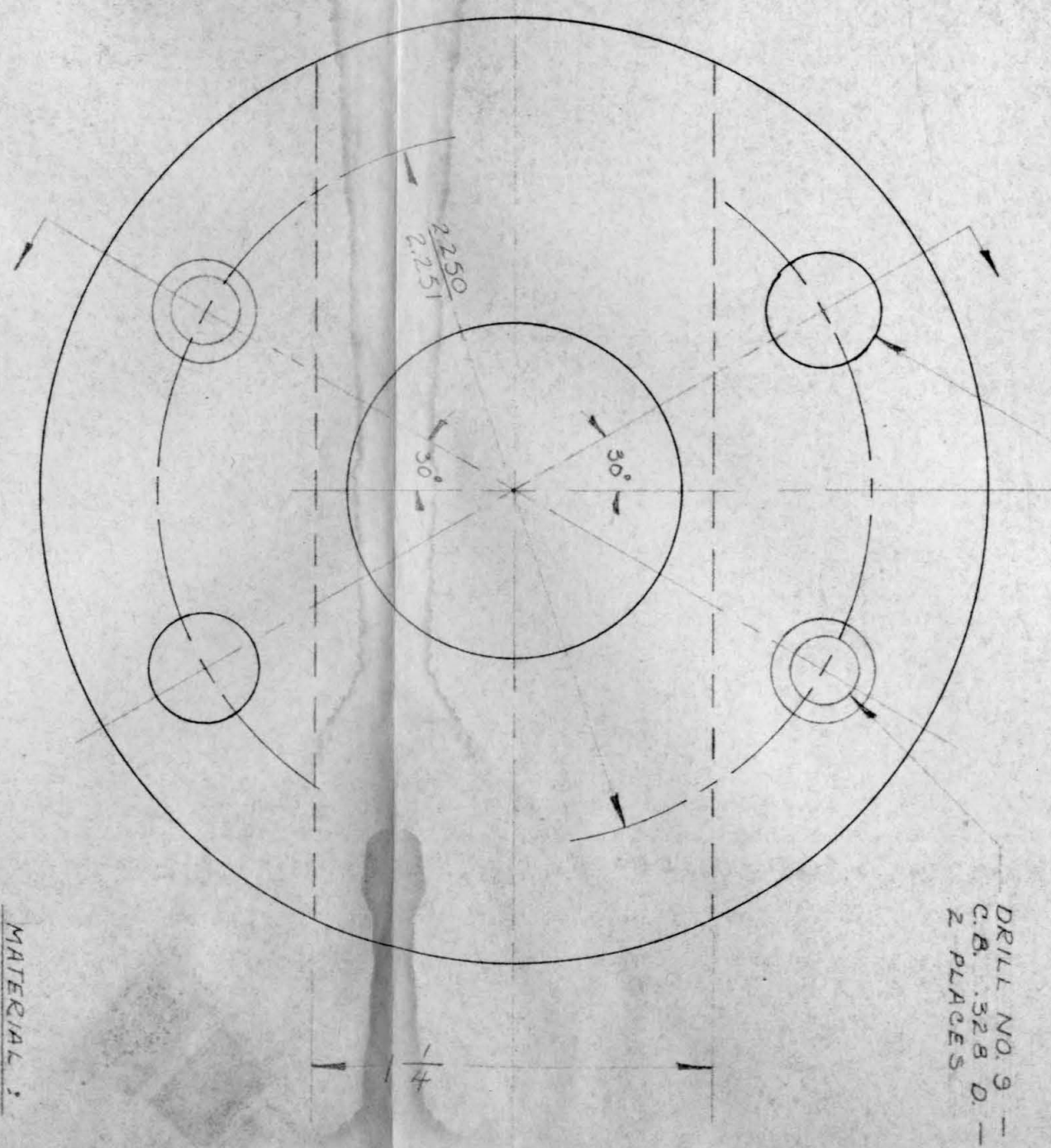


MATERIAL :
 AISI 4340 (C)
 (HEAT TREATED)
 OR EQUIV.

TOLERANCES ANGULAR : $\pm 0.1^\circ$ FRACTIONAL : $\pm 1/64''$ DECIMAL : $\pm 0.005''$	FEMALE DIE HOLDER	4	1	NOTED	64
	NAME		NO. REQ'D.	MAT'L:	DRW'G. NO.
	CALIF. INST. OF TECH.				DR. J. R. BARNES
	RING DIE ASSEMBLY				APPV'D:
				DATE: 6-21-65	
				SCALE: 2X FULL	



MATERIAL:
 AISI 4340 (c)
 OR EQUIV



DRILL # REAM 2500 D. 32°
 2 PLACES
 2505
 DRILL NO. 9 --
 C.B. .528 D. --
 2 PLACES